COMPUTER MODELLING OF THE THERMAL DECOMPOSITION OF SOLIDS

Submitted in fulfilment of the requirements
for the degree of

Master of Science
of
Rhodes University

ANNEMARIE DE LA CROIX

January 1996

ACKNOWLEDGEMENTS

A very special thank you to my supervisors Professor Michael Brown and Professor Leslie Glasser for all their help, expert guidance and encouragement.

I am also grateful to Dr Ron Cosser, Justin Jonas and the computer support team, for their assistance with my computer problems and all the staff and students of the Chemistry Department who have contributed in some way to my stay at Rhodes University.

Finally, I wish to thank my family for their love and support and for believing in me.

ABSTRACT

Decompositions of solids are typically of the form:

$$A(s) \longrightarrow B(s) + \text{gases}$$

Symmetry-controlled routes (based on known and hypothetical crystal structures) for transforming the solid reactant into the solid product were devised as possible decomposition pathways. Lattice energies of the reactants, of the postulated transient intermediate structures and of the final solid products were then estimated by crystal modelling procedures. Profiles of lattice energy changes during the proposed decomposition routes were constructed and any energy barriers were compared with experimental activation energies reported for the thermal decompositions.

The crystal modelling was performed with the computer program WMIN. Calculation of the lattice energies involved the development of a model potential for the perfect lattice and the evaluation of the interatomic parameters. The potential was based on the Born model of ionic solids using the Buckingham potential ($\phi(r) = Ae^{-r/\rho} - C/r^6$) to describe the short-range energy contribution. Empirical fitting was used to establish reliable interatomic energy parameters. The reliability of the interatomic potentials was assessed by calculating crystal structures and lattice energies (which were not included in the fitting).

The particular reactions selected for modelling were the decompositions of the alkaline-earth metal (Ca, Sr, Ba) peroxides and carbonates:

$$MO_2(s) \longrightarrow MO(s) + \tfrac{1}{2}O_2(g)$$

$$MCO_3(s) \longrightarrow MO(s) + CO_2(g)$$

The lattice energies calculated for the known structures were in good agreement with reported values, (except for BaO_2 and $BaCO_3$) which provided support for the adequacy of the potential model used.

Activation energies calculated for the decomposition of the carbonates were in the correct order but higher than experimental values, *i.e.*, 422, 422, 465 and 499 kJ mol^{-1} compared to the experimental values of 205, 87(?), 222 and 283 kJ mol^{-1} for $CaCO_3$ (calcite), $CaCO_3$(aragonite), $SrCO_3$ and $BaCO_3$. The values calculated for the peroxides (91 and 100 kJ mol^{-1} compared to the experimental values of 119 and 185 kJ mol^{-1} for SrO_2 and BaO_2, respectively) were less satisfactory but could be a reflection of the poor structural data used for the peroxides.

The significance of this approach to the modelling of solid decompositions is discussed.

CONTENTS

LIST OF FIGURES

LIST OF TABLES

Chapter 8

LIST OF MAIN SYMBOLS AND ABBREVIATIONS

Crystallographic symbols:

a, b, c, α, β, γ	lattice constants
a, b, c, d, e	Wyckoff positions
(x,y,z)	atomic fractional coordinate
V	unit cell volume
Z	number of formula units
D_o	experimental density
D_c	calculated density
M_r	molar mass
N_A	Avogadro constant, $6.022\ 045 \times 10^{23}\ mol^{-1}$
R-value	refinement factor

Others:

A_{ij}, ρ_{ij}, C_{ij}	interatomic potential parameters
r_{ij}	interatomic radius
q_i, q_j	point charges
W	lattice energy
W_c	Coulombic energy term
W_r	repulsion energy term
W_v	van der Waals energy term
$W_{r,v}$	combined repulsion and van der Waals energy terms
$W_{corrected}$	lattice energy corrected for the removal of evolved gas
ΔW	change in lattice energy
E_a	activation energy
ΔH	enthalpy change
$\Delta H^{\ominus}_f$	standard enthalpy of formation
E	electric field strength
μ	dipole moment
α	polarizability
k	harmonic spring force constant

1. INTRODUCTION

1.1 AIMS OF THIS PROJECT

A typical reaction pattern for the thermal decomposition of some single solid substances is:

$$A(s) \longrightarrow B(s) + C(g)$$

Kinetic studies of such reactions have received a great deal of attention because of both their practical and theoretical importance [1]. Reactions of ionic inorganic solids, in particular, have received much attention; they may be better represented by the reaction pattern,

$$M[XY](s) \longrightarrow M[X](s) + Y(g)$$

where M is a cation, [XY] is a multi-atom anion, [X] is a simple anion and [Y] is a gaseous molecule resulting from disruption of the original anion, *e.g.*, $CO_3^{2-} \longrightarrow O^{2-} + CO_2(g)$.

Numerous factors have been shown to influence the rates and mechanisms of solid decompositions. Attempts have been made to determine, by experiment, the influence of the nature of the cation, M, on the rates of decomposition of a series of salts, M[XY], and the behaviour of various anions [XY] in combination with the same cation, M. Such attempts are complicated by the fact that the crystal structures of a series of salts M[XY] may not be comparable, particularly when the anion varies. Even when structures are comparable, the influence of crystal imperfections on the rates of a solid state decomposition can be greater than any influence of the bulk structure [1].

Lack of progress in both of these approaches has directed attention towards studies of coordination compounds. Although the complexity of the anion (or, possibly, the cation) is increased by coordination, similar crystal structures are often observed for compounds containing a series of different ligands. Attempts may thus be made to determine the influence of the coordinating metal on the release of the different ligands from the complex ion [2].

In this thesis, the relatively unexplored changes of lattice energy of an ionic compound, during its transformation from crystalline reactant to crystalline product with accompanying release of a gaseous molecule, is examined. The possible paths by which such structural transformations may take place are discussed in detail and lattice energies are calculated for postulated structural intermediates.

The particular reactions selected for modelling were the decompositions of the alkaline-earth metal (Ca, Sr, Ba) peroxides and carbonates.

Peroxides: $MO_2(s) \longrightarrow MO(s) + \frac{1}{2}O_2(g)$

Carbonates: $MCO_3(s) \longrightarrow MO(s) + CO_2(g)$

This series of reactions was chosen so that the following aspects could be examined:

1. The effect of the separate removal of O_2 and CO_2 units from the different reactant structures to yield, in each reaction series, the common solid product MO, where $M = Ca^{2+}$, Sr^{2+}, Ba^{2+}.
2. The influence of the cations (Ca^{2+}, Sr^{2+}, Ba^{2+}) on the removal of the above species.

An extensive literature of experimental studies of some of these reactions exists. For example, $CaCO_3$ is used as a model in discussing solid state kinetics [3], while the decompositions of BaO_2 and SrO_2 are well documented [4].

The object of modelling is to reproduce certain features of the system. Because assumptions and approximations are made to derive the model, it is understood that the model is not a perfect representation of the real system. It is the right of the modeller to decide on the features of the model and then it is the responsibility of the modeller to test the model using appropriate and reliable methods. The usefulness of the model can then be assessed. In this study, the main aim has been to test whether the changes in lattice energy of an ionic solid, resulting from a reaction mechanism based on a set of proposed changes in crystal structure, can be used to construct a meaningful energy profile whose maximum (relative to the reactant state) is related to the experimentally determined activation energy, E_{act}, for the reaction considered. (If the energy barrier and E_{act} are very different, then the proposed mechanism cannot be correct; if they are similar, then the mechanism is possible - but never proven). Lattice energy is a bulk property but decomposition of a solid will, at highest resolution, involve breakdown of individual ions, *e.g.*, $CO_3^{2-} \longrightarrow O^{2-} + CO_2(g)$. The stabilities of such ions are known to be greatly influenced by their immediate environment, especially by the presence of defects of various kinds. Experimental studies of decompositions of solids are, with few exceptions [3], low resolution bulk measurements of changes in mass of a sample, or accumulated pressure of gas evolved from the sample [1]. Such measurements thus average out the individual behaviour at the molecular level. This averaging effect of the experimental technique would thus justify comparison of experimentally measured activation energies with a lattice energy profile. No allowance was made in the calculation of lattice energies for the presence of defects of any kind, so the profiles obtained should correspond to the limit of experimental work on perfect crystalline material.

The structure of the thesis is as follows. The first five chapters provide the theoretical background: general introduction to modelling (*Chapter 1*), modelling lattice energy (*Chapter 2*), determination of interatomic potentials (*Chapter 3*), the computer program: WMIN (*Chapter 4*) and structural information (*Chapter 5*). The computation and discussion of results are divided into two parts: **Part I** (*Chapters 6* and *7*), deals with modelling the decomposition of the peroxides, while **Part II** (*Chapters 8* and *9*), models the decomposition of the carbonates. Conclusions and suggestions for future study are given in *Chapter 10*.

1.2 COMPUTER MODELLING

In the last decade or so, computer modelling has become a powerful means of investigating a diverse range of solid state properties, including structural, thermodynamic, transport and reactivity. In the field of **structure**, emphasis has been placed on modelling the stable or equilibrium structures of complex inorganic compounds, the extent to which real structures differ from idealised models, and the effect of altering the chemical composition on the structure. This last interest has led to research into the important and growing area of disorder in solids and defect studies. Defects (*i.e.*, deviations from perfect periodicity in a crystal), although present in small concentrations, often control transport and thermodynamic properties. Closely related to structural studies are calculations of **cohesive properties**, which allow thermodynamic stability to be predicted, and elastic, dielectric and lattice vibrational properties to be calculated. Another major application is in the study of **atomic transport**, in which dynamic simulations of the system yield information on transport mechanisms. Finally, modelling of **surface structure** has led to great advances in the understanding of surface adsorption and **reactivity** in solids.

The availability of high-speed computers has made computer modelling techniques a **reliable** and **routine** procedure for investigating the properties of both perfect and defective materials. Current trends are shifting, with the emphasis moving from reproduction and illumination to prediction of properties. Thus, computer modelling provides a means for "estimating quantities that are experimentally inaccessible or difficult to obtain" [5]. The field is unique in the way in which, *via* the agency of the computer, it allows fundamental theory to interact with complex experimental problems. The evident power of computational modelling provides considerable incentive for fundamental studies.

In static-lattice techniques, the basic procedure is to evaluate the appropriate energy (for example, the lattice energy in the simulation of ionic crystals) for a given configuration and then to minimize the configuration with respect to all relevant structural variables, *i.e.*, the structural parameters (*e.g.*, cell dimensions and atomic coordinates) are adjusted until a minimum energy configuration is attained. The addition of efficient minimization routines to lattice simulations has made the technique more powerful and reliable, opening up new areas of theoretical solid state research.

Care must be taken in the choice of the minimization method. The simplest minimization method involves a *search* procedure in which the parameter space is scanned until the minimum is located. This method is inefficient and is now rarely used. The second class of methods, known as *gradient* techniques, proceeds *via* numerical iterations. First derivatives, or first and second derivatives, of the energy function with respect to the parameters that are being varied, are used as indicators of the direction in which the minimum lies. Techniques which employ information on the second derivatives are found to be particularly efficient, and the most widely used is the *Newton-Raphson* procedure, which works very well when the model is close to the minimum energy configuration. Alternatively, *quasi-Newton methods*, *i.e.*, the *Fletcher-Powell* algorithm, or the closely related *Broyden-Fletcher-Goldfarb-Shanno* (BFGS) algorithm, perform better far from the minimum. More details on minimization techniques are given in *refs.* [17-20].

1.4 LATTICE ENERGY

The lattice energy of an ionic solid is defined as the energy which has to be supplied to separate one mole of the species from their initial crystal lattice positions to infinite separation (where no interactions occur). The lattice energy, W, is related to the lattice enthalpy, ΔH_L, by the relationship:

$$\Delta H_L = -W + \Delta nRT$$

i.e., lattice energy and enthalpy differ by the amount ΔnRT, where Δn is the change in the number of gaseous molecules, $R = 8.3144\ J\ K^{-1}\ mol^{-1}$ and T is the temperature. Since the crystal lattice energy reflects the magnitude of the cohesive energy in the solid phase, it is important in examining the properties and behaviour of solids [21].

There are two principal aspects to the energy calculation, firstly, developing a model potential, or force field, for the perfect lattice and, secondly, evaluating the parameters of the force field. These two

features are further discussed in: modelling lattice energy (*Chapter 2*) and determination of interatomic potentials (*Chapter 3)*. The basic procedures available for calculating interatomic potential parameters are discussed in *Chapter 3*, while the actual parameters are evaluated in **Parts I** and **II** (*Chapters 6* and *8*) , where the computations for the decomposition of the peroxides and carbonates, respectively, are discussed.

1.5 COMMENT ON TERMINOLOGY

There is some argument about the terms *modelling* and *simulation*. The general view is that a "simulation" attempts to represent the dynamic behaviour of a system and to predict or calculate subsequent events, while "modelling" is used in a more static sense [22]. Throughout the literature, the use of *modelling* and *simulation* overlap, and the terms are often used interchangeably. In this project, the term "modelling" will be used in preference to "simulation", to highlight the fact that the dynamic effects have been disregarded.

2. MODELLING LATTICE ENERGY

2.1 INTERATOMIC POTENTIAL MODELS

2.1.1 Introduction

Several standard models describing solids are now in general use. Ionic solids are best described by the classical Born Model, which defines the solid in terms of ions, with formal or partial charges, interacting via analytical pair potentials. The most general interatomic potential function simulating the total potential energy, *i.e.*, the lattice energy (W), is given by [6]:

$$W = W_o + \sum_{ij} \Psi_{ij}(r_{ij}) + \sum_{ijk} \Psi_{ijk}(r_{ijk}) + \ldots \qquad (2.1)$$

where W_o is the zero-point energy. The summations are over all pairs of ions, *i* and *j*, all trios of ions, *ijk*, and all larger groupings (within a specified cut-off radius) in the crystal. Ψ is a function in terms of r, where r is the distance between atoms. In principle, terms involving larger numbers of ions could be included but, in practice, only the second term in this expansion is considered important for static lattice energy calculations [6-8]. For detailed discussion on lattice energy calculations, see the reviews of Tosi [23] and Waddington [24].

Approximating the lattice energy by the second term in the expansion (*eqn* 2.1), is known as the *pair potential approximation*. It is based on the assumption that ions interact via *long-range* electrostatic forces (due to the point charges, q_i and q_j) and *short-range* interactions (where ϕ_{ij} is an analytic function describing the short-range potential) between the pairs of ions *i* and *j* separated by the distance r_{ij}, as in *eqn* (2.2):

$$W = \sum_{ij} \frac{q_i q_j}{r_{ij}} + \sum_{ij} \phi_{ij}(r_{ij}) \qquad (2.2)$$

long-range short-range

2.1.2 Long-range potential

The sum of the electrostatic (Coulombic) interactions between pairs of ions, *i* and *j*, with point charges, q_i and q_j, separated by a distance, r_{ij}, corresponds to the *Coulombic energy*, W_c. This contribution is the dominant attractive interaction and accounts for about 90% of the total lattice energy [21]. Practical difficulties are encountered with the summation of this term due to slow convergence [23,25], but several methods have been proposed for a more rapid convergence of the series involved. These methods include the use of the reciprocal lattice (Madelung [26], Benson [27]); grouping in the summation (Evjen [28], Frank [29]); and use of the superposition of Gaussian charge densities and point charge repartition (Ewald [30]). The Ewald method, which was later revised and expanded to include $1/r^6$ dispersion interactions is referred to as the *Ewald-Bertaut-Williams summation method* [30-32], and provides rapid convergence by evaluating the Coulombic energy and its derivatives using both real and reciprocal space.

2.1.3 Short-range potential

The short-range interactions include the *repulsive energy*, W_r, due to the overlap of electron clouds of neighbouring ions (illustrated in *Fig 2.1*), and the attractive *van der Waals energy*, W_v, due to dispersive interactions. Dispersive interactions are essentially a polarization phenomenon. Due to the electric field, an instantaneous dipole on each of the interacting species is generated resulting in an attractive, induced dipole-dipole interaction. The contribution of the van der Waals energy to the lattice energy is relatively small, of the order of 1%-2% [33].

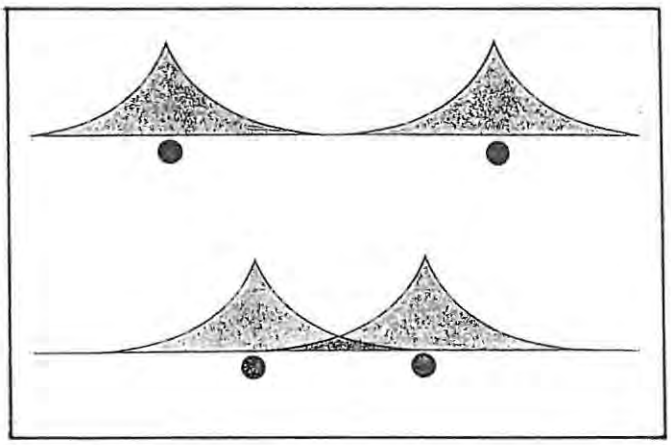

Fig 2.1 Schematic illustration of the overlap of electronic charge distributions as atoms approach. The solid circles denote the nuclei.

The short-range potentials are based on a *pairwise central-force model*, which assumes that the potentials depend only on interatomic distances. This assumption is adequate for ionic systems. The omission of angle-dependent forces and many-body effects results, however, in severe restrictions when applying the

model to covalent systems [7] and, to a lesser extent, to the calculation of elastic and dynamic properties [34] of ionic crystals.

Many analytical functions describing the short-range potential have been proposed; a few typical examples are:

Born potential: $$\phi(r) = \frac{A}{r^n} \qquad (2.3a)$$

Born-Mayer potential: $$\phi(r) = A\, e^{-\frac{r}{\rho}} \qquad (2.3b)$$

Born + v.d.Waals potential: $$\phi(r) = \frac{A}{r^n} - \frac{C}{r^6} \qquad (2.3c)$$

Buckingham potential: $$\phi(r) = A\, e^{-\frac{r}{\rho}} - \frac{C}{r^6} \qquad (2.3d)$$

where A, ρ and C are potential parameters and n is a large integer (10 or 12). The procedures for deriving these parameters are discussed in *Chapter 3*. (Note: The parameter $1/\rho$ is also denoted by B, see *e.g.*, Brink *et al.* [35]).

Sometimes the the Born-Mayer potential, *eqn* (2.3b), is referred to as the exponential or Born-exponential form [33], and potential (d), *eqn* (2.3d), is referred to as the Born-Mayer, exp-6 or Buckingham potential [7,33]. This causes confusion, but the most frequently used names are as shown in *eqns* (2.3a-d).

The "Born" and "Born-Mayer" potentials, *eqn* (2.3a and b), model only the repulsion energy, and no attempt is made to account for the van der Waals forces. These latter forces are normally very weak compared with those acting between electrically charged ions. In a quantitative treatment, however, they should be included. They have been approximated from quantum mechanics by $W_v = -C/r^6$ (a derivation is given in *ref.* 36). The third and fourth expressions, *eqn* (2.3c and d), incorporate both the repulsive and the attractive van der Waals (dispersive) contributions.

Lister [37] tested the above four short-range potentials on a series of alkali metal halides (NaCl, NaBr, NaI, CsCl, CsBr, CsI) and showed that the different expressions generated comparable lattice energies (with small deviations), but that the Buckingham potential yielded the best results (*i.e.*, lattice energies

closest to the observed values) in all cases. Since the Buckingham potential has been the most successful in modelling ionic and semi-ionic materials in numerous studies [38-41], it has become the favoured choice. Hence, the standard potential model used to calculate the lattice energy of perfect, ionic and semi-ionic materials, is

$$W = \sum_{ij} \frac{q_i q_j}{r_{ij}} + \sum_{ij} A_{ij} e^{-\frac{r_{ij}}{\rho_{ij}}} - \sum_{ij} \frac{C_{ij}}{r_{ij}^6} \qquad (2.4)$$

Coulombic repulsion van der Waals

[Notation: (1) The form of the Coulomb interaction has been given in cgs units (q^2/r) but is easily converted to SI units ($q^2/4\pi\epsilon_0 r$), where ϵ_0 is the permittivity of free space. For this conversion, the Coulombic energy, $\Sigma q^2/r$, is multiplied by a factor of 1389.35 in kJ mol^{-1} or 332.07 in kcal mol^{-1}.
(2) The sign convention prescribes a negative energy for electrostatic interactions between oppositely charged ions. Since the Coulombic contribution is predominantly attractive, *i.e.*, negative, the lattice energy is always negative.]

2.2 ALLOWANCE FOR POLARIZATION

2.2.1 Ionic polarizability

The Born model defines the solid in terms of ions, as hard spheres. In solids where the cation is very small and the anion very large, the high charge density of the cation distorts the rather diffuse electron cloud of the anion, as indicated in *Fig 2.2*, and produces in it an induced dipole. This polarization has required a modification of the elementary idea of ions as hard spheres, and has resulted in the development of models based on some representation of ionic polarizability.

The models reviewed below are all *phenomenological models*, being justified largely by the extent to which they can be used to interpret and predict experimental data. These models are based on a spherical representation of the ion. This is in direct opposition to modern quantum theory which shows that the wave function of an electron cannot suddenly drop to zero with increasing distance from the nucleus. In the crystal there is a finite electron density everywhere and, therefore, all treatments of the solid state based on fixed spherical representations are approximations.

Fig 2.2 Diagrammatic representation of ionic polarization in solids with small compact cations and large diffuse anions.

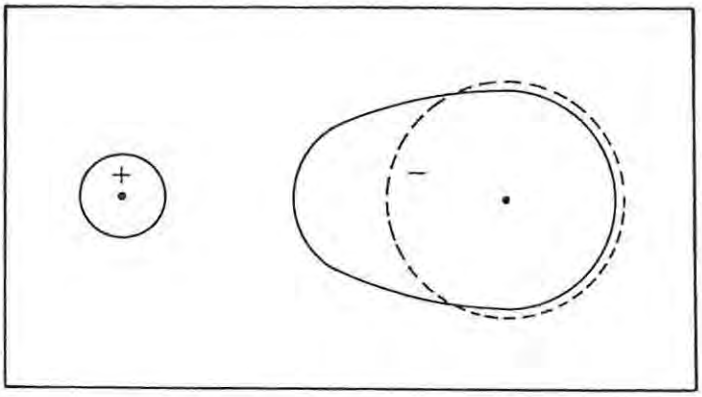

2.2.2 Rigid-ion model

The simplest model is the *rigid ion model* (RIM), which ignores the effects of polarization completely and depicts the ion as a **rigid sphere**, with a point charge concentrated at the atomic nucleus. One effect of ionic polarizability, the dispersion (or van der Waals) energy, can be included implicitly in the short-range interatomic potentials which represent the forces between ions. The model is successful with static lattice simulations of "perfect" ionic material, but it does not provide an adequate description of the dynamic properties of the lattice and fares badly when applied to the calculation of defect energies [7].

2.2.3 Point polarizable ion model

The introduction of an explicit representation of ionic polarizability led to the *point polarizable ion* (PPI) model, proposed by Lyddane and Herzfield [42]. The polarizability was introduced *via* the dipole moment, μ, induced by an electric field, E, *i.e.*,

$$\mu = \alpha E \tag{2.5}$$

where α is the polarizability.

Results were, in general, unsatisfactory. The poor performance was ascribed to the model's fundamental weakness in that it made no allowance for the interdependence of the repulsion forces and ionic polarizability. Since polarization is due to distortions of the valence shell electron distribution by the electric field, short-range repulsion (which arises from overlap of valence shell orbitals on different atoms), is affected by ionic polarizability.

2.2.4 Shell model

The *shell model* (SM), originally developed by Dick and Overhauser [43], is a mechanical model which explicitly accommodates polarization by coupling the ionic polarization to the short-range repulsive forces. The ions are not modelled as single entities but, rather, as consisting of two components: a **core** and a **massless shell**, connected by a harmonic spring, with a force constant, k. Polarization is then generated by the displacement of the shell relative to the core, as illustrated in *Fig 2.3 (b)*. The charge is split between the core and the shell, such that the total charge, $q_t = q_{shell} + q_{core}$. The polarizability is given by

$$\alpha = \frac{q^2_{shell}}{k} \tag{2.6}$$

The short-range forces act only between the shells, while the Coulombic forces act between all cores and shells, except between the core and shell on the same ion. Various attempts have been made to give some physical interpretation to the model, the most common being that the shell represents the valence electrons [44]. This interpretation encountered difficulties when some fitted values of the shell charges turned out to be positive. Harding [8] has suggested that "it is better to consider the shell model simply as a sensible way of coupling the electronic polarization to the ionic distortions".

Fig 2.3 Schematic illustration of the shell model. (a) represents an unpolarized ion, (b) a polarized ion, with the core being displaced by x relative to the shell, and (c) depicts interacting ions separated by a distance, r, and with core displacements of x_1 and x_2. k, k_1, k_2 are harmonic spring force constants.

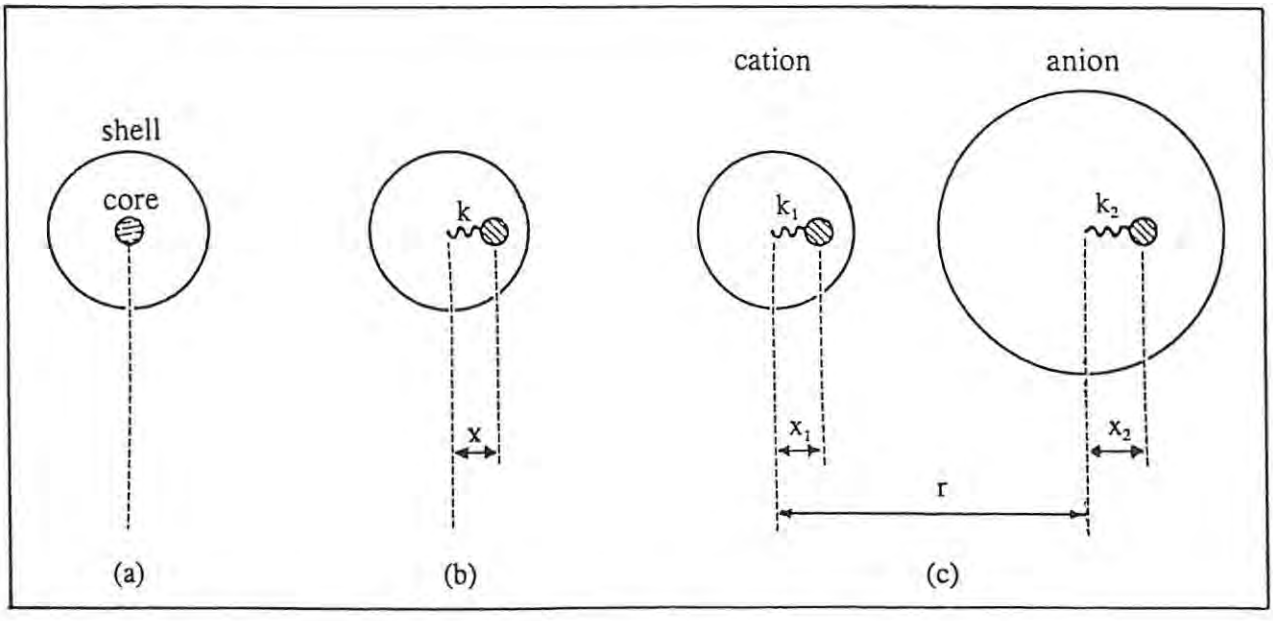

The rigid ion model compares favourably with the shell model when applied to perfect lattices, but fails badly when applied to the calculation of defect energies or dynamic properties. Since no defect calculations or dynamic properties were included in this project, the simpler, rigid ion was selected as a suitable model.

2.3 TREATMENT OF COMPLEX IONS

The rigid ion (point-charge) model has been used successfully to compute lattice energies of simple salts containing spherical ions, *e.g.*, NaCl, CaF_2, CsCl, *etc.* For lattices containing non-spherical complex ions, the simple point charge model performs poorly and has had to be modified. The revised model, the *rigid body model*, described by Busing [45], treats the complex ion as a collection of discrete atoms which are themselves regarded as "point-charged" spheres. The "rigid body" is then assigned the formal charge of the complex, q_f, which is constrained by giving partial charges to the constituent atoms such that

$$nq_i + mq_j = q_f \tag{2.7}$$

where (q_i, q_j) are the partial charges and (n, m) the number of constituent atoms, *i* and *j*. For example, for the carbonate ion (CO_3^{2-}), *eqn* (2.7) would yield

$$q_c + 3q_o = -2 \tag{2.8}$$

where q_c, q_o are the point charges assigned to the carbon and oxygen atoms, respectively, and the 3 specifies the three oxygen atoms in the carbonate ion. The partial charges q_i and q_j are fitted, like the short-range potential parameters, to the structural properties. There is flexibility concerning interatomic interactions within the rigid body, *i.e.*, these may or may not be allowed. If they are not allowed then, for example, no Coulombic or short-range forces between atoms C-O and O-O of the CO_3^{2-} are considered.

More recent work uses models of complex ions which include angle-dependent forces to account for the covalency, thereby ensuring that the potential model is more consistent with the chemical bonding. For example, carbonates typically share chemical bonding features of both ionic and molecular crystals (owing to the strong covalent interactions inside the CO_3^{2-} ion and the presence of the cation, M^{2+}). A model taking into account inter- and intra-molecular interactions in $CaCO_3$ by including two additional potentials (*eqns* (2.9) and (2.10)), has been suggested by Pavese *et al.*[46], *i.e.*, the covalent, directional

bonding in the CO_3^{2-} molecular ion is accounted for by a harmonic angular potential

$$\phi(\theta) = \tfrac{1}{2} k_\theta(\theta - \theta_0)^2 \qquad (2.9)$$

where θ is the actual O-C-O bond angle and θ_0 the equilibrium value. The increase in energy of the CO_3 unit, due to out-of-plane displacements of the C atom, is expressed by

$$\phi(\psi) = k_\psi(1 - \cos 2\psi) \qquad (2.10)$$

where ψ is the torsional angle between the OCO′ and OCO″ planes.

3. DETERMINATION OF INTERATOMIC POTENTIALS

3.1 INTRODUCTION

From *Chapter 2*, *eqn* (2.4), the standard potential model used to calculate the lattice energy for perfect ionic materials is:

$$W = \sum_{ij} \frac{q_i q_j}{r_{ij}} + \sum_{ij} A_{ij} e^{-\frac{r_{ij}}{\rho_{ij}}} - \sum_{ij} \frac{C_{ij}}{r_{ij}^6} \qquad (2.4)$$

Coulombic repulsion van der Waals

where (q_i, q_j) are point charges, r_{ij} are the distances of separation between the pairs of ions *ij* and (A_{ij}, ρ_{ij}, C_{ij}) are the short-range potential parameters.

These interatomic parameters can be evaluated using one of three basic procedures:

(1) *empirical fitting*, where the parameters are fitted directly to known experimental data.

(2) *semi-empirical electron-gas approximation*, where the parameters are determined through fitting the energy surface (obtained from an electron-gas calculation using the Hartree-Fock technique) to experimental data.

(3) *ab initio quantum mechanical calculations*, where the parameters are determined by solving the Schrödinger equation, at some level of approximation, for the system.

3.2 EMPIRICAL FITTING

3.2.1 Optimization

The procedure for fitting potential parameters to experimental data (known as "optimization" of the potentials) involves selecting a set of starting values for the parameters (*i.e.*, A_{ij}, ρ_{ij}, C_{ij}), to compute the lattice energy using an analytical potential function, *eqn* (2.4) above. The potential parameters are then adjusted in a least-squares-fitting routine until the best agreement between calculated and experimental crystal properties is achieved. Crystal properties typically used as observables are crystal structure (cell dimensions and atomic coordinates), relative permittivities and elastic constants, though the elastic properties are often unknown due to the size and the quality of the crystals required to measure

For a small number of materials, phonon dispersion curves may also be available. Experimental lattice energies, determined from the Born-Haber cycle (applying thermochemical data), have also been included by some workers [47], but they are not used extensively due to their variable reliability.

A fundamental difficulty which arises during optimizations is the *multiple-minima problem* [19]. The minimization procedure used only guarantees convergence to the nearest local minimum and not necessarily to the global minimum of the potential energy surface. (*Fig 3.1* illustrates local and global minima for a one-dimensional function). This results in the possible generation of many parameters sets with no assurance of achieving the "best" set, *i.e.*, the perfect fit (see *Fig 3.2*). This is a severe handicap which has prompted extensive research. In the area of conformational-search techniques, suitable algorithms are available for finding all local minima for linear and nonlinear functions of reasonably small problems, *i.e.*, 30 variables or fewer [20]. Also, an optimization procedure, *simulation annealing* [48], which is less suceptible to the local convergence problem, is available.

Fig 3.1 Local and global minima for a one-dimensional function [19].

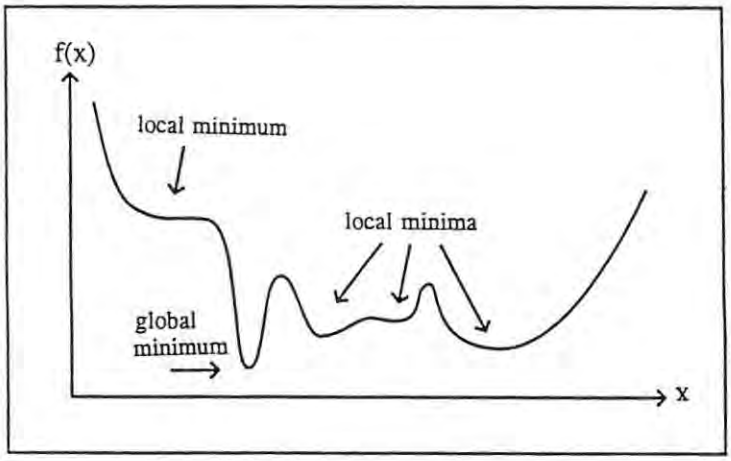

Fig 3.2 schematically illustrates the fitting of the potential energy hypersurface, ϵ, by model potentials ϵ', ϵ'' and ϵ'''. The model potential, obtained by fitting the potential parameters to crystal properties, does not necessarily describe the entire potential energy hypersurface equally well. For example, in *Fig 3.2 (a)*, there is a "perfect fit" of ϵ' for the chosen observations and large deviations from ϵ elsewhere. By increasing the number and quality of crystal properties used as observations in the fitting procedure, the parameters of the potential can be determined with greater certainty. This can be seen in *Fig 3.2 (a)*

and (b), where more observations are used in the fitting of ϵ'', resulting in a better overall fit between ϵ and ϵ'' than is the case for ϵ'. However, since the number of possible observations (which is completely predetermined by the crystal structure/properties) is limited, the probability of determining a model which fits the entire potential hypersurface is small. The hypersurface can, thus, be fitted by a number of distinct models. Two possible models, ϵ' and ϵ''', which fit the hypersurface, ϵ, and its derivatives for the selected observations are shown in *Fig 3.2 (c)*.

Fig 3.2 Schematic illustration of the fitting of a potential energy hypersurface, ϵ, by model potentials ϵ', ϵ'' and ϵ'''. The points marked by vertical lines represent "observations" against which the fitting is measured. Each "observation" is, itself, subject to experimental error. (Diagrams adapted from *ref.* 49).

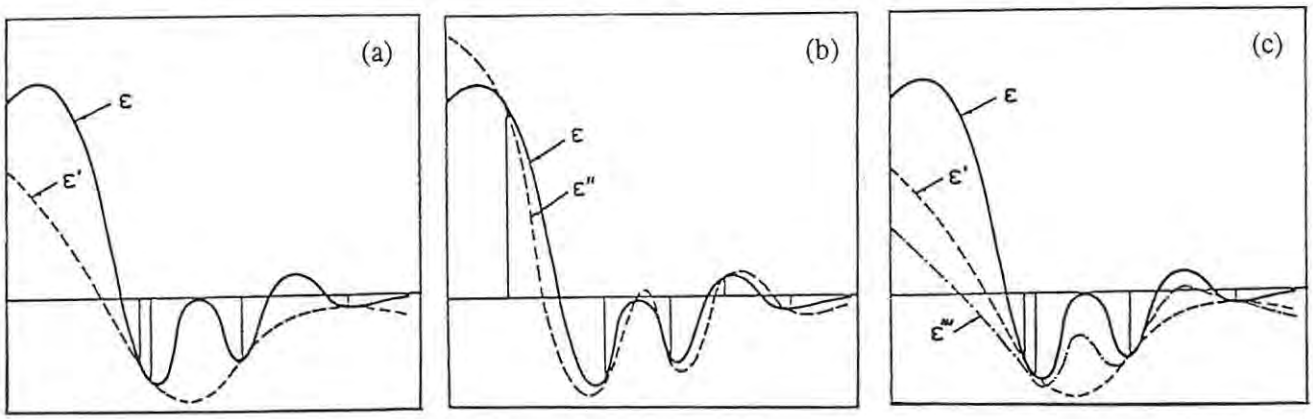

In the optimization or fitting procedure, the potential model is adjusted as a whole, resulting in all energy components becoming mixed after fitting [49]. An important consequence is that, if the Born-Mayer potential, $\phi(r) = Ae^{-r/\rho}$ (*eqn* (2.3b)), which does not include the dispersive energy, is used instead of the Buckingham potential, $\phi(r) = Ae^{-r/\rho} - C/r^6$ (*eqn* (2.3d)), for the short-range potentials, this does not mean that the dispersive component of the interactive energy has been completely neglected. The dispersive interaction will be reflected, at least partially, in the resulting model, even though no explicit term appears in the analytical function. The inclusion of the dispersion term should, however, make the model more flexible and improve the description of the dispersive interaction energy over a range of configurations.

3.2.2 Reliability and transferability of potentials

Interatomic potentials are one of the key factors in determining the reliability of computer modelling studies, hence there have been several studies in recent years where the focus has been on assessing the

reliability and transferability of interatomic potentials (see *e.g.*, reviews by Catlow *et al.* [7], Catlow and Stoneham [50]). The calculation of properties that are not included in the fitting procedure used to derive the potentials provides a useful test of the reliability of the potential parameters [51]. Clearly, the experimental crystal properties used in the optimization must be determined accurately by the fitted model, otherwise a poor fit is implied.

The assumption that a set of potential parameters is transferable from the crystal for which it was derived to another crystal environment, relies on the fact that the environment does not appreciably affect the potentials (*cf.*, second-level model to third-level model below). This is not always the case, since interatomic potentials derived from fitting to the crystal properties contain, at a basic level, inherent physical properties of the atoms involved. In the case where "transferred" potential parameters perform poorly, Catlow *et al.* [40] pointed out that there is no way of determining whether the failure of the transferred parameters is due to the parameters being inappropriate to the changed chemical environment, or to shortcomings in the potential model employed. However, there has been substantial evidence to support the transferability of potential parameters [52,53]. It has also been found that interatomic potentials fitted to multiple lattice models (*i.e.*, where a series of compounds are optimized concurrently) generate parameters that are intrinsically transferable [40].

3.2.3 Potential parameter models

There are three basic "levels of simplicity" used to model the interatomic potentials [49]. In the simplest, first-level model, the potential is assumed to be isotropic and the parameters are assumed to depend only on the **chemical nature** (*i.e.*, on the atomic numbers) of the interacting atoms. In the second-level model, the parameters are assumed to depend also on the **valence state** of the interacting atoms. In the first-level model, for example, the same potential would be assigned to the oxygen atoms in all the alkaline-earth metal oxides and peroxides, while in the second-level model, O^- (oxidation state in the peroxides) would be assigned a different potential to that of O^{2-} (oxidation state in the oxides).

The third-level model goes a step further, and is the most flexible. The potential function is assumed to be anisotropic and the interacting atoms differ not only in their chemical nature and valence state, but also in their **surroundings** in the molecule, *i.e.*, the electron density affects the energy of the atoms. For example, instead of using the same potential for all carbon atoms, one may distinguish between aliphatic and aromatic carbons and treat them as distinct atomic species. The second-level model, where the valence state is taken into consideration, is found to be flexible enough to reproduce the properties of ionic and semi-ionic solids and is used widely thoughout the literature.

As the number of parameters needed to describe the interaction increases, so does the number of observations needed to determine these parameters. Clearly, the fewer the adjustable parameters, the more useful the model. Various combining rules for interactions between different atomic species have been applied to reduce the number of independent parameters. The ones most frequently used are:
(a) *geometric-mean combination rule* for parameters **A** and **C**

$$A_{ij} = \sqrt{A_{ii}\, A_{jj}} \quad , \quad C_{ij} = \sqrt{C_{ii}\, C_{jj}} \tag{3.1}$$

where A_{ij} = parameter **A**, for the interaction between atoms *i* and *j*. Similarly, A_{ii}, A_{jj}, ρ_{ij}, ρ_{ii}, ρ_{jj}, C_{ij}, C_{ii} and C_{jj} are the potentials of interaction between the indicated atoms.
(b) *arithmetic-mean combining rule* for ρ

$$\rho_{ij} = \frac{\rho_{ii} + \rho_{jj}}{2} \tag{3.2}$$

For example, these combining rules could be applied to compounds with mixed oxidation states, *i.e.*, if the parameters for the interactions O^{2-}-O^{2-} and O^{-}-O^{-} were known, then the parameters for the interaction O^{2-}-O^{-} could be calculated using *eqns* (3.1) and (3.2).

3.2.4 Guidelines for the optimization

In general, the number of observations (*i.e.*, experimental crystal properties used in the fitting procedure) must be greater than or equal to the number of variables (*i.e.*, adjustable parameters, A_{ij}, ρ_{ij} and C_{ij}, for each interatomic interaction). If this is not the case, it becomes an under-determined problem or "limited optimization" in that the optimization is constrained to the surface on which the optimization was started. The results of the optimization will not necessarily be faulty, but could result in "over-fitting" on the chosen observations. Going outside that range may yield irrelevant results, *i.e.*, in such a case, the parameter set would not be transferable [49].

The crystal symmetry influences the number of independent observations that are available for the fitting, *i.e.*, the "higher" the symmetry, the fewer the observables. For example, in cubic symmetry (where $a=b=c$ and $\alpha=\beta=\gamma=90°$) only one cell dimension, a, is available as an observation, compared to the "low" symmetry triclinic system, $a\neq b\neq c$ and $\alpha\neq\beta\neq\gamma$, where all six cell dimensions are available. The availability of atomic coordinates as observations depends on whether the atoms are in symmetry-determined positions or not.

To increase the number of observables, two strategies have been adopted in the present work:

(1) The number of crystals with common properties (*e.g.*, MgO, CaO, SrO and BaO) involved in the fitting is increased. This procedure compromises the reliability of the parameters for a particular compound, but enhances the transferability of the parameters among a number of systems [39]. The number of observables increases relative to the number of variables. For example, using the Born-Mayer potential ($\phi(r) = Ae^{-r/\rho}$) in the fitting of one oxide (*e.g.*, CaO, which is cubic and has all atoms in special positions), the ratio of variables (A_{OO}, ρ_{OO}, A_{CaO}, ρ_{CaO}) to observables (a and experimental lattice energy, W_o) is 4:2. When optimizing four oxides concurrently, however, the ratio becomes 10:8 since the variable parameters, A_{OO}, ρ_{OO}, are common to all four oxides (*i.e.*, the variables are A_{OO}, ρ_{OO}, A_{MgO}, ρ_{MgO}, A_{CaO}, ρ_{CaO}, A_{SrO}, ρ_{SrO}, A_{BaO}, ρ_{BaO}, while there are two observables, a and W_o, for each of the four oxides). It can be seen that the number of variables approximately doubles but the number of observables increases by a factor of four.

(2) The crystal structure is relaxed to that of a triclinic system, with no symmetry constraints applied. This is done by entering all the symmetry-generated atoms in the full unit cell and including only the identity symmetry operation. For example, when changing from the cubic (for CaO) to a triclinic system, the observables increase from one to six (or more, if the atomic coordinates are treated as independent).

4. THE COMPUTER PROGRAM: WMIN

4.1 INTRODUCTION

The FORTRAN program WMIN by Busing [45] was used to optimize short-range potentials and perform the energy calculations and minimizations. A copy of the program was obtained from Prof L Glasser of the University of the Witwatersrand, who also provided invaluable guidance on the installation and running of what is a complex and user-unfriendly program.

Of central importance is the energy of the molecule or crystal, and this is always calculated by the function subroutine WCALC. This energy (see *Chapter 2* for lattice energy) is a function of parameters which can be divided into two categories:

(a) the structural parameters, which define the geometrical positions of the atoms in the molecule or crystal

(b) the energy parameters, which are coefficients in the expressions for the potential energy of the model.

The principal purpose of the program is to manipulate either the energy parameters or the structual parameters for one or more substances in a way which depends on the MODE of the calculation. Thus, WMIN may be used for calculating potential energies for systems ranging from ionic crystals to large organic molecules with options for (1) minimizing the energy, (2) optimizing energy parameters, (3) calculating vibrational frequencies and normal modes, and (4) mapping energy as a function of the minimised energy. These options may be selected by setting the indicator called MODE.

4.2 MODES OF OPERATION

Optimization of potential parameters is performed with MODE 0 (which provides a least-squares fitting routine) by adjusting energy parameters using structual parameters and the experimental lattice energy (if it is available) as observations. This procedure converges only when the initial energy parameters (which can be deduced by mapping with MODE -1 or adjusting the structure with MODE 3) are nearly correct. It is the only option for which the observed energy can be used.

Energy minimizations are done with MODE 1, MODE 2, MODE 3 and MODE 5, each using different techniques to adjust structural parameters and rigid-body positions. Corresponding to the modes, these techniques are:

(1) *Newton's method* (using first and second derivatives); (2) *method of steepest descent* (first derivatives); (3) *Rosenbrock search* (using a search technique which requires no derivatives); and (5) *Powell's method* (a variant of the basic coordinate descent scheme which requires no derivatives)*.

MODE 3, unlike the other modes, converges even if the structure is far from the minimum, however, it may be slow to attain final convergence and is generally followed by a re-run using MODE 1. MODE 4 is used to calculate vibration frequencies and MODE -1 is used to map energy as a function of from 1 to 3 parameters.

* Powell's method was introduced into WMIN by Glasser.

4.3 ENERGY CALCULATION

4.3.1 Types of interactions

The energy, calculated by the subroutine WCALC, can be divided into **non-bonded** interactions and interactions between **bonded** atoms. Bonded interactions, which apply to flexible molecules (either isolated or in a crystal), include terms for bond stretching, bond angle deformation and changes in conformation (torsion) angles. The energy terms included in the non-bonded interactions are the Coulomb energy, van der Waals attraction and repulsion terms. These typically apply to intermolecular interactions in crystals, but can also arise due to intramolecular terms for flexible groups in crystals or isolated molecules.

4.3.2 Lattice energy

Lattice energy, W (*Chapter 2, eqn* (2.4)), includes the following interactions.

$$W = \sum_{ij} \frac{q_i q_j}{r_{ij}} + \sum_{ij} A_{ij} e^{-\frac{r_{ij}}{\rho_{ij}}} - \sum_{ij} \frac{C_{ij}}{r_{ij}^6} \qquad (2.4)$$

Coulombic repulsion van der Waals

The *Coulombic energy* is easily calculated using the Ewald-Bertaut-Williams summation method [30-32], which achieves rapid convergence by including terms in reciprocal space. This calculation is built into WMIN, in the subroutine WCALC, and operates by summing all interactions within prescribed radii in the direct and reciprocal lattice of each particle in the asymmetric unit of the crystal.

By contrast, the *repulsive energy* is not as straightforward and several functions have been used to represent this short-range interaction (see *eqns* (2.3a-d). A standard repulsion energy term is built into the program (*eqn* 4.1) of the form suggested by Gilbert [54]:

$$W_r = \sum_{ij} (b_i+b_j)\, e^{\frac{a_i+a_j-r_{ij}}{b_i+b_j}} \qquad (4.1)$$

where a_i and a_j are radii and b_i and b_j are "softness" parameters for atoms *i* and *j*. The program permits considerable flexibility in the form of the potential, by allowing the user to prepare subroutines (in user's function subprograms REPL and GPOT), which define the repulsive term.
The *van der Waals* energy, given by

$$W_v = -\sum_{ij} \frac{C_{ij}}{r^6} \qquad (4.2)$$

is also built into WCALC.

For this project, the short-range energy terms (*i.e., repulsion* and *van der Waals* energy) were combined in the form of the *Buckingham potential* (*eqn* (2.3d)) and programmed into the subroutine GPOT (see *Appendix D*). Optimized interatomic parameters (A_{ij}, ρ_{ij}, C_{ij}) were derived using MODE 0.

4.4 OPTIMIZATION PROCEDURE

4.4.1 Program features

Optimizations are performed in MODE 0, which provides a *least-squares fitting routine*. The program has a number of features which enable the user to modify the course of refinement. These are:

(a) Specification of the parameters which are to be varied in any given cycle.

(b) Damping factors, which reduce the magnitude of the calculated change in the parameters (as selected in (a)), *i.e.*, the step size in the evaluated derivative is reduced giving more reliable local results, but the process is slowed down. Damping is used to control ill-behaved variables.

(c) Implementation of Marquardt's compromise *i.e.*, to approximate the method of steepest descent. The constant for Marquardt's compromise (CMPR) is added to the diagonal elements of the scaled matrix of normal equations. This has the effect of damping an ill-conditioned problem by reducing the contributions of each eigenvector, especially those with small eigenvalues.

4.4.2 Guidelines for the optimization

(1) Good starting values for the energy parameters have to be available for WMIN, otherwise the optimization process diverges rapidly [45].

(2) The optimization will be ineffective if the energy sum has not converged. Each term in the sum (*e.g.*, Coulombic and short-range energy terms) must converge individually. The Coulombic and van der Waals energy are calculated in both direct and reciprocal space within a specified cut-off radius. QLIM and RLIM (radii of convergence in the reciprocal and direct lattices, respectively) should be set to a series of values such that convergence to a chosen criterion (about 0.1 kJ mol^{-1} has been chosen here) can be seen. The convergence affects the reliability and stability of the results. A balance between the computational cost of the lengthier calculations for large values of QLIM and RLIM, and the reliability which needs to be achieved, has to be made.

(3) The measure of convergence of the optimization is the overall discrepancy factor (SDWS or SDWST, see below) which is the sum of the squares of the derivatives of the lattice energy with repect to each parameter, plus the square of the difference between the observed and calculated data. The value of RDWS or RDWST (defined below), which also gauges the "discrepancy" between the fitted and observed data, should fall monotonically, converging to a steady value.
RDWS = SQRT(SDWS) and RDWST = SQRT(SDWST), where SDWS is the discrepancy factor for one substance and SDWST is the discrepancy factor summed over all substances.

4.5 WMIN INPUT DATA FILE

A brief overall description of the input data file is given in *Appendix C.* Complete instructions are available in the WMIN manual [45].

5. STRUCTURAL INFORMATION

5.1 INTRODUCTION

The accuracy of lattice energy calculations depends on the quality of the crystal data used as reference. There are numerous problems associated with the determination of experimental crystal data, especially when only powder data are available, since much information is lost or degraded with the use of an aggregate instead of a single crystal [55,56]. Single crystal X-ray and neutron diffraction generally yield reliable results, but these techniques depend on high quality, single crystals, which are not always available. Since diffraction methods average the information available over a vast number of structural units, crystal impurities (due to sample contamination or deterioration) are not directly detected and further structural inaccuracies result.

A review of the structural data for the alkaline-earth metal (Ca, Sr, Ba) oxides, peroxides and carbonates is given in *Sections 5.2*, *5.3* and *5.4*. For the oxides and the carbonates, data for MgO and $MgCO_3$ are also included, because they were required (to increase the number of observables) in the optimization of the short-range energy parameters. The crystal data (mostly derived from powder data) were obtained from the Inorganic Crystal Structure Database (ICSD) [57]. The criterion to gauge the refinement of the crystal parameters, *i.e.*, the R-value, was not available in most of the studies. Thus, as an alternative measure, the density ratio, D_o/D_c, (where D_c is the density calculated from the crystal structure and D_o is the experimental density) was used as a guide for assessing the accuracy of the crystal data. The calculated density is expected to be slightly (~5%) higher than the experimental density because no allowance is made for crystal defects in D_c. The density calculated from crystal data is given by:

$$D_c = \frac{\text{mass}}{\text{volume}} = \frac{M_r . Z}{V . N_A} \qquad (5.1)$$

where M_r = molar mass, Z = number of formula units per unit cell, V = unit cell volume, and N_A = the Avogadro constant ($6.022\ 045 \times 10^{23}$ mol^{-1}). In general, the volume of the unit cell is:

$$V = abc\sqrt{1 - \cos^2\alpha - \cos^2\beta - \cos^2\gamma + 2\cos\alpha\cos\beta\cos\gamma} \qquad (5.2)$$

where (a, b, c) are the unit cell lengths and (α, β, γ) are the interaxial angles.

For orthogonal axes (cubic, tetragonal, orthorhombic crystal systems), the volume is simplified to:

$$V = abc \tag{5.3}$$

and for rhombohedral axes to:

$$V = a^3 \sqrt{1 - 3\cos^2\alpha + 2\cos^3\alpha} \tag{5.4}$$

5.2 CRYSTAL DATA FOR THE ALKALINE-EARTH METAL OXIDES

The crystal structures of MgO, CaO, SrO and BaO (*Fig 5.1*) belong to the face-centered cubic system (NaCl-type), with unit cell lengths $a=b=c$ and interaxial angles, $\alpha=\beta=\gamma=90°$. The space group in the International Tables for X-ray Crystallography [58] is $Fm\bar{3}m$, #225, with the number of formula units, $Z=4$. The unit cell dimensions and quality factors are listed in *Table 5.1*. The large density discrepancies for SrO and BaO suggest caution in accepting the corresponding lattice constants, a. (The program PLUTO [59] was used to plot all unit cell diagrams; data files for CaO, CaO_2 and $CaCO_3$ (calcite and aragonite) are shown in *Appendix F*).

Fig 5.1 The face-centered cubic unit cells of CaO, SrO and BaO.

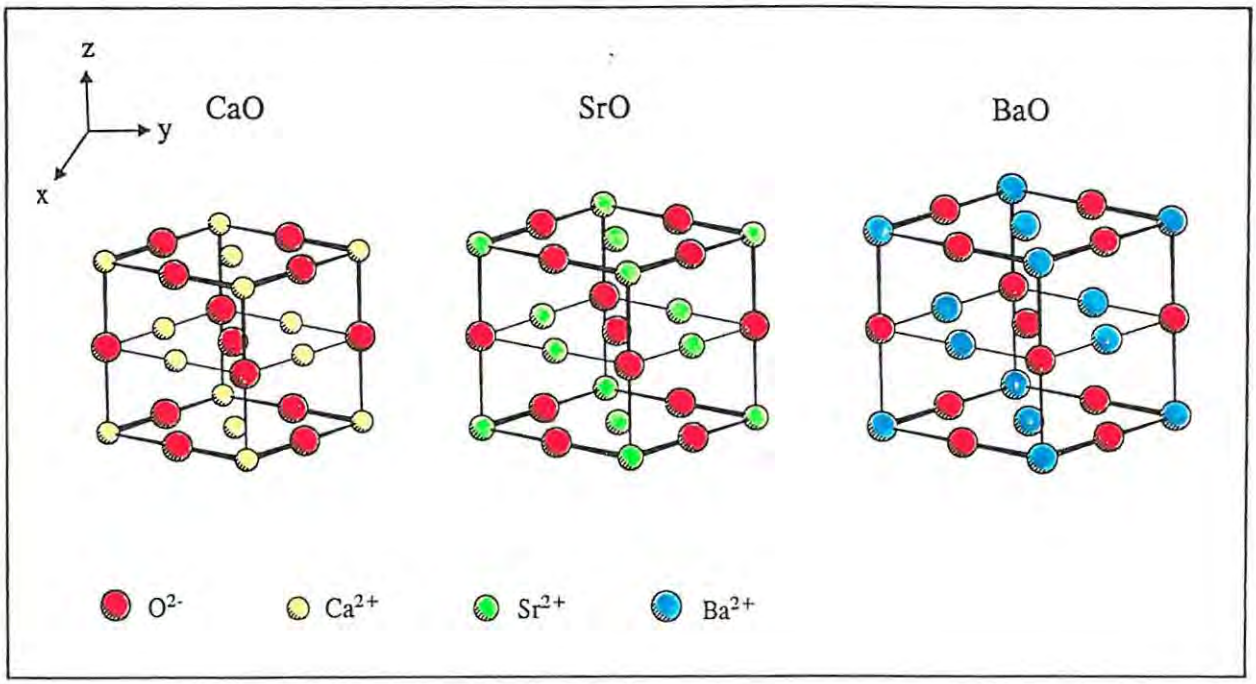

Table 5.1 Crystal data for the cubic alkaline-earth metal oxides: lattice constant (a), number of formula units (Z), unit cell volume (V) and fractional atomic coordinates showing Wyckoff position (Wy) for M=Mg, Ca, Sr and Ba. The density ratio (D_o/D_c), where D_o is the experimental density [60] and D_c the calculated density, is used as a quality factor. D_c is calculated using *eqn* (5.1).

(1) Lattice Dimensions:

		a/Å	Z	V/Å^3	D_o/g cm^{-3}	D_o/D_c
MgO	[61]	4.217	4	74.99	3.58	1.003
CaO	[62]	4.795	4	110.25	3.35	0.991
SrO	[63]	5.1396	4	135.77	4.7	0.921
BaO	[64]	5.496	4	166.01	5.72	0.927

(2) Atomic Fractional Coordinates:

	Wy	MO
M^{2+}	4a	(0, 0, 0)
O^{2-}	4b	(½, ½, ½)

Space group $Fm\bar{3}m$ (#225) has 192 symmetry operations but, since both M^{2+} and O^{2-} are located at positions of high point symmetry (m3m), only four symmetry operations are needed to generate the atoms in the unit cell. Every symmetry operation has a matrix representation consisting of two elements, *i.e.*, a translational vector and a rotational matrix, which permits the analytical calculation of the symmetry related positions (for more information on symmetry operations see *ref.* 65) The four symmetry operations required are:

$$\begin{pmatrix}0\\0\\0\end{pmatrix}+\begin{pmatrix}1&0&0\\0&1&0\\0&0&1\end{pmatrix} \qquad \begin{pmatrix}0\\½\\½\end{pmatrix}+\begin{pmatrix}1&0&0\\0&1&0\\0&0&1\end{pmatrix} \qquad \begin{pmatrix}½\\0\\½\end{pmatrix}+\begin{pmatrix}1&0&0\\0&1&0\\0&0&1\end{pmatrix} \qquad \begin{pmatrix}½\\½\\0\end{pmatrix}+\begin{pmatrix}1&0&0\\0&1&0\\0&0&1\end{pmatrix}$$

The first matrix, the identity operation, is always included although it does not generate any equivalent positions. The subsequent matrices generate atoms at the face centers. The equivalent positions generated are:

M^{2+}	(0,0,0)	(0,½,½)	(½,0,½)	(½,½,0)
O^{2-}	(½,½,½)	(½,0,0)	(0,½,0)	(0,0,½)

For ready comparison of the peroxide and oxide structures, an alternative unit cell for the oxides was constructed. A body-centred tetragonal unit cell of half the volume ($Z=2$) was generated, by rotating the x- and y-axes through 45° about the z-axis (*Fig 5.2 (b)*). The dimensions of the unit cells are related by dividing the lattice constants, a and b, of the cubic face-centred unit cell by a factor of $\sqrt{2}$ to obtain the values for the tetragonal body-centred lattice. The dimension c is the same for both cells, since the body-centred unit cell was derived by rotation about the z-axis.

Fig 5.2 A comparison of the crystal structures of BaO and BaO_2. (a) The conventional, face-centered cubic unit cell of BaO, $Z=4$. (b) The alternative body-centered tetragonal unit cell, $Z=2$. (c) The conventional body-centered, tetragonal BaO_2 unit cell, $Z=2$.

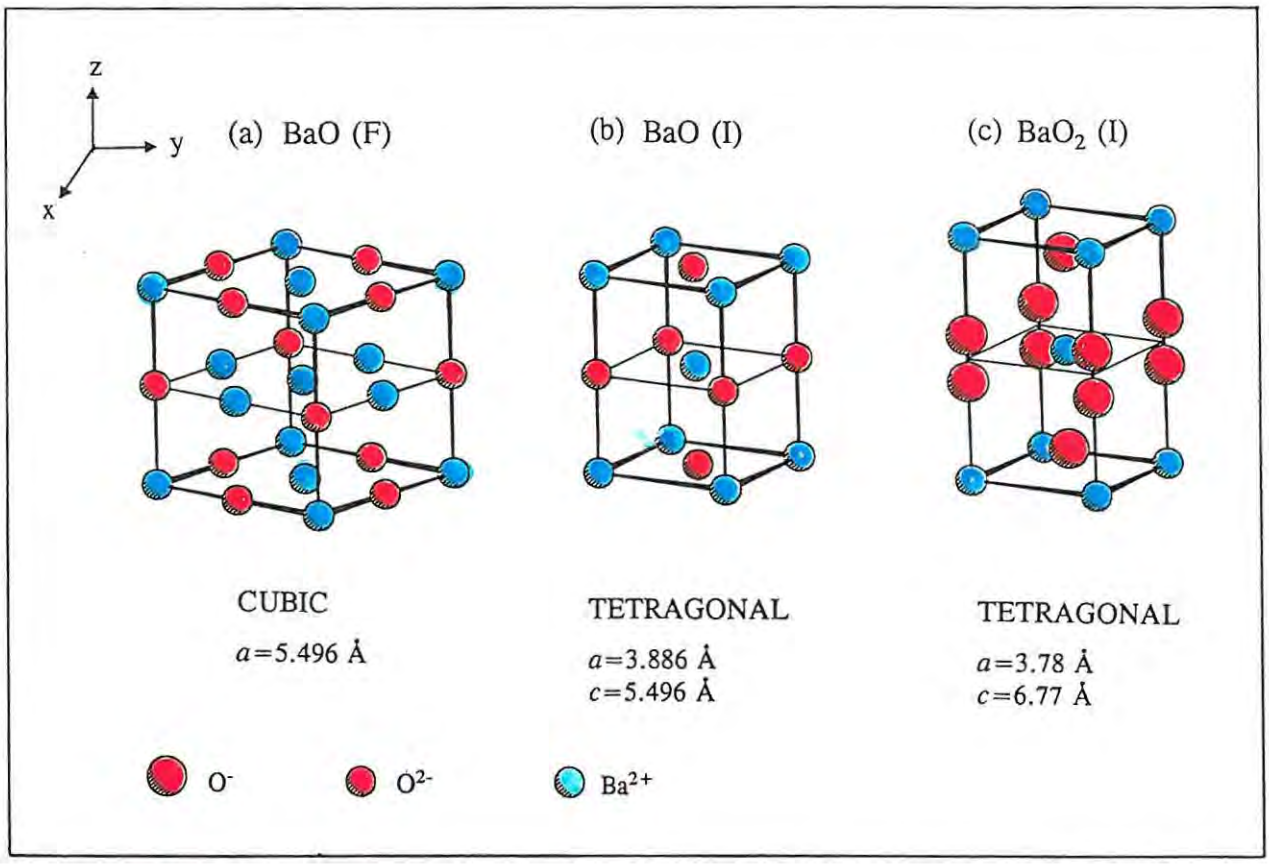

5.3 CRYSTAL DATA FOR THE ALKALINE-EARTH METAL PEROXIDES

The crystal structures of CaO_2, SrO_2 and BaO_2 (*Fig 5.3*) belong to the body-centered tetragonal system (CaC_2-type) with unit cell lengths, $a=b\neq c$ and interaxial angles, $\alpha=\beta=\gamma=90°$. The space group is *I4/mmm*, #139 with $Z=2$.

Fig 5.3 The body-centered tetragonal unit cells of CaO_2, SrO_2 and BaO_2. Lattice parameters are those from *Set A* (see below).

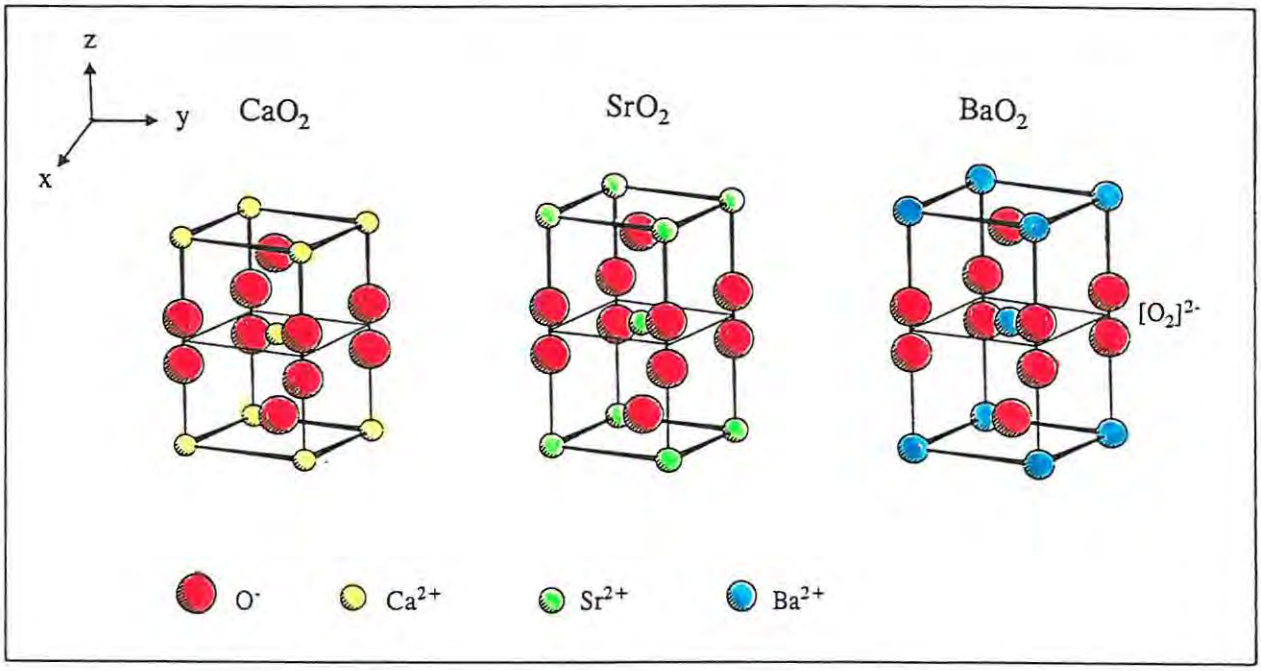

The structural data for SrO_2 and BaO_2 reported by Bernal, *et al.*, [66] in 1935, and for CaO_2 by Kotov and Reichstein [67] in 1941 were used. On examination of these crystal parameters, the peroxide bond length was found be 1.30 Å, 1.35 Å and 1.30 Å for Ca, Sr and Ba peroxide, respectively, which conflicts with the more recently established value of 1.49 Å [68].

Due to the apparent shortness of the $[O\text{-}O]^{2-}$ bond in these early studies on alkaline-earth metal peroxides, the nature of the oxygen-oxygen bond in the peroxide ion has been the subject of repeated investigation. The crystal structures of $CaO_2.8H_2O$, $SrO_2.8H_2O$ and $BaO_2.8H_2O$ were determined by Harr [69] and the values obtained for the O-O separation are given as 1.48 Å, 1.49 Å and 1.48 Å, respectively. In a single crystal study, Abrahams and Kalnajs [70] measured the peroxide bond length in BaO_2 to be 1.49 ± 0.04 Å, while Vannerberg [71] found it to be 1.49 Å in MgO_2.

A possible explanation for the shortness of the $[O\text{-}O]^{2-}$ bond in the early structures came from a study by Brosset and Vannerberg [72]. They found that CaO_2 obtained by the dehydration of $CaO_2.8H_2O$ was not pure. Some of the peroxide ions (O_2^{2-}) were substituted by superoxide ions (O_2^-), oxide ions (O^{2-}) and hydroxide ions (OH^-), with the following approximate composition: Ca^{2+} $(O_2^{2-})_{0.87}$ $(O_2^-)_{0.05}$ $(O^{2-})_{0.11}$ $(H_2O)_{0.10}$. The bond lengths of $[O\text{-}O]^-$ and $[O\text{-}H]^-$ are approximately 1.33 Å and 0.98 Å, respectively. Since X-ray crystallography generates an average structure over the space and time of the diffraction record, the partial substitution of peroxide ions by ions with shorter bond lengths could result in the perceived shortness of the O-O separation in $[O\text{-}O]^{2-}$.

It was decided that, even though the early crystal structures of CaO_2, SrO_2 and BaO_2 are in error, these data (*Set A*) would be used because more accurate crystal data were available only for BaO_2. However, a second set (*Set B*) of structural data was compiled using the BaO_2 data (with O-O = 1.49 Å) measured by Abrahams and Kalnajs [70]. The data for CaO_2 and SrO_2 were then constructed, using the latest reported lattice constants and adjusting the O-O separation to 1.49 Å. All calculations were done using both sets, *i.e.*,

Set A: structures with O-O = ~1.30 Å and

Set B: structures with O-O = 1.49 Å.

All the atoms are in special positions, Wyckoff positions "2a" for M^{2+} and "4e" for O^-, with fractional coordinates (0,0,0) and (0,0,z), respectively. Three symmetry operations, instead of the 32 symmetry operations for space group *I4/mmm*, are needed to generate the atoms in the unit cell, *viz.*,

$$\begin{pmatrix}0\\0\\0\end{pmatrix} + \begin{pmatrix}1&0&0\\0&1&0\\0&0&1\end{pmatrix} \qquad \begin{pmatrix}½\\½\\½\end{pmatrix} + \begin{pmatrix}1&0&0\\0&1&0\\0&0&1\end{pmatrix} \qquad \begin{pmatrix}0\\0\\0\end{pmatrix} + \begin{pmatrix}1&0&0\\0&1&0\\0&0&\bar{1}\end{pmatrix}$$

The equivalent positions for the metal ions are (0,0,0) and (½,½,½). There are two peroxide ions, O_2^{2-}, per unit cell (each containing two O^- ions) with fractional coordinates (0,0,z), (0,0,$\bar{z}$) and (½,½,½+z) (½,½,½-z) respectively. The values of z for both *Sets A* and *B*, are given in *Table 5.2*. An R-value (0.0381) is available only for the BaO_2 structure [70] in *Set B*. The SrO_2 and BaO_2 lattice parameters for *Set B* appear to be reliable since the respective densities (*Table 5.2*) fall within the expected 5% deviation range. The 10.6% deviation for CaO_2, however, indicates inaccuracies in either the lattice constants of CaO_2 or the experimental density, D_o.

Table 5.2 Crystal data for the orthorhombic alkaline-earth metal peroxides: lattice constants (a, c), number of formula units (Z), unit cell volume (V) and fractional atomic coordinates are shown for both *Set A* (structures with O-O=1.30 Å) and *Set B* (structures with O-O=1.49 Å). The density ratio (D_o/D_c), where D_o is the experimental density and D_c the calculated density, is used as a quality factor. D_c is calculated using *eqn* (5.1).

(1) Lattice dimensions:

		a/Å	c/Å	c/a	Z	V/Å^3	D_o/g cm^{-3}	D_o/D_c
Set A:								
CaO_2	[67]	3.54	5.92	1.67	2	74.19	2.92*	0.904
SrO_2	[66]	3.55	6.55	1.85	2	82.55	4.56*	0.948
BaO_2	[66]	3.78	6.77	1.79	2	96.73	5.43*	0.935
Set B:								
CaO_2	[67]	3.54	5.92	1.67	2	74.19	2.92*	0.904
SrO_2	[73]	3.568	6.616	1.85	2	84.23	4.56*	0.966
BaO_2	[70]	3.807	6.841	1.80	2	99.15	5.43*	0.958

(2) Atomic Fractional Coordinates:

	M^{2+}	O^-	O^-	O-O/Å
		(0,0,z)	**(0,0,$\bar{z}$)**	
Set A:				
CaO_2	(0,0,0)	(0, 0, 0.39)	(0, 0, 0.61)	1.30
SrO_2	(0,0,0)	(0, 0, 0.397)	(0, 0, 0.603)	1.35
BaO_2	(0,0,0)	(0, 0, 0.404)	(0, 0, 0.596)	1.30
Set B:				
CaO_2	(0,0,0)	(0, 0, 0.374)	(0, 0, 0.626)	1.49
SrO_2	(0,0,0)	(0, 0, 0.3875)	(0, 0, 0.6125)	1.49
BaO_2	(0,0,0)	(0, 0, 0.3911)	(0, 0, 0.6089)	1.49

* The experimental densities for CaO_2 and SrO_2 are from "The Handbook of Chemistry and Physics" [74] while the value measured by Reichstein and Kazarnovskii [75] is used for BaO_2.

NOTE: Different lattice constants for SrO_2 appear in *Set A* (O-O=1.35 Å) and *Set B* (O-O=1.49 Å), because the more accurate lattice dimensions of *ref.* 73 (no atomic fractional coordiates were given) were used to construct the crystal data of SrO_2 for *Set B* (as described in *Section 5.3*).

For CaO_2 only the positions (*i.e.*, atomic fractional coodinates) of the peroxide ions in the original unit cell were changed to achieve the O-O separation of 1.49 Å in O_2^{2-} for *Set B*. For BaO_2 a completely new set of crystal data was available for *Set B*.

5.4 CRYSTAL DATA FOR THE ALKALINE-EARTH METAL CARBONATES

5.4.1 Introduction

Calcium carbonate crystallizes naturally as calcite, aragonite or vaterite. The two most important polymorphs are calcite (which is the thermodynamically stable phase at atmospheric pressure and room temperature) and aragonite (which is the stable high-pressure phase). Little experimental data is available on the structure and properties of vaterite and the reported structures have been found to be disordered [76,77].

The calcite and aragonite structures are found in a large number of ABO_3 compounds. The choice of structure is determined by the size of the cation. When the cation is small, the calcite structure is favoured, otherwise the aragonite structure is preferred, with the transition taking place at a cation radius of about 0.98 Å [78]. The cation radii and crystal structures for the alkaline-earth metal carbonates [78] are listed in *Table 5.3*. Since the radius of the Ca^{2+} ion is so close to the critical value of 0.98 Å, calcium carbonate occurs in both structures.

Table 5.3 Dependence of structure on cation radius.

Compound	Cation radius/Å	Crystal structure
$MgCO_3$	0.65	calcite
$CaCO_3$	0.99	calcite, aragonite
$SrCO_3$	1.13	aragonite
$BaCO_3$	1.35	aragonite

The ionic arrangements in the two polymorphic structures are very similar (*Fig 5.4*), and only slight alterations to the packing are needed to convert between the calcite structure and the aragonite structure. The CO_3^{2-} group is planar in the calcite structures ($MgCO_3$, $CaCO_3$) and slightly, but significantly, non-planar in the aragonite structures ($CaCO_3$, $SrCO_3$, $BaCO_3$), where the carbon atom lies 0.020 Å out of the plane of the oxygen atoms.

Fig 5.4 Packing diagrams showing the ionic arrangements of $CaCO_3$ in (a) calcite and (b) aragonite. The bond angles and bond lengths in the CO_3^{2-} group are shown.

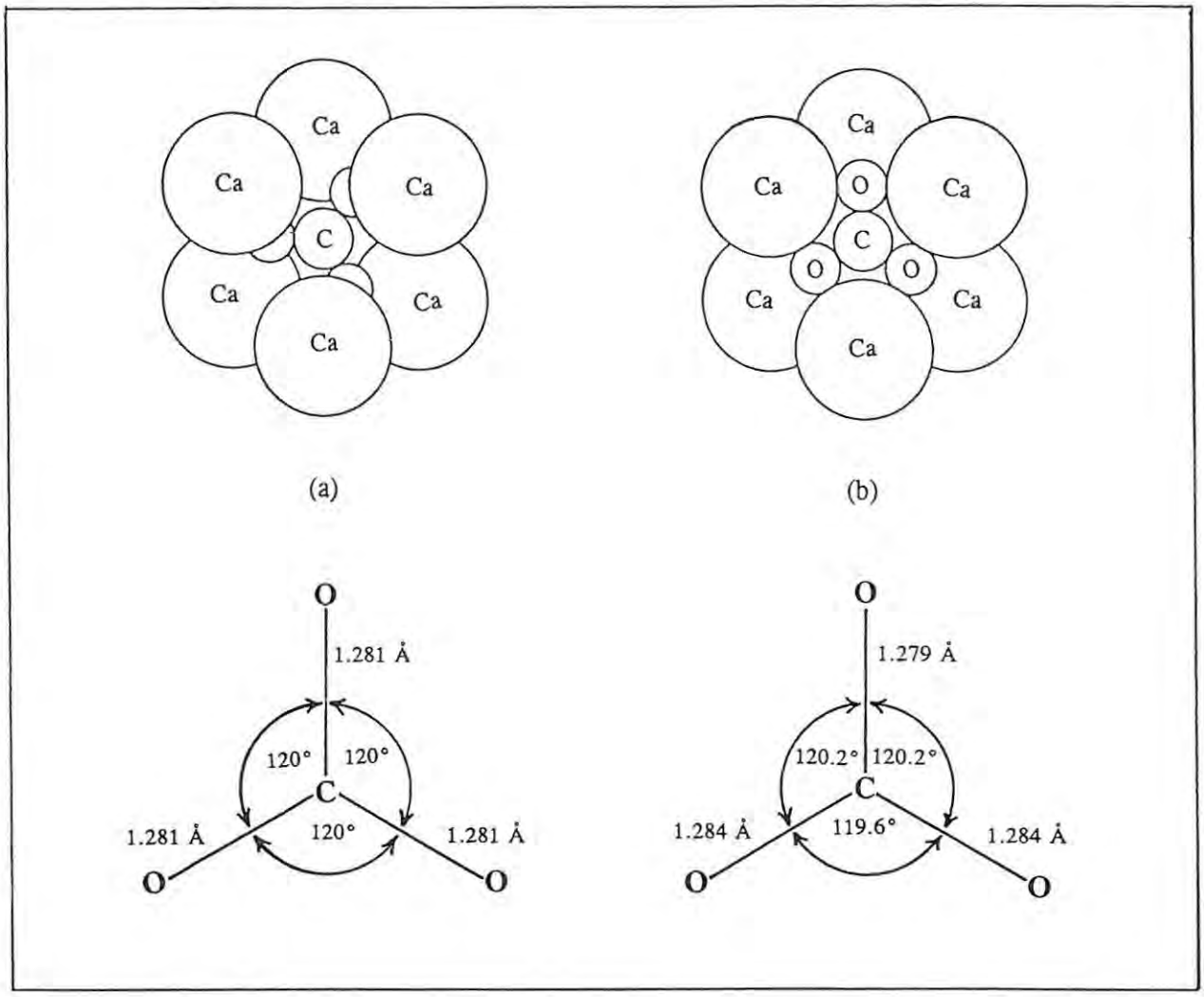

The following discussion of the crystal data of the carbonates is divided into the two isomorphous series, **calcite structures**: $MgCO_3$ (magnesite), $CaCO_3$ (calcite) and **aragonite structures**: $CaCO_3$ (aragonite), $SrCO_3$ (strontianite), $BaCO_3$ (witherite).

5.4.2 Calcite structures

The crystal structures of $MgCO_3$ and $CaCO_3$ belong to the trigonal system, space group $R\bar{3}c$, #167, which can be defined in terms of either hexagonal ($a=b\neq c$ and $\alpha=\beta=90°$, $\gamma=120°$) or rhombohedral ($a=b=c$ and $\alpha=\beta=\gamma$) axes. For comparison with the cubic oxides, the rhombohedral unit cell (which can be considered to be a distorted cubic cell), was preferred. The crystal data for $MgCO_3$ [79] and $CaCO_3$ [79], listed in *Table 5.4*, are recorded in the literature in hexagonal space and had to be transformed to rhombohedral space.

Table 5.4 Crystal data for hexagonal axes of the calcite-structured carbonates, $MgCO_3$ (magnesite) and $CaCO_3$ (calcite).

(1) Lattice Dimensions:

	a/Å	*c*/Å	Z	*V*/Å^3
$MgCO_3$ [79]	4.6328	15.0129	6	279.06
$CaCO_3$ [79]	4.9896	17.0609	6	367.85

(2) Atomic Fractional Coordinates:

	Wy	$MgCO_3$	$CaCO_3$
M	6b	(0, 0, 0)	(0, 0, 0)
C	6a	(0, 0, ¼)	(0, 0, ¼)
O	18e	(0.2774, 0, ¼)	(0.2568, 0, ¼)
R-value		0.02	0.022

The relationship between the hexagonal parameters, (a_{hex}, c_{hex}) and rhombohedral parameters, (a_{rhom}, α_{rhom}), is given by [58]:

$$a_{rhom} = \frac{c_{hex}}{3\sin\theta} \qquad \text{where} \qquad \theta = \tan^{-1}\left(\frac{c_{hex}}{\sqrt{3}\, a_{hex}}\right) \tag{5.5}$$

$$\alpha_{rhom} = \cos^{-1}\left(1 - \frac{a_{hex}^2}{2\, a_{rhom}^2}\right) \tag{5.6}$$

From *eqns* (5.5) and (5.6), the rhombohedral unit cell dimensions were calculated and are listed in *Table 5.5*. The conversion of the Wyckoff positions from hexagonal to rhombohedral axes can be obtained from "International Tables for X-ray Crystallography", Volume 1 [58]. The Wyckoff positions and fractional coordinates for the rhombohedral unit cell are as follows (those for hexagonal unit cell are listed in *Table 5.4*): Mg and Ca are located at "2b", (0,0,0); C at "2a", (¼,¼,¼); O at "6a", (x,½-x,¼). The oxygen position is a function of the x-parameter and, therefore, to calculate x (and hence the oxygen position), the oxygen hexagonal parameter has to be transformed to the corresponding rhombohedral parameter. This transformation depends on the orientation of the rhombohedral axes, which can be orientated in two ways relative to the corresponding hexagonal axes, see *Fig 5.5*. Different terms have been used to define these orientations, *viz.*, *obverse* (also called *positive* or *direct*), and *reverse* (*negative* or *inverse*).

Fig 5.5 (a) *Obverse* and (b) *Reverse* settings of rhombohedron and the corresponding hexagonal non-primitive unit cell [58].

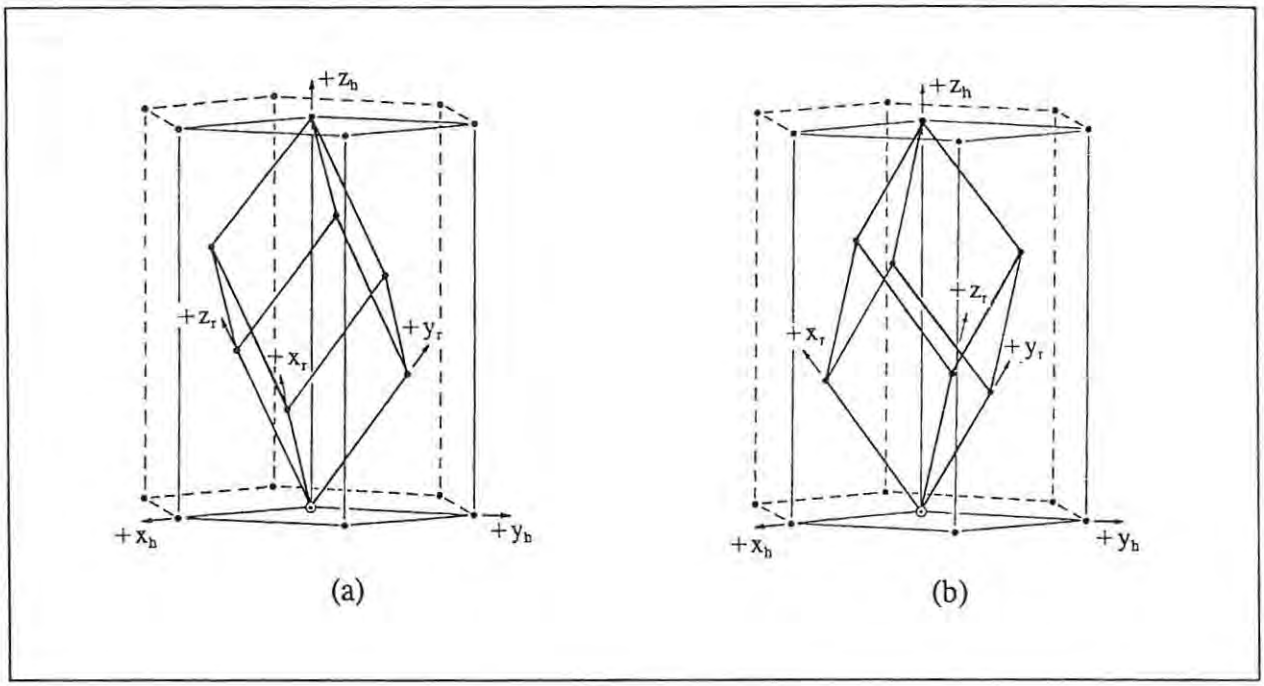

The *obverse* is the standard orientation and the matrix (T), for transforming the hexagonal coordinates to the *obverse* rhombohedral coordinates is:

$$T = \begin{pmatrix} 1 & \bar{1} & 0 \\ 0 & 1 & \bar{1} \\ 1 & 1 & 1 \end{pmatrix} \tag{5.7}$$

The conversion from hexagonal, $(x,y,z)_{hex}$ to rhombohedral, $(x,y,z)_{rhom}$ coordinates is calculated by:

$$T^t \cdot \begin{pmatrix} x \\ y \\ z \end{pmatrix}_{hex} = \begin{pmatrix} x \\ y \\ z \end{pmatrix}_{rhom} \qquad \text{with} \qquad T^t = \begin{pmatrix} 1 & 0 & 1 \\ \bar{1} & 1 & 1 \\ 0 & \bar{1} & 1 \end{pmatrix} \tag{5.8}$$

where T^t is the transpose of the transformation matrix, T.

The hexagonal coordinates in *Table 5.4* are thus transformed to rhombohedral coordinates in *Table 5.5*. These are of the form, (x , ½-x , ¼), required by Wyckoff position "6e", using x = 0.5274 for $MgCO_3$ and x = 0.5068 for $CaCO_3$. *Fig 5.6* shows the rhombohedral unit cells for $CaCO_3$.

Table 5.5 Crystal data for rhombohedral (*obverse*) axes of the calcite-structured carbonates: lattice constants (a, α), number of formula units (Z) and fractional atomic coordinates showing Wychoff positions (Wy). The R-value and density ratio (D_o/D_c), where D_o is the experimental density and D_c the calculated density, are included as quality factors.

(1) Lattice Dimensions:

		a/Å	α/deg	Z	V/Å^3	D_o/g cm^{-3}	D_o/D_c
$MgCO_3$	[79]	5.6751	48.18	2	93.02	2.96	0.983
$CaCO_3$	[79]	6.3750	46.08	2	122.62	2.71	1.000

(2) Atomic Fractional Coordinates:

	Wy	$MgCO_3$	$CaCO_3$
M	2b	(0, 0, 0)	(0, 0, 0)
C	2a	(¼, ¼ ¼)	(¼, ¼, ¼)
O	6e	(0.5274, -0.0274, ¼)	(0.5068, -0.0068, ¼)
R-value		0.02	0.022

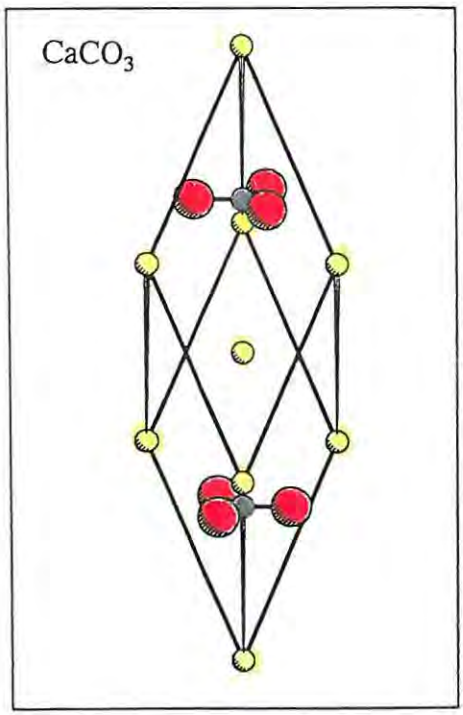

Fig 5.6 The rhombohedral unit cell of $CaCO_3$ (calcite)

Ca^{2+} C^+ O^-

Space group *R3c* has twelve symmetry operations, but only six of these are needed to generate the complete set of atoms for the unit cell. The symmetry operations are:

$$\begin{pmatrix}0\\0\\0\end{pmatrix}+\begin{pmatrix}1&0&0\\0&1&0\\0&0&1\end{pmatrix} \qquad \begin{pmatrix}0\\0\\0\end{pmatrix}+\begin{pmatrix}0&0&1\\1&0&0\\0&1&0\end{pmatrix} \qquad \begin{pmatrix}0\\0\\0\end{pmatrix}+\begin{pmatrix}0&1&0\\0&0&1\\1&0&0\end{pmatrix}$$

$$\begin{pmatrix}½\\½\\½\end{pmatrix}+\begin{pmatrix}0&1&0\\1&0&0\\0&0&1\end{pmatrix} \qquad \begin{pmatrix}½\\½\\½\end{pmatrix}+\begin{pmatrix}0&0&1\\0&1&0\\1&0&0\end{pmatrix} \qquad \begin{pmatrix}½\\½\\½\end{pmatrix}+\begin{pmatrix}1&0&0\\0&0&1\\0&1&0\end{pmatrix}$$

The equivalent positions for the metal and carbon are the same for both magnesium and calcium carbonate, *i.e.*, Mg and Ca have fractional coordinates (0,0,0); (½,½,½) and C, (¼,¼,¼); (¾,¾,¾). There are six equivalent positions (Wyckoff position "6e") for the oxygen, *i.e.*, (x,½-x,¼); (½-x,¼,x); (¼,x,½-x); ($\bar{x}$,½+x,¾); (½+x,¾,$\bar{x}$); (¾,$\bar{x}$,½+x). The six equivalent positions for O are:

$MgCO_3$	$CaCO_3$
(0.5274, -0.0274, 0.2500)	(0.5068, -0.0068, 0.2500)
(-0.0274, 0.2500, 0.5274)	(-0.0068, 0.2500, 0.5068)
(0.2500, 0.5274, -0.0274)	(0.2500, 0.5068, -0.0068)
(-0.5274, 1.0274, 0.7500)	(-0.5068, 1.0068, 0.7500)
(1.0274, 0.7500, -0.5274)	(1.0068, 0.7500, -0.5068)
(0.7500, -0.5274, 1.0274)	(0.7500, -0.5068, 1.0068)

5.4.3 Aragonite structures

The crystal structures of $CaCO_3$, $SrCO_3$ and $BaCO_3$ (*Fig 5.7*) belong to the orthorhombic system, with unit cell lengths, $a \neq b \neq c$ and interaxial angles, $\alpha=\beta=\gamma=90°$. The space group is #62 and is defined in terms of a non-standard setting, *Pmcn* (order of axes is "*bca*"), with a tetramolecular unit cell, $Z=4$. There are six settings of the same unit cell; the standard setting, *Pnma*, has the axes ordered "*abc*".

The crystal data for the three isostructural carbonates were taken from de Villiers [80]. There are two sets of oxygen positions, O(1) and O(2). The former, O(1), as well as the (Ca, Sr or Ba) metal ion and C atom lie in Wyckoff position "4c", with coordinates (¼,y,z). The latter, O(2), is in a general position, (x,y,z), Wyckoff position "8d". The atomic coordinates and cell dimensions as well as quality factors, are given in *Table 5.6*. Both the R-values (range between 0.031 and 0.033) and the density ratio (calculated densities all fall within the 5% error range) indicate that the crystal data are of high quality.

Table 5.6 Crystal data for the orthorhombic aragonite-structured carbonates: lattice constants (a, b, c), number of formula units (Z), unit cell volume (V) and fractional atomic coordinates showing Wychoff positions (Wy). The R-value and density ratio (D_o/D_c), where D_o is the experimental density [60] and D_c the calculated density, are included as quality factors.

(1) Lattice dimensions:

	a/Å	b/Å	c/Å	Z	V/Å^3	D_o/g cm^{-3}	D_o/D_c
$CaCO_3$ [80]	4.9614	7.9671	5.7404	4	226.91	2.93	1.000
$SrCO_3$ [80]	5.090	8.358	5.997	4	254.97	3.70	0.961
$BaCO3$ [80]	5.3126	8.8958	6.4284	4	303.81	4.43	1.027

(2) Atomic Fractional Coordinates:

	Atom	Wy	Fractional coordinates	R-value
CaCO3:	Ca	4c	(0.2500 0.4150 0.7597)	0.031
(aragonite)	C	4c	(0.2500 0.7622 -0.0862)	
	O(1)	4c	(0.2500 0.9225 -0.0962)	
	O(2)	8d	(0.4736 0.6810 -0.0862)	
$SrCO_3$:	Sr	4c	(0.2500 0.4160 0.7569)	0.031
(strontianite)	C	4c	(0.2500 0.7601 -0.0864)	
	O(1)	4c	(0.2500 0.9119 -0.0946)	
	O(2)	8d	(0.4694 0.6821 -0.0839)	
$BaCO_3$	Ba	4c	(0.2500 0.4163 0.7549)	0.033
(witherite)	C	4c	(0.2500 0.7570 -0.0810)	
	O(1)	4c	(0.2500 0.9011 -0.0878)	
	O(2)	8d	(0.4595 0.6839 -0.0790)	

Since O(2) lies in a general position, all the eight symmetry operations of space group *Pmcn* are needed to generate the atoms in the unit cell. The symmetry operations are,

$$\begin{pmatrix}0\\0\\0\end{pmatrix}+\begin{pmatrix}1&0&0\\0&1&0\\0&0&1\end{pmatrix} \quad \begin{pmatrix}\tfrac{1}{2}\\\tfrac{1}{2}\\\tfrac{1}{2}\end{pmatrix}+\begin{pmatrix}1&0&0\\0&\bar{1}&0\\0&0&\bar{1}\end{pmatrix} \quad \begin{pmatrix}0\\\tfrac{1}{2}\\0\end{pmatrix}+\begin{pmatrix}\bar{1}&0&0\\0&1&0\\0&0&\bar{1}\end{pmatrix} \quad \begin{pmatrix}\tfrac{1}{2}\\0\\\tfrac{1}{2}\end{pmatrix}+\begin{pmatrix}\bar{1}&0&0\\0&\bar{1}&0\\0&0&1\end{pmatrix}$$

$$\begin{pmatrix}0\\0\\0\end{pmatrix}+\begin{pmatrix}\bar{1}&0&0\\0&\bar{1}&0\\0&0&\bar{1}\end{pmatrix} \quad \begin{pmatrix}\tfrac{1}{2}\\\tfrac{1}{2}\\\tfrac{1}{2}\end{pmatrix}+\begin{pmatrix}\bar{1}&0&0\\0&1&0\\0&0&1\end{pmatrix} \quad \begin{pmatrix}0\\\tfrac{1}{2}\\0\end{pmatrix}+\begin{pmatrix}1&0&0\\0&\bar{1}&0\\0&0&1\end{pmatrix} \quad \begin{pmatrix}\tfrac{1}{2}\\0\\\tfrac{1}{2}\end{pmatrix}+\begin{pmatrix}1&0&0\\0&1&0\\0&0&\bar{1}\end{pmatrix}$$

The equivalent positions for:

(a) the metal ion (Ca, Sr or Ba), C and O(1) are: $(\frac{1}{4},y,z)$; $(\frac{3}{4},\bar{y},\bar{z})$; $(\frac{3}{4},\frac{1}{2}+y,\frac{1}{2}-z)$; $(\frac{1}{4},\frac{1}{2}-y,\frac{1}{2}-z)$

(b) O(2) are: (x,y,z); $(\bar{x},\bar{y},\bar{z})$; $(\frac{1}{2}-x,\frac{1}{2}-y,\frac{1}{2}+z)$; $(\frac{1}{2}+x,\frac{1}{2}+y,\frac{1}{2}-z)$; $(\frac{1}{2}+x,\bar{y},\bar{z})$; $(\frac{1}{2}-x,y,z)$; $(\bar{x},\frac{1}{2}+y,\frac{1}{2}-z)$; $(x,\frac{1}{2}-y,\frac{1}{2}+z)$

(The atomic fractional coordinates are shown in *Appendix B*)

Fig 5.7 The orthorhombic unit cells of $CaCO_3$ (aragonite), $SrCO_3$ (strontianite) and $BaCO_3$ (witherite).

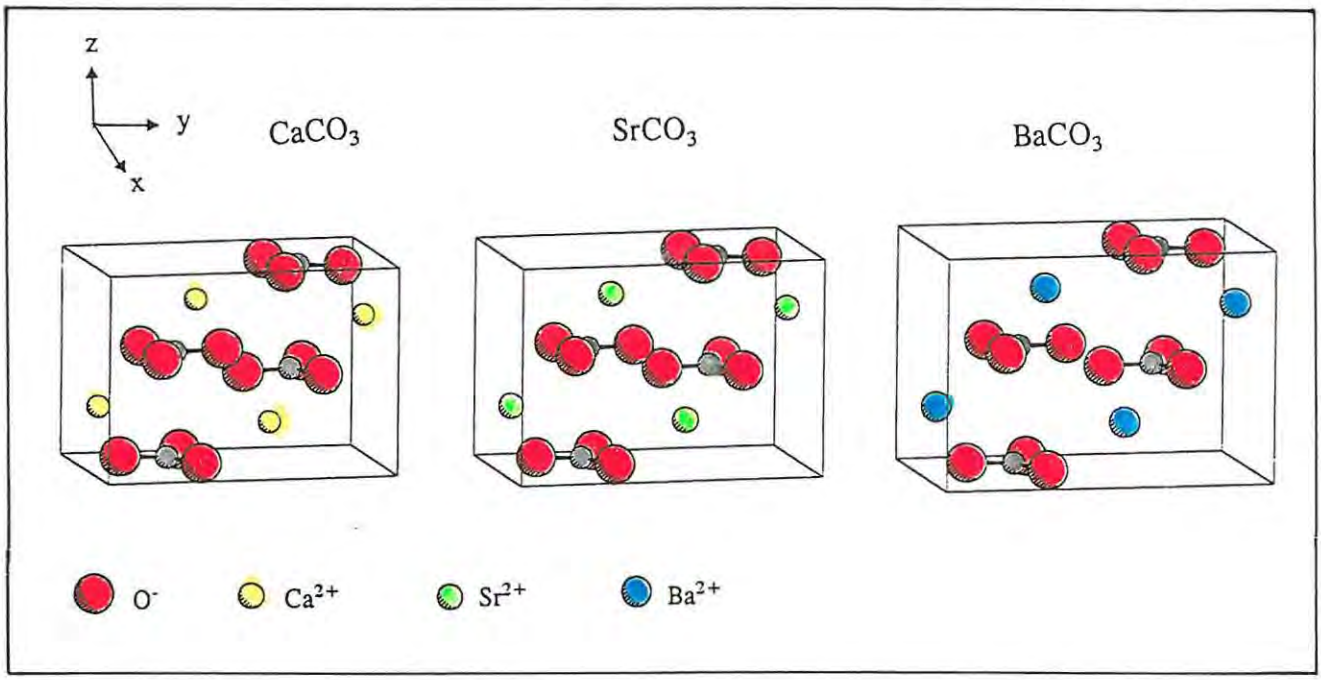

Fig 5.8 The orthorhombic unit cell (showing half the number of atoms) of $CaCO_3$. (a) unshaded white atoms are in the plane $x=\frac{3}{4}$ and (b) black shaded atoms are in the plane $x=\frac{1}{4}$. Atom types are indicated in *Fig 5.7*.

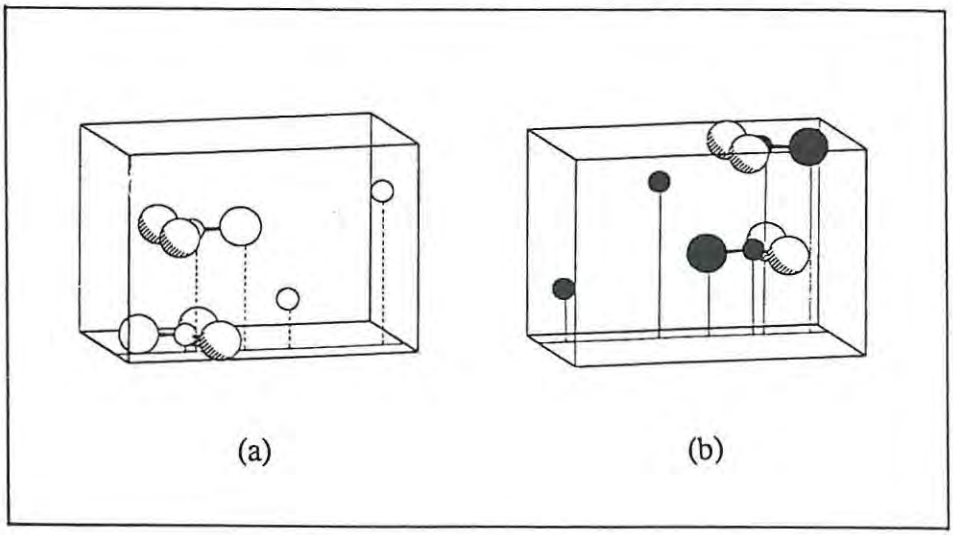

PART 1

Modelling the thermal decomposition of alkaline-earth metal peroxides to oxides

$$MO_2 \longrightarrow MO + \tfrac{1}{2}O_2$$

6. COMPUTATIONAL PROCEDURES

6.1 INTRODUCTION

To investigate the changes in lattice energy during the thermal decomposition of alkaline-earth metal peroxides to their respective solid oxides and gaseous O_2, *i.e.*,

$$MO_2(s) \longrightarrow MO(s) + \tfrac{1}{2}O_2(g)$$

symmetry-controlled routes were devised for transforming the reactant structure into the solid product structure. These routes, regarded as possible solid state reaction pathways, provide the crystal structures for which lattice energies at various stages of the transformation can be calculated. Energy barriers in these proposed decomposition routes can then be compared with experimentally determined activation energies.

Lattice energies were calculated using the standard potential model (*eqn 2.4*) as described in *Chapter 2*

$$W = \sum_{ij} \frac{q_i q_j}{r_{ij}} + \sum_{ij} A_{ij} e^{-\frac{r_{ij}}{\rho_{ij}}} - \sum_{ij} \frac{C_{ij}}{r_{ij}^6}$$

and energy minimizations were performed for all known structures. To use the potential function above, the variable short-range interatomic potential parameters (A_{ij}, ρ_{ij}, C_{ij}) had first to be determined. Literature values for the parameters are available for the oxides (MgO, CaO, SrO, BaO) [40,81,82] but not for the peroxides. The available parameters, however, were not used directly since different models were used in deriving them, *i.e.*, ionic polarisation was treated by the shell model in *refs.* [40,81] and in *ref.* [82] the parameters were derived from a fit to Hartree-Fock calculations.

6.2 OPTIMIZATION OF SHORT-RANGE PARAMETERS

6.2.1 Assumptions

The following assumptions (proposed by Catlow, *et al.*,[82] and by Sangster and Stoneham [81]) were used in obtaining the short-range potentials:

(a) the oxygen-oxygen interactions were taken to be the same in all the crystals where the oxidation

states are equivalent, *i.e.*, O^{2-}- O^{2-} in the oxides and O^-- O^- in the peroxides. This interaction is represented by the Buckingham potential $\phi(r) = Ae^{-r/\rho} - C/r^6$ (*eqn 2.3d*).

(b) cation-cation interactions were assumed to be purely Coulombic. Modified electron gas calculations [83] indicate that, for the separation distances normally encountered in crystals, short-range cation-cation (which are second neighbours) interactions are insignificant and can be ignored.

(c) the anion-cation interactions were represented by the Born-Mayer potential $\phi(r) = Ae^{-r/\rho}$ (*eqn 2.3b*), *i.e.*, the attractive r^{-6} term was ignored. The small contribution of such terms to the short-range potential is incorporated by small modifications of the Born-Mayer parameters (A_{ij} and ρ_{ij}) [49].

6.2.2 Computational procedure

The optimization of the energy parameters was performed using WMIN, MODE 1. The stages in the process of finding optimized energy parameters are outlined below:

I. Oxides

The initial optimization of the energy parameters for Mg, Ca, Sr and Ba oxides was done with reference to the crystal structures (*Table 5.1*) and lattice energies calculated by Huggins and Sakamoto [84] (*Table 6.5*). Of all the parameters available, the lattice constants are the best determined. Thus, even when other structural properties (*e.g.*, elastic constants) are used in fitting, the weighting is often strongly biased towards the lattice parameters at the expense of the other structural properties (see *e.g.*, Bush, *et al.* [40]). As starting values for A_{ij}, ρ_{ij} and C_{ij}, those reported by Sangster and Stoneham [81] (listed in *Table 6.1*) were used. The calculations were performed with radii of summation of 14 Å in the direct lattice and 0.7 Å in the reciprocal lattice.

This was a "limited" optimization, since for this set of cubic oxides there were 11 variables ($A_{O\text{-}O}$, $A_{Mg\text{-}O}$, $A_{Ca\text{-}O}$, $A_{Sr\text{-}O}$, $A_{Ba\text{-}O}$, $\rho_{O\text{-}O}$, $\rho_{Mg\text{-}O}$, $\rho_{Ca\text{-}O}$, $\rho_{Sr\text{-}O}$, $\rho_{Ba\text{-}O}$ and $C_{O\text{-}O}$, where the subscripts indicate the interaction between the two atoms listed) but only 8 observables (4 unit cell lengths, one from each oxide, plus 4 lattice energies). Considerable difficulty was experienced with the optimization. To stabilise the process, one set of potential parameters was varied at a time, starting with the Ba parameters ($A_{Ba\text{-}O}$, $\rho_{Ba\text{-}O}$) and then adding, consecutively, those of Sr, Ca, Mg, the last added being the O-O parameters ($A_{O\text{-}O}$, $\rho_{O\text{-}O}$, $C_{O\text{-}O}$). In this way, the optimized set of parameters, OPT1, shown in *Table 6.1*, was obtained. The "fitting" factor, RDWST = 0.02, pointed to an extremely good fit for the chosen observables but, since there were fewer observables than variables, it could indicate "over-fitting". Because of possible problems with the transferability of the parameters, a second optimization was performed, where the cubic oxide structures were relaxed to those of the triclinic system, *i.e.*, all

the

symmetry constraints were removed, thus allowing all the cell dimensions to be used as independent observables.

Since experimental lattice energies determined from the thermochemical Born-Harber cycle are of "variable reliability" [74] (and there are considerable discrepancies in reported energies), calculated lattice energies should be more reliable if they are determined from optimized parameters in which the experimental lattice energy is not used in the fitting. Bush, *et al.*, [40] and Sangster and Stoneham [81] did not include the lattice energies. It was thus decided to omit the "known" lattice energy as an observation and to use it only for comparison with calculated values. There were still 11 variables, but the number of observables was increased from 8 to 24 (6 cell dimensions, a, b, c, α, β, γ, for each of the 4 oxides). The starting parameter values were those used previously, and the necessary changes to the input file were made to account for the removal of all symmetry constraints.

The values converged rapidly, needing only about 40 cycles. The second parameter set, OPT2, also shown in *Table 6.1*, followed the same trend as that followed by the set reported by Sangster and Stoneham [81], *i.e.*, the A_{ij} values (for the M^{2+}- O^{2-} interactions) decreased as the cation size increased. Parameter set OPT2 was used for modelling the decomposition. Differences between the optimized parameters reported [81] and those calculated using WMIN were expected, since Sangster and Stoneham used the shell model [43] to treat ionic polarization, while the rigid ion model was used in this investigation. The value of RDWST = 0.1452×10^{-5} was even better than in the first optimization, *i.e.*, RDWST = 0.01981. Since "sufficient" observables (more than the number of variables) were used in the fitting, the excellent fit could be due to the very symmetrical nature of the oxides.

Table 6.1 Optimized short-range parameters (A_{ij}, ρ_{ij} and C_{ij}) for each ion in the oxides. Values in column 2 are those reported by Sangster and Stoneham (SS) [81] and in columns 3 and 4 are values optimized using WMIN.

Parameters	SS	OPT1 cubic	OPT2 symmetry-released
A_{ij} /kJ mol^{-1}			
O-O	219.64130×10^4	121.84850×10^4	803.80900×10^4
Mg-O	12.30377×10^4	3.34116×10^4	12.13607×10^4
Ca-O	11.37848×10^4	5.47833×10^4	11.17443×10^4
Sr-O	9.16704×10^4	7.09582×10^4	8.97697×10^4
Ba-O	7.54609×10^4	8.51326×10^4	7.56742×10^4
ρ_{ij} /Å			
O-O	0.1490	0.0173	0.1733
Mg-O	0.3012	0.3824	0.3004
Ca-O	0.3401	0.3837	0.3391
Sr-O	0.3736	0.3875	0.3722
Ba-O	0.4084	0.3971	0.4049
C_{ij} /kJ mol^{-1} Å^6			
O-O	19.6540×10^2	19.5384×10^2	20.4964×10^2
RDWST	—	0.01981	0.1452×10^{-5}

The optimized parameter sets, OPT1 and OPT2, were then used in the calculation and minimization (by allowing the structure to relax) of the lattice energies for the oxides. The initial symmetry constraints of the cubic space group $Fm\bar{3}m$ were reinstated since there were slight deviations from the cubic structure with the removal of all symmetry constraints (*e.g.*, the lattice constants for the symmetry released BaO were $\alpha=\beta=5.490$ Å, $\gamma=5.489$ compared to the experimental cubic values of $\alpha=\beta=\gamma=5.490$ Å. All the angles remained 90°). From the results, shown in *Tables 6.2* and *6.3* (for OPT1 and OPT2, respectively), it can be seen that the lattice parameters and cell volume are reproduced with errors of the order of 0.5% The parameter set, OPT1 (in which the lattice energies were used as observables) yielded lattice energies closer to the observed values, *i.e.*, with errors of at most 0.03%, while the lattice energies calculated with parameter set OPT2 (in which lattice energies were excluded from the fitting) compared well with recently reported values, *i.e.*, values generally fell between those calculated by Sangster and Stoneham [81] and Bush, *et al.*, [40] (see *Tables 6.3* and *6.5*).

Table 6.2 Cell dimension (a), cell volume (V) and lattice energy (W) for fitted alkaline-earth metal oxides, using parameters OPT1.

		a/Å	V/Å^3	W/kJ mol^{-1}
MgO	expt.	4.2123	74.74	-3795*
	calc.	4.2059	74.40	-3795
	% error	0.15	0.45	0.00
CaO	expt.	4.795	110.25	-3414*
	calc.	4.789	109.83	-3415
	% error	0.15	0.45	-0.03
SrO	expt.	5.1396	135.76	-3217*
	calc.	5.1346	135.37	-3218
	% error	0.10	0.27	-0.03
BaO	expt.	5.496	166.01	-3029*
	calc.	5.493	165.74	-3029
	% error	0.06	0.16	0.00

*Lattice energies reported by Huggins and Sakamoto [84].

Table 6.3 Cell dimension (a), cell volume (V) and lattice energy (W) for fitted alkaline-earth metal oxides, using parameters OPT2.

		a/Å	V/Å^3	W/kJ mol^{-1}	W/kJ mol^{-1}
MgO	expt.	4.2123	74.74	-3956*	-3955**
	calc.	4.2059	74.40	-3968	-3968
	% error	0.15	0.45	-0.3	-0.3
CaO	expt.	4.795	110.25	-3473*	-3509**
	calc.	4.791	109.97	-3486	-3486
	% error	0.08	0.25	-0.4	0.7
SrO	expt.	5.1396	135.76	-3223*	-3281**
	calc.	5.1328	135.23	-3240	-3240
	% error	0.13	0.39	-0.5	1.2
BaO	expt.	5.496	166.01	-3001*	-3132**
	calc.	5.490	165.47	-3020	-3020
	% error	0.11	0.33	-0.6	3.6

*Lattice energies reported by Sangster and Stoneham [81].
**Lattice energies reported by Bush, *et al.* [40]

NOTE: The lattice energies calculated by Huggins and Sakamoto [84] were used as observables in the optimization of OPT1 and thus these energies appear as "experimental energies" in *Table 6.2*. In *Table 6.3*, the energies calculated using parameters OPT2 are compared to more recent values, *i.e.*, those reported by Sangster and Stoneham [81] and Bush, *et al.* [40].

Finally, using parameters OPT2, the contributions of the long-range Coulombic energy and the short-range (repulsive and dispersive energy, calculated by the Buckingham potential) energy terms, to the total lattice energy were examined. It was found that the $W_{r,v}/W_c$ ratio is consistent (*cf.* to the peroxides) and that the short-range component is, on average, 14.7% of the Coulombic energy (see *Table 6.4*).

Table 6.4 Contributions to the lattice energies of the alkaline-earth metal oxides, according to WMIN,using OPT2 parameter set.
W= total lattice energy. W_c= Coulombic energy and $W_{r,v}$= short-range energy (repulsion plus van der Waals energy calculated from the Buckingham potential).

	W_c /kJ mol^{-1}	$W_{r,v}$ /kJ mol^{-1}	$W_{r,v}/W_c$ %	W /kJ mol^{-1}
MgO	-4168	650	15.6	-3968
CaO	-4054	568	14.0	-3486
SrO	-3784	544	14.4	-3240
BaO	-3538	517	14.6	-3021

Table 6.5 A comparison of the lattice energies (kJ mol^{-1}) reported for the alkaline-earth metal oxides.

Reference	MgO	CaO	SrO	BaO
Kapust. eqn.	-3865	-3489	-3250	-3088
Therm. cycle	-3791	-3401	-3223	-3054
1957: HS	-3795	-3414	-3217	-3029
1980: SS	-3956	-3473	-3223	-3001
1993: B	-3955	-3509	-3281	-3132
1995: WMIN (OPT2)	-3968	-3486	-3240	-3021

Kapust. eqn. = Kapustinskii equation [85] (see *Appendix A)*
Therm. cycle = experimental lattice energy determined from the thermochemical cycle [74].
HS = Huggins and Sakamoto [84]
SS = Sangster and Stoneham [81]
B = Bush, *et al.* [40]
WMIN (OPT2) = lattice energies calculate using optimized parameter set, OPT2

II. Peroxides

The optimization of the energy parameters for Ca, Sr and Ba peroxides was done with reference to the two sets of crystal structures as defined in *Section 5.3*, *i.e.*, *Set A*: structural data with peroxide bond length O-O= ~1.30 Å, and *Set B*: O-O=1.49 Å, given in *Table 5.2*. All symmetry constraints were removed from the tetragonal system (*I4/mmm*) and the structures were entered as triclinic, with only the identity operation. This allowed all six cell dimensions to be used as observables. For the three peroxides, there were 9 variables ($A_{O\text{-}O}$, $A_{Ca\text{-}O}$, $A_{Sr\text{-}O}$, $A_{Ba\text{-}O}$, $\rho_{O\text{-}O}$, $\rho_{Ca\text{-}O}$, $\rho_{Sr\text{-}O}$, $\rho_{Ba\text{-}O}$ and $C_{O\text{-}O}$) and 18 observables (6 cell dimensions for each of the peroxides).

Since potential parameters for use as starting values for the peroxides could not be found in the literature, the oxide parameter set, OPT2 (*Table 6.1*), together with a "mixed oxide-peroxide" structure was used. The "mixed" structure was constructed by collapsing the O-O onto itself, so that the oxygen would be in the same oxidation state as in the oxide, but otherwise retaining the space group and lattice dimensions of the peroxide structures (see *Fig 6.1*). The parameters optimized in this way proved to be unsuitable for use as starting values for the actual peroxide structures, probably due to the mixed hypothetical structures being too unstable.

Fig 6.1 Unit cell structures for cubic BaO, tetragonal BaO_2 and the hypothetical "mixed" structure, tetragonal BaO.

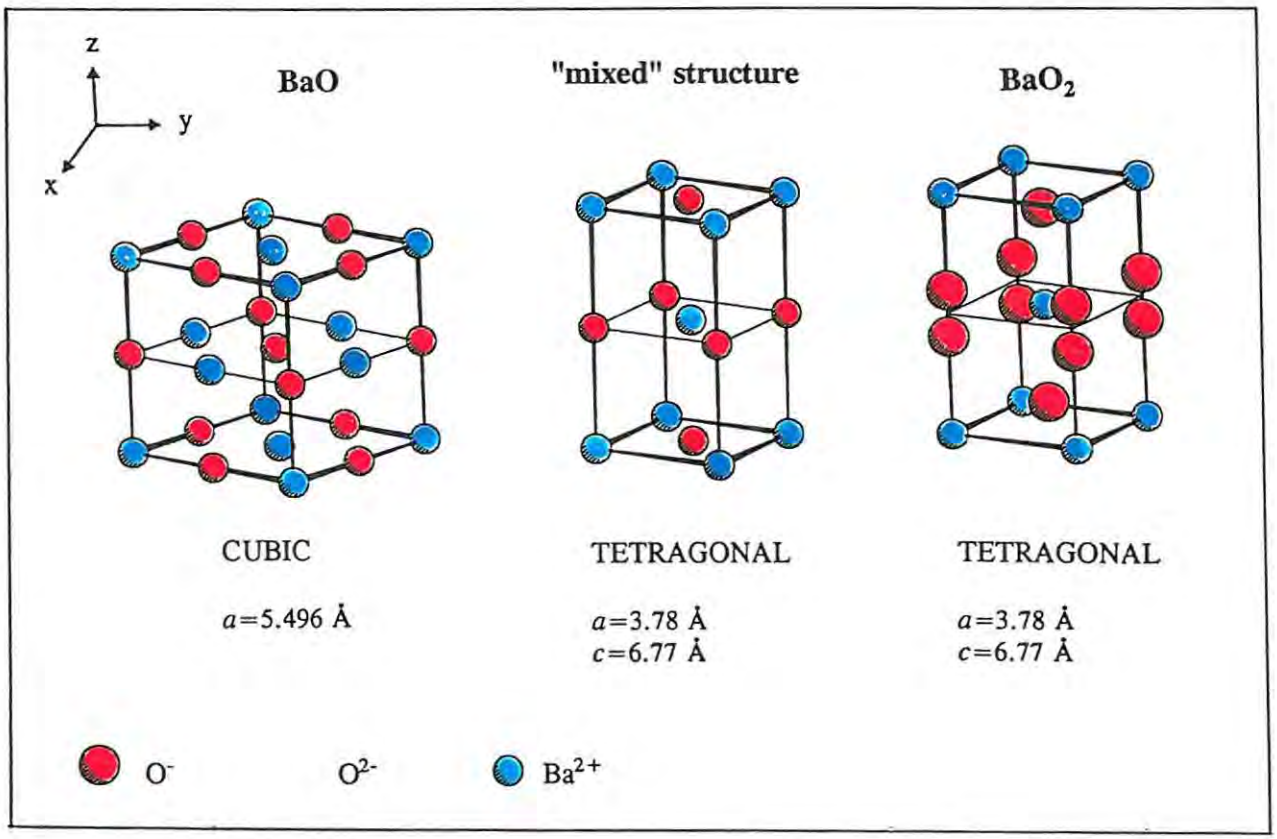

Further attempts at obtaining approximate starting values were made on a trial-and-error basis, by combining oxide and carbonate parameters. The parameters were varied for one substance at a time, but when the parameters for CaO_2 were added to the list of variables, they (*i.e.*, $A_{Ca\text{-}O}$, $\rho_{Ca\text{-}O}$) diverged rapidly. The CaO_2 parameters were thus omitted from the first two optimized sets, OPT3 (using structural data *Set A*) and OPT4 (using structural data *Set B*), shown in *Table 6.6*.

The accuracy of the crystal data reported for CaO_2 [67] is questionable, since there is a 10.6% deviation in the calculated density compared to the experimental density (see *Section 5.3* and *Table 5.2*). Once the final optimized sets for SrO_2 and BaO_2 had been completed, however, the optimization process was rerun with CaO_2 included. The optimization proceeded with difficulty, but finally the parameters OPT5 (using structural data *Set B*) and OPT6 (using structural data *Set A*) were derived and are shown in *Table 6.6*. If the experimental crystal data are in error, these inaccuracies will be reflected in the short-range potentials. Values of the lattice energy, calculated from these optimized parameters, will reflect such errors.

Table 6.6 Optimized short-range parameters (A_{ij}, ρ_{ij} and C_{ij}) for each ion in the alkaline-earth metal peroxides.

Parameters	**CaO_2 omitted**		**CaO_2, SrO_2, BaO_2**	
	OPT3 (O-O=1.30 Å)	OPT4 (O-O=1.49 Å)	OPT5 (O-O=1.49 Å)	OPT6 (O-O=1.30 Å)
A_{ij} /kJ mol^{-1}				
O-O	76.40414×10^{6}	35.86485×10^{8}	33.78811×10^{8}	58.03570×10^{6}
Ca-O			0.45257×10^{4}	0.49063×10^{4}
Sr-O	6.99418×10^{4}	7.31160×10^{4}	7.32199×10^{4}	5.91456×10^{4}
Ba-O	6.15959×10^{4}	1.70120×10^{4}	1.44845×10^{4}	7.07321×10^{4}
ρ_{ij} /Å				
O-O	0.1793	0.1546	0.1540	0.1765
Ca-O			0.6346	0.6026
Sr-O	0.3581	0.3751	0.3733	0.3671
Ba-O	0.3829	0.5152	0.5305	0.3737
C_{ij} /kJ mol^{-1} Å^{6}				
O-O	72.5239×10^{2}	338.9678×10^{2}	339.9418×10^{2}	56.9617×10^{2}
RDWST	0.4060×10^{-5}	0.1831×10^{-3}	1.189	0.5015

The optimized parameter sets, OPT3, OPT4, OPT5 and OPT6, were then used to calculate the lattice energies of the peroxides. When the parameters OPT5 and OPT6 were used in the energy minimization, erroneous results were obtained. For OPT5, although the relaxed structures (*i.e.*, cell dimensions and volume) deviated by at most 0.5% from the observed values (see *Table 6.7*), the calculated lattice energies did not compare well with observed values. Of more importance, however, was the deviation in the trend of the lattice energies. Reported lattice energies (see *Table 6.10*) decrease down the group from CaO_2 to SrO_2, while the reverse occurred for the values calculated using OPT5 in this investigation, *i.e.*, CaO_2 (-2997 kJ mol^{-1}) had a smaller lattice energy than SrO_2 (-3112 kJ mol^{-1}). Energy minimizations using parameter set OPT6, immediately gave "overflow" error messages and thus yielded no results.

Table 6.7 Cell dimensions (*a*, *c*), volume (*V*) and lattice energies (W) for fitted peroxides using optimized parameters OPT5.

		a/Å	*c*/Å	*V*/Å^3	W/kJ mol^{-1}
OPT5 (*Set B*: O-O=1.49 Å)					
CaO_2	expt.	3.54	5.92	74.19	-3050*
	calc.	3.54	5.92	74.19	-2997
	% error	0.00	0.00	0.00	1.7
SrO_2	expt.	3.568	6.616	84.23	-2865*
	calc.	3.565	6.620	84.14	-3113
	% error	0.08	-0.06	0.11	-8.7
BaO_2	expt.	3.807	6.841	99.15	-2738*
	calc.	3.821	6.815	99.50	-2693
	% error	-0.37	0.38	-0.35	1.6

*Lattice energies calculated from the Kapustinskii equation [85] (see *Appendix A*).

The structural data for CaO_2, determined from X-ray powder data in 1941 [67], were re-examined. The original reference had two obvious errors, *i.e.*, the Ca was in Wyckoff position 2b (0, 0, ½) instead of 2a (0, 0, 0) and the number of formula units was given as Z=2 with a=5.01 Å and c=5.92 Å (*I4/mmm*, #139) giving a 44.9% deviation in D_c (1.61 g cm^{-3}) compared to D_o (2.92 g cm-*3*). For the cell dimensions given, the number of formula units should clearly be Z=4 (*F4/mmm*, #139). Dimensions for the corresponding body-centered unit cell (*I4/mmm*, #139) are easily obtained by rotating the xy-plane through 90° about the z-axis, giving a bimolecular unit cell with a=3.54 Å and c=5.92 Å. Even for the corrected unit cell, D_c (3.23 gcm^{-3}) still deviates from D_o by 10.6%. The cell dimension ratio, *c/a*, (see *Table 5.2*) for CaO_2 is also out of sequence, *i.e.*, the *c/a* ratios for Ca, Sr and Ba peroxide are 1.67,

1.85 and 1.79, respectively. Because of the lack of accurate data, CaO_2 was omitted from further investigation.

The results from the parameter sets with CaO_2 excluded, OPT3 and OPT4, are given in *Table 6.8*. The relaxed structures of both SrO_2 and BaO_2 are very close to their respective experimental structures (errors of 0.5%), but the calculated lattice energies show deviations when compared to values reported by Vedeneev, *et al.* [86], and to values calculated from the Kapustinskii equation [85] (see *Appendix A*). However, the discrepancies are not consistent (*i.e.*, deviations in the calculated lattice energies (for *Set A*) compared to values reported by Vedeneev, *et al.* [86], are small, but large when compared to values determined from the Kapustinskii equation. This trend is also reversed for the lattice energies of Set B), which suggests that the reference lattice energies are not accurate. Both sets of lattice energies calculated with WMIN *i.e.*, using potentials OPT3 (-3085, -2918 kJ mol^{-1} for SrO_2 and BaO_2, respectively) and using OPT4 (-3113, -2718 kJ mol^{-1}), fall within the range of reported values (*Table 6.10*). The difference between the lattice energies for SrO_2 and BaO_2, *i.e.*, $W(BaO_2) - W(SrO_2)$ ranges between 120 - 220 kJ mol^{-1}. The lattice energies generated from OPT3 give a difference which falls into this range, *i.e.*, 165 kJ mol^{-1} while the difference in lattice energies for SrO_2 and BaO_2 using OPT4 is much larger, *i.e.*, 395 kJ mol^{-1}. The reason could be due to the high $W_{r,v}/W_c$ ratio discussed below.

Table 6.8 Cell dimensions (*a*, *c*), volume (*V*) and lattice energies for fitted peroxides using OPT3 and OPT4.

		a/Å	*c*/Å	*V*/Å^3	W/kJ mol^{-1}	W/kJ mol^{-1}
OPT3 (*Set A*: O-O=1.30 Å)						
SrO_2	expt.	3.55	6.55	82.55	-3150*	-2865**
	calc.	3.555	6.550	82.78	-3085	-3085
	% error	-0.1	0.00	-0.28	2.1	-7.6
BaO_2	expt.	3.78	6.77	96.73	-3000*	-2738**
	calc.	3.78	6.77	96.73	-2918	-2918
	% error	0.00	0.00	0.00	2.7	-6.6
OPT4 (*Set B*: O-O=1.49 Å)						
SrO_2	expt.	3.568	6.616	84.23	-3150*	-2865**
	calc.	3.565	6.621	84.15	-3113	-3113
	% error	0.08	-0.07	0.10	1.2	-8.6
BaO_2	expt.	3.807	6.841	99.15	-3000*	-2738**
	calc.	3.823	6.821	99.69	-2718	-2718
	% error	-0.40	0.30	-0.54	9.4	-0.7

*Lattice energies calculated by Vedeneev, *et al.* [86].
**Lattice energies calculated with the Kapustinskii equation [85] (see *Appendix A*).

Finally, an evaluation of the $W_{r,v}/W_c$ ratio shows that the lattice energies calculated with the optimized parameter set OPT3 (where O-O=1.30 Å) yield consistent $W_{r\text{-}v}/W_c$ ratios (as is seen for the oxides), with ratios that are slightly lower than in the oxides (*cf. Tables 6.4* and *6.9*), *i.e.*, ~12% (peroxides) compared to ~15% (oxides). The calculations with parameter set OPT4 yield $W_{r\text{-}v}/W_c$ ratios which are much more diverse (*i.e.*, 10.3% and 17.3% for SrO_2 and BaO_2, respectively).

Since there is not sufficient evidence to confirm which set of lattice energies is more accurate, both sets, *i.e.*, WMIN(OPT3) with O-O=1.30 Å and WMIN(OPT4) with O-O=1.49 Å, were used for modelling the thermal decomposition of the peroxides.

Table 6.9 Contributions to the lattice energies of the alkaline-earth metal peroxides using WMIN. W= total lattice energy, W_c= Coulombic energy and $W_{r,v}$= short-range energy (repulsion plus van der Waals energy calculated from the Buckingham potential).

	W_c /kJ mol-1	$W_{r,v}$ /kJ mol^{-1}	$W_{r,v}/W_c$ %	W /kJ mol^{-1}
OPT3 (*Set A*: O-O=1.30 Å)				
SrO_2	-3509	424	12.1	-3085
BaO_2	-3343	425	12.7	-2918
OPT4 (*Set B* O-O=1.49 Å)				
SrO_2	-3468	356	10.3	-3113
BaO_2	-3285	568	17.3	-2718

Table 6.10 A comparison of lattice energies (kJ mol^{-1}) reported for the alkaline-earth metal peroxides.

Reference	CaO_2	SrO_2	BaO_2	$W(BaO_2)$ - $W(SrO_2)$
Kapust. eqn.	-3050	-2865	-2738	127
Therm. cycle	-3133	-2849	-	
1949: EU	-3075	-2920	-2707	213
1952: V	-	-3150	-3000	150
1965: WD	-3144	-3037	-	
1995: WMIN(OPT3)	-	-3085	-2918	165
1995: WMIN(OPT4)	-	-3113	-2718	395

Kapust. eqn. = Kapustinskii equation [85] (see *Appendix A*).
Therm. cycle = experimental lattice energy determined from the thermochemical (Born-Haber) cycle [74].
EU = Evans and Uri [87].
V = Vedeneev, *et al.* [86].
WD = Wood and D'Orazio [88]

WMIN (OPT3) = lattice energies calculated using OPT3
WMIN (OPT4) = lattice energies calculated using OPT4

6.3 SETTING THE DECOMPOSITION PATHWAY

6.3.1 Assumptions

The following assumptions were made in modelling the decomposition route:

1. The starting reactants are pure crystalline peroxides (SrO_2 or BaO_2), both of which have tetragonal structures with space group *I4/mmm*.
2. The final solid products are the corresponding pure crystalline (Sr or Ba) oxides, both of which have cubic structures with space group $Fm\bar{3}m$.
3. Reaction is assumed to occur *via* a series of solid intermediates with structures changing along a symmetry route (see below) connecting *I4/mmm* to $Fm\bar{3}m$.
4. Parameters needed for the lattice energy calculation are assumed to be transferable. For the intermediate structures, the parameter set for either the peroxides or the oxides was used, depending on whether the oxidation state of oxygen was -1 or -2.
5. The crystal structures were assumed to be perfect, *i.e.*, no allowance is made for the influence of any kind of defect on the lattice energy. (Defects are, however, known to be important in the mechanisms of decompositions of solids.)

6.3.2 Initial symmetry-controlled decomposition routes

During the overall decomposition, the peroxide ions, which are aligned parallel to the tetragonal *c*-axis, become converted to oxide ions and the tetragonal *c*-axis shrinks to its value in the cubic structure, with only relatively small changes in the *a* dimension (see in *Fig 6.2*, *i.e.*, *structure 1* ⟶ *structure 3**).

Two symmetry-controlled transformations for the decomposition were investigated (see *Fig 6.2*), *i.e.*,

PATH I: removal of O_2 from the peroxide, followed by adjustments to the unit cell dimensions to achieve those of the oxide structure.

PATH II: adjustment of the peroxide unit cell dimensions to those of the oxide, followed by the removal of O_2 to yield the product oxide structure.

(Note: *Fig 6.2* shows the O_2 being removed in stages in PATH I. This divided sequence was only performed at a later stage).

Most calculations were done with both sets of structural data (see *Section 5.3*), *i.e.*, *Set A* (data with O-O=1.30 Å) and *Set B* (data with O-O=1.49 Å).

Reactant, *structure 1*: Tetragonal, body-centred unit cell with

Set A: a=3.55 Å, c=6.55 Å for SrO_2; a=3.78 Å, c=6.77 Å for BaO_2, (Z=2).
Set B: a=3.568 Å, c=6.616 Å for SrO_2; a=3.807 Å, c=6.841 Å for BaO_2, (Z=2)

PATH I: Removal of O_2 gives *structure 2b*, which is followed by compression of the unit cell volume by adjusting cell dimensions to a=3.634 Å, c=5.1396 Å for Sr, and a=3.886 Å, c=5.496 Å for Ba (for both *Set A* and *Set B*), giving *structure 3**.

PATH II: The first step is compression of the peroxide unit cell dimensions to a=3.634 Å c=5.1396 Å for Sr, and a=3.886 Å, c=5.496 Å for Ba (for both *Set A* and *Set B*), giving structure 2c. Since the positions of the atoms are recorded in fractional coordinates (and the coordinates of the peroxide ion (O^--O^-) are (0,0,z) and (0,0,$\bar{z}$)), the z-coordinates of the O^- ions have to be corrected to keep the O-O bond length constant. Once the peroxide ion has been converted to the oxide ion, O^{2-}, as in the next stage (*i.e.*, *structure 3**), this problem no longer exists. The original and corrected coordinates are shown in *Table 6.11*.

Product, *structure 3*: This is a cubic, face-centred unit cell with a=5.1396 Å for SrO, and a=5.496 Å for BaO, (Z=4). To obtain *structure 3* from *structure 3**, the unit cell has only to be redefined to convert the initial body-centred arrangement to a face-centred arrangement (described in *Section 5.2*), *i.e.*, this is done by rotating the xy-plane through 90° about the z-axis. The dimensions of the unit cells are related by multiplying the lattice constants, a and b, of the tetragonal body-centred lattice by a factor of $\sqrt{2}$ to obtain the values for the cubic face-centred lattice. The dimension c is the same for both cells, since the cubic unit cell was derived by rotation about the z-axis. Lattice energies for *structures 3* and *3** are identical, since they have identical lattices.

Table 6.11 The original (for *structure 1*) and corrected (*structure 2c)* fractional z-coordinates for Sr and Ba peroxide. *Set A*: O-O=~1.30 Å and *Set B*: O-O=1.49 Å.

		original		corrected		O-O/Å
		z	$\bar{z}$	z	$\bar{z}$	
Set A:	SrO_2	0.397	0.603	0.369	0.631	1.35
	BaO_2	0.404	0.596	0.382	0.618	1.30
Set B:	SrO_2	0.3875	0.6125	0.3550	0.6450	1.49
	BaO_2	0.3911	0.6089	0.3645	0.6355	1.49

Fig 6.2 Initial symmetry-controlled transformations for the decomposition of BaO_2 to BaO. Dimensions are shown for *Set A*: O-O=1.30 Å.

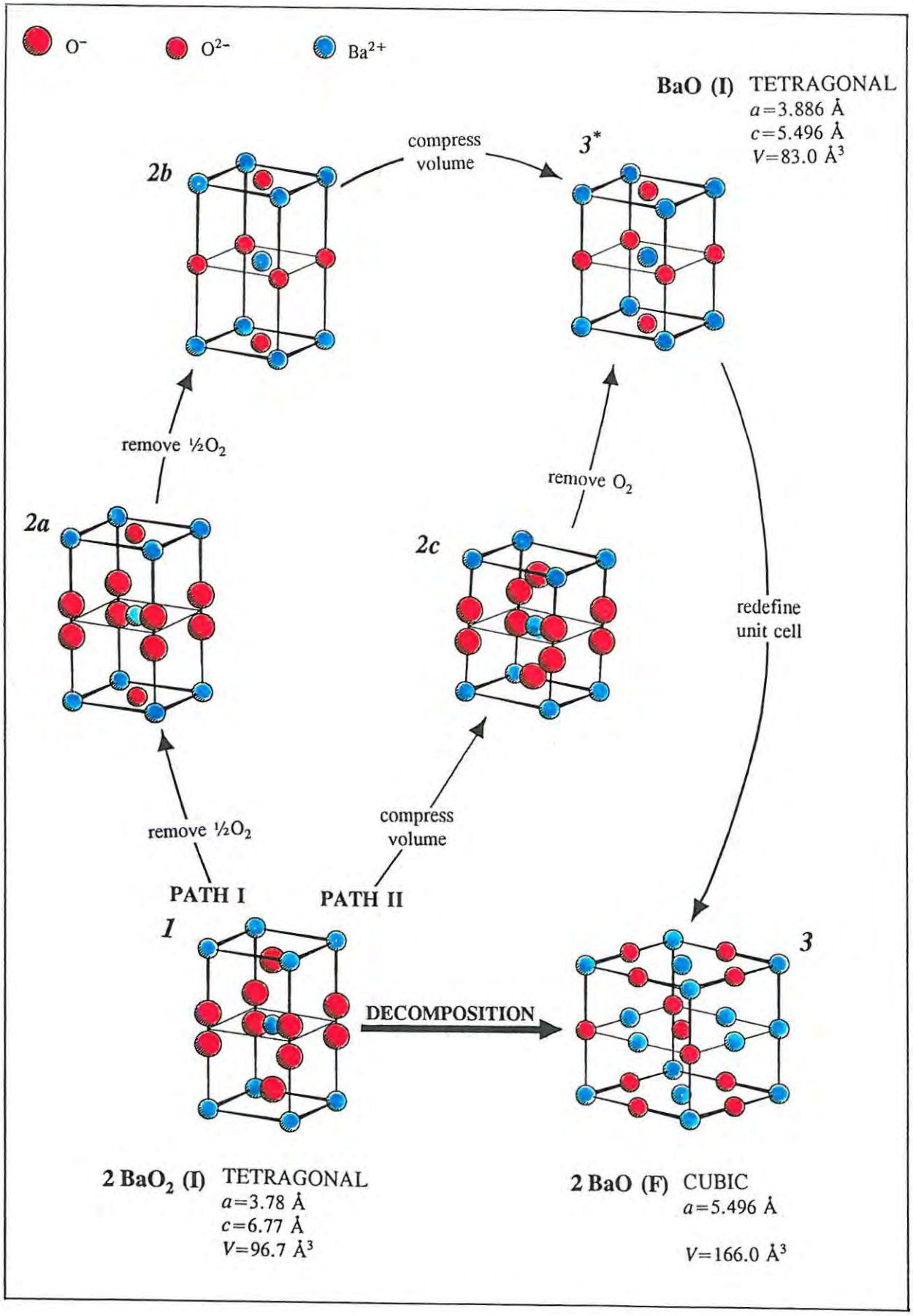

6.3.3 Extended decomposition routes

After the trends in the changes of lattice energies along PATH I and PATH II were established, refinements to the cross-over point between compressing the unit cell (*i.e.*, decreasing the volume) and removing the O_2 were investigated and the effects of these processes on the activation energy for the decomposition were determined.

Since there are two O_2^{2-} per unit cell, the effect of removing $\frac{1}{2}O_2$ (*i.e.*, $O_2^{2-} \longrightarrow O^{2-} + \frac{1}{2}O_2$) at a time was also explored. In *structure 2a* (*Fig 6.2*), oxygen is in a mixed oxidation state, thus there are additional interactions, *viz.*, there are three oxygen-oxygen interactions, O^{2-}- O^{2-}, O^- - O^- and O^{2-}- O^- (instead of only one in the oxides and peroxide). The energy parameters for the first two interactions are those derived for the oxides and peroxides, respectively, while the parameters for the last interaction were calculated from the combining rules, *eqns (3.1)* and *(3.2)*, see *Section 3.2.3*. *Table 6.12* gives the energy parameters (for SrO_2 and BaO_2, *Set A*: O-O=1.30 Å) needed to calculate the lattice energy of structures with a mixed oxidation state. Corrections to the z-coordinates of the peroxide ion were made for all unit cell deformations in which the peroxide ion(s) were still present.

Table 6.12 Optimized short-range parameters (A_{ij}, ρ_{ij} and C_{ij}) for structures with oxygen in a mixed oxidation state.

	A_{ij} /kJ mol^{-1}	ρ_{ij} /Å	C_{ij} /kJ mol^{-1} Å^6
O^{2-}- O^{2-}	8.03809x10^6	0.1733	20.49640x10^2
O^- - O^-	76.40414x10^6	0.1793	72.52390x10^2
O^{2-}- O^-	24.78192x10^6	0.1763	38.55488x10^2
Sr^{2+}- O^{2-}	8.97697x10^4	0.3722	
Sr^{2+}- O^-	6.99418x10^4	0.3581	
Ba^{2+}- O^{2+}	7.56742x10^4	0.4049	
Ba^{2+}- O^-	6.15959x10^4	0.3829	

7 RESULTS AND DISCUSSION

7.1 CALCULATED LATTICE ENERGIES

The lattice energies calculated for PATH I (excluding *structure 2a*) and PATH II in the proposed decomposition route (see *Fig 6.2*) are listed in *Table 7.1*. The energies of the known structures, *i.e.*, reactant peroxides (*structure 1*) and solid product oxides (*structure 3*), were compared with values reported by Vedeneev, *et al.* [86] for SrO_2 and BaO_2, and Bush, *et al.* [40] for SrO and BaO, and with values determined from the Kapustinskii equation [85] (*Table 7.2*). In general, the WMIN values are in good agreement with reported values. The difference in lattice energy between the reactant and product (*i.e.*, $\Delta W = W(MO_2) - W(MO)$) was also examined and, is shown in *Table 7.2*. The uncertainties in the values of ΔW are large and the parameter *Sets A* and *B* give different trends with the change of cation.

Table 7.1 Calculated lattice energies for structures in the proposed symmetry-controlled routes (*i.e.*, PATH I and PATH II), see *Fig 6.2*. *Set A*: O-O=1.30 Å and *Set B*: O-O=1.49 Å.

	Set A		*Set B*	
W/kJ mol^{-1}	SrO_2	BaO_2	SrO_2	BaO_2
PATH I:				
structure 1	-3085	-2918	-3113	-2718
structure 2b	-3205	-2998	-3201	-2993
structure 3	-3240	-3020	-3240	-3020
PATH II:				
structure 1	-3085	-2918	-3113	-2718
structure 2c	-2845	-2785	-2802	-2604
structure 3	-3240	-3020	-3240	-3020

Table 7.2 Comparison of lattice energies for the reactant peroxides and solid product oxides, calculated with WMIN, with reported values. The differences between the lattice energies, $\Delta W = W(MO_2) - W(MO)$, are also shown. *Set A*: O-O=1.30 Å and *Set B*: O-O=1.49 Å.

W/kJ mol^{-1}	WMIN *Set A*	WMIN *Set B*	Reported	Kapustinskii equation [85]
SrO_2	-3085	-3113	-3150 [86]	-2865
SrO	-3240	-3240	-3281 [40]	-3250
ΔW	**155**	**127**	**131**	**385**
BaO_2	-2918	-2718	-3000 [86]	-2738
BaO	-3020	-3020	-3132 [40]	-3088
ΔW	**102**	**302**	**132**	**350**

The decompositions of the alkaline-earth peroxides, *i.e.*, $MO_2 \longrightarrow MO + \frac{1}{2}O_2$, are endothermic [4]. The enthalpy changes for the decompositions can be calculated from standard enthalpies of formation [89], *i.e.*, $\Delta H = \Delta H_f^{\ominus}(MO) - \Delta H_f^{\ominus}(MO_2)$. ΔH was calculated to be 52.3 kJ mol^{-1} for SrO_2 and 71.6 kJ mol^{-1} for BaO_2. The enthalpy changes have also been measured from DSC traces and those recorded by Tribelhorn and Brown [4], *i.e.*, 51.7 and 76.2 kJ mol^{-1}, compare favourably.

7.2 CORRECTION FOR THE REMOVAL OF O_2

To relate the changes in lattice energy to the changes in energy associated with the decomposition of the peroxides, corrections have to be made for the removal of O_2 from the lattice.
From the definition of lattice energy, the processes under consideration are:

$$MO_2(s) \longrightarrow M^{2+}(g) + O_2^{2-}(g) \quad .....\Delta H_1 \qquad (1)$$

$$MO(s) \longrightarrow M^{2+}(g) + O^{2-}(g) \quad .....\Delta H_2 \qquad (2)$$

Using the standard thermodynamic relationship: $\Delta H = \Delta U + p\Delta V = \Delta U + \Delta nRT$ (where Δn is the change in the number of gaseous molecules), for reaction (1) and (2), $\Delta n=2$. Therefore, using T=298 K, $\Delta nRT \approx 5$ kJ mol^{-1}. This is within the uncertainty of the lattice energy values, and hence, $\Delta H \approx \Delta U = -W$ for the formation of gaseous ions.

For the reaction (1) - (2) = (3), $\Delta H_3 = \Delta H_1 - \Delta H_2$

$$MO_2(s) \longrightarrow MO(s) + O_2^{2-}(g) - O^{2-}(g) \quad .....\Delta H_3 \qquad (3)$$

For the decomposition (4), ΔH_4 is calculated from tables of standard thermodynamic data.

$$MO_2(s) \longrightarrow MO(s) + \tfrac{1}{2}O_2(g) \quad .....\Delta H_4 \qquad (4)$$

Finally, (4) - (3) yields reaction (5) with $\Delta H_5 = \Delta H_4 - \Delta H_3$.

$$O_2^{2-}(g) \longrightarrow \tfrac{1}{2}O_2(g) + O^{2-}(g) \quad .....\Delta H_5 \qquad (5)$$

Reaction (5) represents the reaction that takes place on removal of O_2 from the lattice and therefore the value of ΔH_5 must be added to those energies calculated from the lattice devoid of O_2. *Table 7.3* gives the enthalpies for reactions (1) to (5) for Sr and Ba.

Table 7.3 Enthalpies of reaction (in kJ mol^{-1}) of the reactions defined in the text.

	Set A		*Set B*	
	Sr	Ba	Sr	BaO_2
$\Delta H_1 \approx -W(MO_2)^*$	3085	2918	3113	2718
$\Delta H_2 \approx -W(MO)^{**}$	3240	3021	3240	3021
$\Delta H_3 = \Delta H_1 - \Delta H_2$	-155	-103	-127	-303
ΔH_4	52	72	52	72
$\Delta H_5 = \Delta H_4 - \Delta H_3$	207	175	179	374

*Lattice energies calculated for the peroxides with OPT3 (*Set A*: O-O=1.30 Å) and OPT4 (*Set B*: O-O=1.49 Å)
**Lattice energies calculated for the oxides with OPT2.

The energies corrected for the removal of O_2 are plotted against course of reaction in *Fig 7.1* (for Sr, *Set A*: O-O=1.30 Å). From the corrected decomposition profile, the activation energy (E_a) can be calculated.

For the initial proposed decomposition route (PATH I), E_a was calculated to be:
87 and 95 kJ mol^{-1} for SrO_2 and BaO_2 (*Set A*: O-O = 1.30 Å) and
91 and 100 kJ mol^{-1} for SrO_2 and BaO_2 (*Set B*: O-O = 1.49 Å), respectively.
The activation energies calculated from PATH II were considerably higher for SrO_2 and in the reverse order, *i.e.*,
240 and 133 kJ mol^{-1} for SrO_2 and BaO_2 (*Set A*: O-O=1.30 Å) and
311 and 114 kJ mol^{-1} for SrO_2 and BaO_2 (*Set B*: O-O=1.49 Å)

Fig 7.1 Lattice energies (corrected for the removal of O_2) plotted against reaction course for the postulated decomposition route, PATH I (omitting *structure 2a*), for SrO_2 (*Set A*: O-O=1.30 Å). Processes (3) to (5) are also depicted.

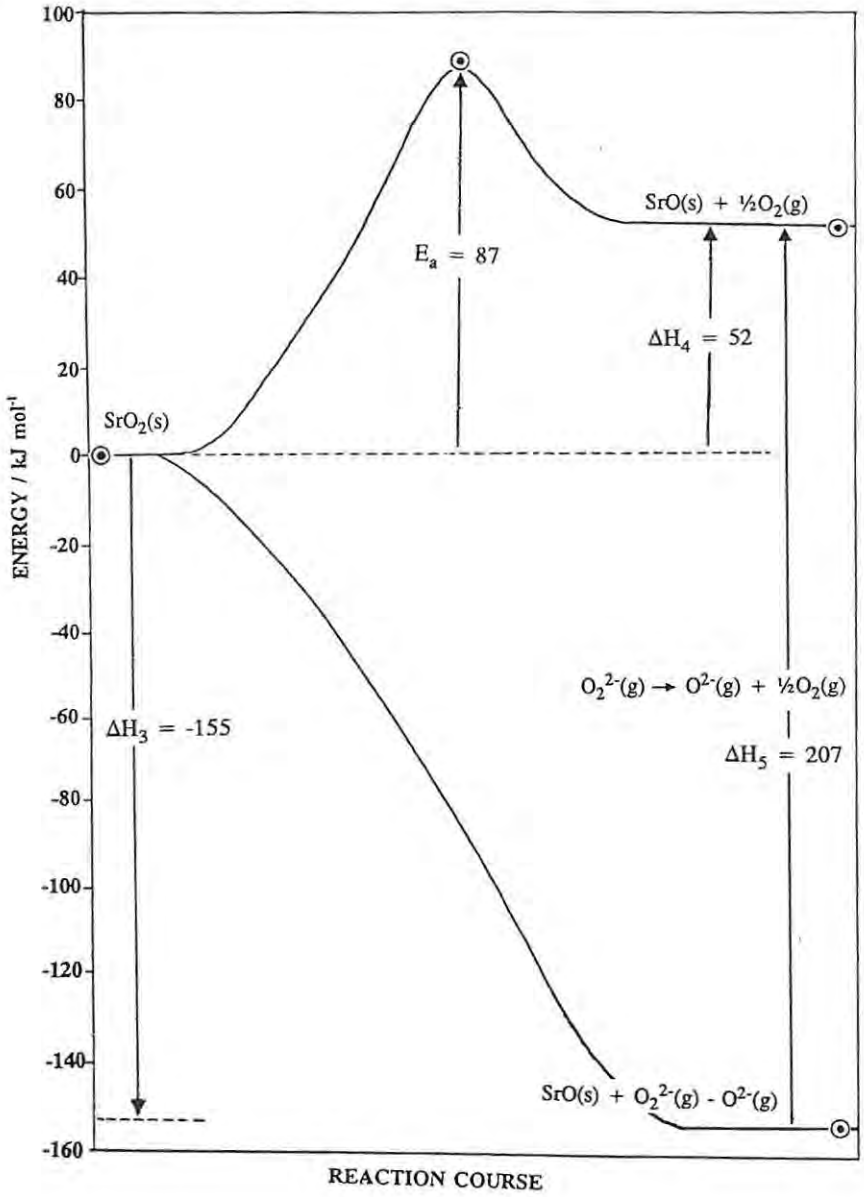

7.3 EXTENDED DECOMPOSITION ROUTES

7.3.1 Activation energies for refined symmetry-controlled routes

Small reductions in the energy barrier were achieved by slightly compressing the unit cell (*i.e.*, for SrO_2: the initial cell constants a=3.55 Å, c=6.55 Å were decreased to a=3.57 Å, c=6.22 Å and for BaO_2: from a=3.78 Å, c=6.77 Å to a=3.80 Å, c=6.43 Å) before removing the oxygen. E_a changed from 87 to 83 kJ mol^{-1} for SrO_2 and from 95 to 93 kJ mol^{-1} for BaO_2 (calculations were only performed for *Set A*: O-O=1.30 Å).

7.3.2 Removal of the O_2

All oxygen positions in the peroxide lattice (for both Sr and Ba) are identical and therefore the removal of one oxygen is not favoured over another. However, the lattice energy increases on removal of the first oxygen (*i.e.*, $\frac{1}{2}O_2$) from the unit cells and then increases further with removal of the second oxygen, so that the maximum energy barrier is associated with the removal of O_2 from the unit cell. For example, in *Fig 6.2*, PATH I (for *Set A*: O-O=1.30 Å) *structure 2a* ($-\frac{1}{2}O_2$) yielded lattice energies of -3130 and -2946 kJ mol^{-1} for Sr and Ba, respectively, and *structure 2b* ($-O_2$), values of -3205 and -2998 kJ mol^{-1}. These values, corrected for the removal of O_2 and plotted against reaction course show for both SrO_2 (E_a=87 kJ mol^{-1}) and BaO_2 (E_a=95 kJ mol^{-1}) a higher activation energy on the release of the second oxygen (see *Fig 7.2* for SrO_2).

In studies on the decomposition of Li_2O_2 in vacuum, the rate limiting step was identified as O-O bond rupture [90] and it was suggested that a large part of the energy required to rupture the peroxide (O-O) link is compensated by the decrease in the lattice energy of the product[91].

Fig 7.2 Lattice energies (corrected for the removal of O_2) plotted against reaction course for the postulated decomposition route, PATH I (including *structure 2a*, see *Fig 6.2*), for SrO_2 (*Set A*: O-O=1.30 Å).

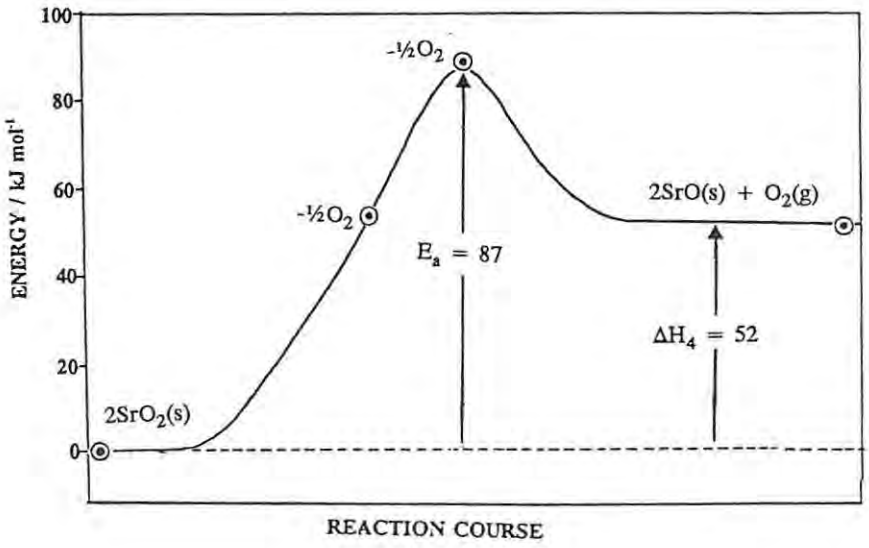

7.4 EXPERIMENTAL VALUES FOR THE ACTIVATION ENERGY OF DECOMPOSITION OF SrO_2 AND BaO_2

Several experimental studies of the decomposition of the alkaline-earth metal peroxides have been reported (reviewed in *ref.* 4). It is clear that the thermal decomposition is more complicated than the simple process represented by

$$MO_2(s) \longrightarrow MO(s) + \tfrac{1}{2}O_2(s)$$

Only a few of the studies report values for the kinetic parameters. E_a values for decomposition of SrO_2 (119 to 165 kJ mol^{-1}) and BaO_2 (135 to 360 kJ mol^{-1}), calculated from isothermal and nonisothermal kinetic studies, are shown in *Table 7.4*. Brunere, *et al.* [92] represented the decomposition of BaO_2 by a three-step process: nucleus formation (E_a=12 kJ mol^{-1}), grain growth (E_a=104 kJ mol^{-1}) and oxygen diffusion (E_a=2 kJ mol^{-1}). The activation energies calculated for the proposed symmetry-controlled decomposition routes (PATH I and PATH II) are listed in *Table 7.4*. The values for PATH I (*Set A* and *Set B*) appear to be too low, but are in the correct order with BaO_2 having the higher E_a, while the values for PATH II are much higher but in the reverse order, *i.e.*, $E_a(Sr) > E_a(Ba)$.

Table 7.4 Reported activation energies (kJ mol^{-1}) for the decompositions of Sr and Ba peroxides.

	SrO_2		BaO_2	
Reference	Isothermal	Nonisothermal	Isothermal	Nonisothermal
1963: Erofeev and Sokolova [93]	—	—	192	360±20
1983: Fahim and Ford [94]	—	—	135	141
1994: Tribelhorn and Brown [4]	119	165	185	165
1995: WMIN (PATH I, *Set A*)	87		95	
1995: WMIN (PATH I, *Set B*)	91		100	
1995: WMIN (PATH II, *Set A*)	240		133	
1995: WMIN (PATH II, *Set B*)	311		114	

The decompositions of the peroxides are known to be reversible, *i.e.*,

$$MO_2(s) \rightleftharpoons MO(s) + \tfrac{1}{2}O_2(s)$$

and, in the lattice energy calculations, no account can be taken of any influence of the reverse process, which may be considerable when removal of product oxygen gas is not rapid or complete. Ideally then, the values from lattice energy calculations should be closest to experimental values obtained for the decomposition of the peroxides in vacuum.

The apparent energy barriers for the highly symmetry-controlled reaction route (PATH I) for both Sr and Ba are lower than the experimental values. The opposite might have been expected if the role of defects is to provide a lower energy pathway for decomposition *via* some sort of cooperative mechanism analogous to the movement of a line dislocation through a crystal lattice. The postulated reaction route of PATH I could be kinetically inaccessible, but inconsistencies in the activation energies calculated for PATH II, *i.e.*, $E_a(Sr) > E_a(Ba)$, suggest possible errors in the modelling process. The lattice energies calculated for intermediate structures in PATH II (for *Set A* and *Set B*) are mainly dependent on the peroxide parameters. since the peroxide ion is retained longer in the unit cell (*cf.* PATH I where O_2 has been removed and the oxide parameters have been used, *i.e.*, $2O_2^{2-} \longrightarrow 2O^{2-} + O_2$). The peroxide interatomic parameters are probably less reliable than those of the oxides.

Possible errors involved in the modelling process fall into three categories.

(1) **Accuracy of the crystal data used as reference**: the crystal data for the peroxides *Set A*, are inaccurate since the peroxide bond lengths of 1.35 Å and 1.30 Å for SrO_2 and BaO_2, respectively, differ from the more recently established value of 1.49 Å. Accurate crystal data were available only for BaO_2 (*Set B*), reported by Abrahams and Kalnajs [70] with an R-value of 0.0381 and D_o/D_c = 0.958. The crystal structure of SrO_2 (*Set B*) was constructed on the basis of the BaO_2 structure and using the latest reported lattice constants.

(2) **Accuracy of the potential model**: the accuracy of the model is assessed by calculating structural properties and lattice energies (which were not included in the fitting). The parameters have successfully modelled the ionic alkaline-earth oxide and peroxide structures, except for BaO_2. Further evidence for the poor modelling of BaO_2 is given by the inconsistency in the $W_{r,v}/W_r$ ratio (for *Set B*). BaO_2 may have some covalent character in its bonding and thus to describe the bonding in BaO_2, potential parameters may have to be introduced to account for covalent interactions. The accuracy of the lattice energies calculated for the peroxides could not be determined because the reference lattice energies were inconsistent. The values calculated for the oxides agreed well with experimental values.

(3) **Transferability of the interatomic potentials**: the transferability of the interatomic potentials (A_{ij}, ρ_{ij}, C_{ij}) could not be assessed and thus the extent to which the potentials are valid for interatomic separations which differ considerably from those in the perfect lattice (*i.e.*, for the proposed intermediate structures in the proposed decomposition routes) is not known. There is however, substantial evidence which indicates that potentials of the present form are transferable.

PART II

Modelling the thermal decomposition of alkaline-earth metal carbonates to oxides

$$MCO_3 \longrightarrow MO + CO_2$$

8. COMPUTATIONAL PROCEDURES

8.1 INTRODUCTION

The changes in lattice energy during the thermal decomposition of alkaline-earth metal carbonates to their respective solid oxides and gaseous CO_2, *i.e.*,

$$MCO_3(s) \longrightarrow MO(s) + CO_2(g)$$

were investigated using the same basic assumptions and computational steps as in the peroxides. A few additional aspects had to be considered. In the optimization of the short-range energy parameters for the oxides and peroxides, only isomorphous structures were examined, while the carbonates exist in several polymorphic structures. The charge distribution in the carbonate ion (CO_3^{2-}), is also more complicated than in the peroxide ion (O_2^{2-}).

8.2 OPTIMIZATION OF SHORT-RANGE PARAMETERS

8.2.1 The charge distribution in CO_3^{2-}

The charge distribution in CO_3^{2-} has been extensively investigated, *e.g.*, by Ladd [95,96], Jenkins and Waddington [97], Jenkins, *et al.* [98], Yuen, *et al.* [99] and Pavese, *et al.* [46]. The values published by the various authors are very different and are shown in *Table 8.1*. Discrepancies between the first two sets of results [96,97] have been the subject of published correspondence [100].

Table 8.1 Reported values for the charge distribution in CO_3^{2-}.
q_c and q_o are the charges on the carbon and oxygens, respectively.

	calcite		aragonite	
	q_c	q_o	q_c	q_o
1971: JW*	-1.22	-0.26		
1972: L*	0.31	-0.77		
1976: J*	-0.38	-0.54		
1978: Y	0.95	-0.98	0.89	-0.96
1992: P	0.985	-0.995	0.817	-0.939

*Authors did not give separate values for the charge distribution of CO_3^{2-} in calcite and aragonite.
JW = Jenkins and Waddington [97]; L = Ladd [96]; J = Jenkins, *et al.* [98];
Y = Yuen, *et al.* [99]; P = Pavese, et al.[46].

Several methods are available for estimating the fractional atomic charge in a complex ion. Charge distribution is one of the terms contributing to the crystal lattice energy, thus a reliable method must ensure that the other energy parameters, those due to dispersion and to repulsion, are accurately estimated. Empirical fitting was used in the last two investigations [99,46] (a procedure suggested by Busing [100] and applied by him to a number of ionic crystals), with the application of different models, *i.e.*, the fractional atomic charges developed by Yuen, *et al.* [99] were estimated on the basis of a pure Born model, which was fitted only to structural properties of calcite and aragonite, while Pavese *et al.* [46] included bond-bending terms in the CO_3 group and the interatomic potentials were fitted to elastic and vibrational data. The fact that the charge distributions derived by such different models are consistent with each other (see the last two authors in *Table 8.1*) supports the physical soundness of these values. Molecular orbital calculations on the isolated CO_3^{2-} ion [99] gave values of $q_c = 0.907$ and 0.906 for calcite and aragonite, respectively, which lends further support to the use of more recent charge distributions, rather than those derived in the earlier studies. Thus, a good valence-bond representation of the carbonate ion is:

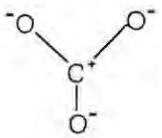

in which carbon is associated with six rather than the eight electrons depicted in resonance hybrid structures.

8.2.3 Computational procedure

The energy parameters for the two polymorphic series, *i.e.*, the rhombohedral calcite structures ($MgCO_3$, $CaCO_3$) and the orthorhombic aragonite stuctures ($CaCO_3$, $SrCO_3$, $BaCO_3$) were optimized separately. The fitting was done with reference to the crystal data listed in *Table 5.5* and 5.6 for the calcite and aragonite structures, respectively. To increase the number of observables, all symmetry constraints were removed, so that the compounds were treated as triclinic structures (with only the identity symmetry operation), a procedure which worked adequately for the oxides and peroxides. As starting values for the energy parameters, those reported by Pavese, *et al.* [46] for $CaCO_3$ (calcite and aragonite) and listed in *Table 8.7* were used. Since no values were available for $MgCO_3$, $SrCO_3$ and $BaCO_3$, estimates of these parameters, on the basis of the $CaCO_3$ values, were made.

Various tactics were used to stabilize the optimization process. Starting values were altered; one set of parameters was varied at a time (*i.e.*, $A_{Ca\text{-}O}$, $\rho_{Ca\text{-}O}$ then $A_{Sr\text{-}O}$, $\rho_{Sr\text{-}O}$, *etc.*, finally $A_{O\text{-}O}$, $\rho_{O\text{-}O}$, $C_{O\text{-}O}$); damping was increased (reducing the magnitude of the calculated change allowed for the parameter); the increment to be added to, or subtracted from, the parameter in calculating the numerical derivative was decreased, and the constant for Marquardt's compromise (which is added to each eigenvalue before its reciprocal is taken, reducing the contribution of each eigenvector, especially those with small eigenvalues) was increased. Once the parameters started converging, the above values (*i.e.*, damping, increments and constants) were set at the WMIN-recommended optimum values. It was found that the C-O parameters, *i.e.*, $A_{C\text{-}O}$, $\rho_{C\text{-}O}$ had no effect on the optimization (no interactions *within* a rigid body are calculated and the term is most probably small at the distances between C and O in other ions) and thus they were removed.

Since the charge distribution of a complex ion differs slightly according to the crystal in which it is contained [99], a series of trial charges (see *Table 8.2*) was tested. For each set, the short-range energy parameters were optimized and then the energy was minimized to see the effect on the calculated lattice energy and relaxed cell dimensions. For *Trial 1*, the fractional charges determined by Pavese, *et al.* [46], were assigned to all the carbonate ions (*i.e.*, both calcite structures, $MgCO_3$ and $CaCO_3$, were given the calcite charge distribution and all three aragonite structures, $CaCO_3$, $SrCO_3$ and $BaCO_3$, were given the charge distribution of aragonite). For *Trial 2*, the charge distribution calculated by Yuen, *et al.* [99] was used and, for *Trials 3, 4* and *5*, the charge distribution was varied, with q_c either increasing or decreasing down the group, as shown in *Table 8.2*. Lastly, for *Trial 6*, $q_c = 1.00$ was assigned to all the compounds.

Table 8.2 Charge distributions of CO_3^{2-} in the calcite structures ($MgCO_3$, $CaCO_3$) and the aragonite structures ($CaCO_3$, $SrCO_3$, $BaCO_3$). Only the charge on the carbon atom, q_c, is shown. The charge on the oxygens is assigned such that: $q_c + 3q_o = -2.000$

q_c	calcite structures		aragonite structures		
Trial	$MgCO_3$	$CaCO_3$	$CaCO_3$	$SrCO_3$	$BaCO_3$
1.	0.985	0.985	0.817	0.817	0.817
2.*	0.949	0.949	0.889	0.889	0.889
3.	1.000	0.985	0.817	0.760	0.700
4.	0.949	0.985	0.817	0.850	0.910
5.	0.886	0.985	0.817	0.910	1.000
6.	1.000	1.000	1.000	1.000	1.000

* The original values quoted by Yuen *et al.* [99] were q_c=0.95 and q_c=0.89 for calcite and aragonite, respectively (see *Table 8.1*). These were adjusted so that $q_c + 3q_o = -2.000$

Once the lattice energies had been calculated using the optimized energy parameters, it became clear that the Coulombic energy was rather insensitive to the charge distribution and changed only slightly (by 0.1% - 0.3%) over the six trials. The lattice energy varied by approximately 1% - 5%, with $MgCO_3$ and $BaCO_3$ being the least influenced. The $W_{r,v}/W_c$ ratio remained at ~2% and ~14% for $MgCO_3$ and $BaCO_3$, respectively, and was independent of the charge distribution, while for the other carbonates it fluctuated between ~4% and ~8%. Both the lattice energy and the $W_{r,v}/W_c$ ratio for $MgCO_3$ and $BaCO_3$ appear to be out of sequence (see *Table 8.5*). This occurred for all the trial distributions.

The choice of one set of empirical interatomic parameters over others depends largely on the correct predictions of experimentally observed crystal properties [51]. The charge distribution of *Trial 1* led to the most accurate relaxed structures and was thus selected. The optimized short-range parameters, $OPT7^c$ (for the calcite isomorphous structures; $MgCO_3$, $CaCO_3$) and $OPT8^a$ (for the aragonite isomorphous structures; $CaCO_3$, $SrCO_3$, $BaCO_3$) are shown in *Table 8.3*. A comparison of experimental and relaxed properties is given in *Table 8.4*, and the energy contributions to the lattice energy for *Trial 1* are shown in *Table 8.5*.

Table 8.3 Optimized short-range parameters (A_{ij}, ρ_{ij} and C_{ij}) for the alkaline-earth metal carbonates. All energy parameters were optimized using the CO_3^{2-} charge distribution as indicated for *Trial 1*, (see *Table 8.2*).

Parameters	$OPT7^c$	$OPT8^a$	OPT^{c+a}
A_{ij}/kJ mol^{-1}			
O-O	6.46542x10^5	2.83041x10^5	4.73143x10^5
Mg-O	9.09465x10^5		
Ca-O	5.64031x10^5	8.92411x10^5	4.50897x10^5
Sr-O		6.69437x10^5	3.21931x10^5
Ba-O		0.18677x10^5	0.15098x10^5
ρ_{ij}/Å			
O-O	0.2761	0.2828	0.2694
Mg-O	0.2193		
Ca-O	0.2595	0.2492	0.2625
Sr-O		0.2674	0.2860
Ba-O		0.4796	0.4903
C_{ij}/kJ mol^{-1} Å^6			
O-O	1.73014x10^4	1.25212x10^4	0.782344x10^4
RDWST	1.85	14.07	51.40

$OPT7^c$ = optimized parameter set for calcite isomorphous structures
$OPT8^a$ = optimized parameter set for aragonite isomorphous structures
OPT^{c+a} = optimized parameters set for the calcite and aragonite structures (excluding $MgCO_3$)

Table 8.4 Cell constants (a, b, c, α), Volume (V) and lattice energies (W) for fitted carbonates using OPT7[c] and OPT8[a].

		a/Å	α/deg	V/Å^3	W/kJ mol^{-1}
OPT7[c] (*calcite structures*)					
$MgCO_3$	expt.	5.6751	48.18	93.02	-3282
	calc.	5.6752	48.18	93.20	-3414
	% error	0.00	0.00	-0.2	-4 0
$CaCO_3$	expt.	6.3750	46.08	122.62	-3004
	calc.	6.3527	46.31	122.95	-2986
	% error	0.35	0.50	-0.3	0 6

		a /Å	b /Å	c /Å	V /Å^3	W/kJ mol^{-1}
OPT8[a] (*aragonite structures*)						
$CaCO_3$	expt.	4.9614	7.9671	5.7404	226.91	-3004
	calc.	4.9583	7.9843	5.7406	227.26	-2964
	% error	0.06	-0.22	0.00	-0.15	-1 3
$SrCO_3$	expt.	5.090	8.358	5.997	254.97	-2824
	calc.	5.090	8.312	6.023	254.82	-2825
	% error	0.00	0.55	-0.07	0.06	0 0
$BaCO_3$	expt.	5.3126	8.8958	6.4284	303.81	-2700
	calc.	5.3170	8.8182	6.5056	305.02	-2439
	% error	-0.44	0.87	-1.20	-0.40	9 6

*Lattice energies calculated with the Kapustinskii equation [85] (see *Appendix A*).
OPT7[c] = optimized parameter set for calcite isomorphous structures
OPT8[a] = optimized parameter set for aragonite isomorphous structures

Table 8.5 Contributions to the lattice energy (using parameters OPT7[c] and OPT8[a]) for the alkaline-earth metal carbonates.
W= total lattice energy, W_c= Coulombic energy and $W_{r,v}$= short-range energy (repulsion plus van der Waals energy calculated from the Buckingham potential)

	W_c /kJ mol^{-1}	$W_{r,v}$ /kJ mol^{-1}	$W_{r,v}/W_c$ %	W /kJ mol^{-1}
Trial I (using OPT7[c] and OPT8[a])				
$MgCO_3$	-3494	80	2.3	-3414
[c]$CaCO_3$	-3160	179	5.5	-2986
[a]$CaCO_3$	-3107	143	4.6	-2964
$SrCO_3$	-2997	172	5.7	-2825
$BaCO_3$	-2835	396	14.0	-2439

[c]$CaCO_3$ = calcite [a]$CaCO_3$ = aragonite

The agreement between the calculated and experimental structural properties is good. Deviations are generally less than 0.5% (except for $BaCO_3$). The lattice energies, compared to the values calculated from the Kapustinskii equation [85], show irregularities in the energies calculated for $BaCO_3$ (and perhaps $MgCO_3$), which are supported by the out-of-sequence $W_{r,v}/W_c$ ratios (see *Table 8.5*).

The potentials, OPT7[c] and OPT8[a], were fitted independently, either to the physical properties of the calcite or to those of the aragonite structures. Since it is highly desirable to obtain a transferable unique potential that would account simultaneously for the properties of all the carbonates ($CaCO_3$ (calcite), $CaCO_3$ (aragonite), $SrCO_3$ and $BaCO_3$), an optimization was performed on the combined carbonate structures (excluding $MgCO_3$, since sufficient observables were available). The charge distribution of CO_3^{2-} indicated by *Trial 1* (*Table 8.2*) was used and, as starting values for the short-range parameters, an average of OPT7[c] and OPT8[a] was used. The fitting proceeded surprisingly well, and converged to the parameter set OPT9[c+a] reported in *Table 8.3*. The structural properties computed with OPT9[c+a] are as would be expected, not as accurate as the values determined from OPT7[c] and OPT8[a] individually (compare *Table 8.4* and *8.6*), but the deviations are still acceptable (except, perhaps for $BaCO_3$).

Table 8.6 Cell constants (*a, b, c,* α), Volume (*V*) and lattice energies (W) for fitted carbonates using OPT9[c+a].

		a/Å	α/deg	V/Å^3	W/kJ mol^{-1}
OPT9[c+a] *(calcite and aragonite structures)*					
[c]$CaCO_3$ expt.		6.3750	46.08	122.62	-3004*
	calc.	6.4847	44.98	124.96	-2986
	% error	-1.7	2.4	-1.9	0.6
		a /Å	*b* /Å	*c* /Å	*V* /Å^3	W/kJ mol^{-1}
[a]$CaCO_3$ expt.		4.9614	7.9671	5.7404	226.91	-3004*
	calc.	4.9719	7.8846	5.7666	226.06	-2921
	% error	-0.21	1.0	-0.46	-0.4	2.7
$SrCO_3$	expt.	5.090	8.358	5.997	254.97	-2824*
	calc.	5.098	8.221	6.076	254.65	-2782
	% error	-0.16	1.6	-1.3	0.1	1.5
$BaCO_3$	expt.	5.3126	8.8958	6.4284	303.81	-2700*
	calc.	5.3155	8.7109	6.6335	307.15	-2431
	% error	-0.05	2.1	-3.2	-1.1	10.0

*Lattice energies calculated with the Kapustinskii equation [85] (see *Appendix A*).
OPT9[c+a] = optimized parameter set for the calcite and aragonite structures (excluding $MgCO_3$).
[c]$CaCO_3$ = calcite; [a]$CaCO_3$ = aragonite

Table 8.7 Contributions to the lattice energy (using parameters $OPT9^{c+a}$) for the alkaline-earth metal carbonates.
W= total lattice energy, W_c= Coulombic energy and $W_{r,v}$= short-range energy (repulsion plus van der Waals energy calculated from the Buckingham potential)

	W_c /kJ mol^{-1}	$W_{r,v}$ /kJ mol^{-1}	$W_{r,v}/W_c$ %	W /kJ mol^{-1}
Trial 1 (using $OPT9^{c+a}$)				
$^cCaCO_3$	-3151	244	7.7	-2907
$^aCaCO_3$	-3112	192	6.2	-2921
$SrCO_3$	-3000	218	7.3	-2782
$BaCO_3$	-2833	40	14.2	-2431

$^cCaCO_3$ = calcite $^aCaCO_3$ = aragonite

Finally, the parameters of $CaCO_3$ (calcite and aragonite) were refined (by excluding all other carbonates, *i.e.*, $MgCO_3$, $SrCO_3$ and $BaCO_3$ from the optimization) so that comparisons with other reported studies on $CaCO_3$ could be made. This was done in two stages:

(1) calcite and aragonite were optimized separately (as was done by Pavese, *et al.* [46]), yielding optimized parameter sets $OPT10^c$ and $OPT11^a$

(2) calcite and aragonite were optimized together (as was done by Yuen, *et al.* [99]), yielding parameters $OPT12^{c+a}$

The optimized parameters for the sets $OPT10^c$, $OPT11^a$ and $OPT12^{c+a}$ are shown in *Table 8.8*. The results of relaxing the structure to equilibrium geometry with the derived parameters are given in *Table 8.9*, and the calculated lattice energies in *Table 8.10*. (The notation for the recorded lattice energies is as follows: *e.g.*, in $WMIN^s$ ($OPT10^c$, $OPT11^a$) and $WMIN^t$ ($OPT12^{c+a}$), the subscripts "s" and "t" indicate that the parameters were optimized *separately* or *together* for calcite and aragonite, and the optimized parameters which were used in the energy calculation appear in brackets). The optimized parameters are quite different (with the oxygen parameters showing the largest variation, *i.e.*, the A_{o-o} decrease by three orders of magnitude from the values reported by Pavese, *et al.* [46]. The C-O parameters had no effect on the optimization (no CO_3^{2-} intramolecular interactions were considered as was done in the study by Pavese *et al.* and the C-O intermolecular terms were insignificant) and were removed. No direct comparison could be made with the values reported by Yuen *et al.*, because a different analytical form for the repulsion term was used, *i.e.*,

$$\phi(r) = f(\rho_i + \rho_j)\, e^{\frac{B_i + B_j\, r_{ij}}{\rho_i + \rho_j}} \quad \text{in place of} \quad \phi(r) = A_{ij}\, e^{-\frac{r_{ij}}{\rho_{ij}}}$$

where ρ_i, ρ_j, A_i, A_j and f are adjustable energy parameters.

Table 8.8 Optimized parameters for $CaCO_3$ (calcite and aragonite). Values in columns 2 and 3 are those reported by Pavese, *et al.* [46], and, in columns 4, 5 and 6, those derived with WMIN.

	Pavese, *et al.*		WMIN		
	calcite	aragonite	OPT10^c	OPT11^a	OPT12^{c+a}
A_{ij}/kJ mol^{-1}					
O-O	1.50856x10^8	1.36704x10^8	6.32018x10^5	3.50641x10^5	4.54312x10^5
Ca-O	1.97144x10^5	1.80461x10^5	5.68909x10^5	8.34780x10^5	3.63886x10^5
C-O	1.39531x10^{13}	5.22287x10^{14}			
ρ_{ij}/Å					
O-O	0.1366	0.2107	0.2754	0.2751	0.2632
Ca-O	0.2886	0.2892	0.2597	0.2490	0.2688
C-O	0.0458	0.0402			
C_{ij}/kJ mol^{-1} Å^6					
O-O	3.34815x10^2	3.34815x10^2	1.75353x10^4	1.03669x10^4	0.55908x10^4
RDWST	—	—	0.8446	0.1475x10^{-4}	23.26

OPT10^c = optimized parameter set for calcite
OPT11^a = optimized parameter set for aragonite
OPT12^{c+a} = optimized parameter set for calcite and aragonite

Table 8.9 Cell dimensions (a, b, c, α) and volumes (V) calculated for calcite and aragonite using OPT10^c, OPT11a and OPT12$c+a$.

		a/Å	α/deg	V/Å^3
Calcite	expt.	6.3750	46.08	122.62
OPT10^c	calc.	6.3326	46.53	121.79
	% error	0.67	-0.98	0.68
OPT12^{c+a}	expt.	6.5042	44.80	124.28
	% error	-2.0	2.8	-1.35

		a/Å	b/Å	c/Å	V/Å3
Aragonite	expt.	4.9614	7.9671	5.7404	226.91
OPT11^a	calc.	4.9587	7.9491	5.7608	227.07
	% error	0.05	0.23	0.36	0.07
OPT11^{c+a}	calc.	4.9661	7.8942	5.7888	226.94
	% error	-0.09	0.92	-0.84	-0.01

OPT10^c = optimized parameter set for calcite
OPT11^a = optimized parameter set for aragonite
OPT12^{c+a} = optimized parameter set for calcite and aragonite

Table 8.10 A comparison of the lattice energies (kJ mol^{-1}) reported for $CaCO_3$ (calcite and aragonite). $\Delta W = W_{aragonite} - W_{calcite}$

W /kJ mol^{-1}	calcite	aragonite	W /kJ mol^{-1}
Therm. cycle	-2810	—	
1976: J	-2814	-2820	6
1978: Y	-3017	-3046	29
1995: $WMIN^s$ ($OPT7^c$, $OPT8^a$)	-2986	-2964	-22
1995: $WMIN^t$ ($OPT9^{c+a}$)	-2907	-2921	4
1995: $WMIN^s$ ($OPT10^c$, $OPT11^a$)	-2987	-2949	-38
1995: $WMIN^t$ ($OPT12^{c+a}$)	-2882	-2890	8

Therm. cycle = W determined from the thermochemical cycle [74].
J = Jenkins, *et al.* [98]
Y = Yuen, *et al.* [99]
$WMIN^s$ = W calculated from parameters in which the calcite and aragonite structures were optimized separately, showing in brackets which parameters were used.
$WMIN^t$ = W calculate from parameters in which the calcite and aragonite structures were optimized together.

The lattice energy of aragonite is reported [97-99] to be slightly higher than that for calcite. Reported values for the enthalpy of transition (ΔH_{tr}) for the calcite-aragonite transformation range between 0.21 and 4.88 kJ mol^{-1} (see *Table 8.12*). Both Jenkins, *et al.* [98], and Yuen *et al.* [99], found that aragonite had the higher lattice energy, but the difference in the two energies ($\Delta W = W_{aragonite} - W_{calcite}$ in *Table 8.10*) is higher than the reported values, *i.e.*, 6 and 29 kJ mol^{-1}, respectively. From this investigation, it is interesting to note that only the lattice energies calculated from energy parameters in which the calcite and aragonite structures were optimized together, *i.e.*, $WMIN^t(OPT9^{c+a})$ and $WMIN^t(OPT12^{c+a})$, show this trend, with the ΔW values being 14 and 8 kJ mol^{-1}, respectively. The other calculated energies ($WMIN^s$) are in the reverse order. A comparison with the study by Pavese, *et al.* [46], (in which the parameters were optimized separately for calcite and aragonite) could not be made since no lattice energies were reported.

The optimized parameters set $OPT9^{c+a}$ was used for modelling the decomposition of the carbonates since all the carbonates were involved in the fitting and the resultant lattice energies appeared to be the most accurate (except for $BaCO_3$)

8.3 SETTING THE DECOMPOSITION PATHWAY

8.3.1 Overview

Modelling the thermal decomposition of the carbonates on the basis of symmetry-controlled transformations is more complicated than modelling decomposition of the peroxides. The same basic assumptions (p 51) apply to the carbonate decompositons, except that the reactant may have either:

(a) the rhombohedral calcite structure, space group $R\bar{3}m$, e.g., $CaCO_3$, or

(b) the orthorhombic aragonite structure, space group *Pmcn, e.g.*, $CaCO_3$, $SrCO_3$ or $BaCO_3$.

The decompositions of calcite ($CaCO_3$) and the aragonite-structured carbonates ($CaCO_3$, $SrCO_3$, $BaCO_3$) were modelled separately. It has been reported [102] that, on heating, the aragonite-structured carbonates first undergo a phase transition to the calcite structure (discussed in *Section 8.3.3*) before decomposing.

8.3.2 Calcite

Three symmetry-controlled routes, *viz.*, PATH I, PATH II and PATH III were investigated. *Fig 8.1* outlines part of the decomposition route, *i.e.*, to *structure 4** (a common structure through which all three pathways pass) while *Fig 8.2* shows the complete route for PATH III.

PATH I: Removal of CO_2 (*structure 2a*) is followed by dilation of the angles from 46.08° to 90° (*structure 3*) and then compression of the sides from 6.3750 Å to $a = c = 3.3905$ Å, $b = 4.795$ Å (*structure 4**).

PATH II: Dilation of the angles from the initial 46.08° to 90° to form a cubic structure (*structure 2b*) is followed by removal of CO_2 (*structure 3*) and then compression of the sides as in PATH I (*structure 4**).

PATH III: The first step involves both dilating the angles to 90° and compressing the sides to 4.795 Å (*cubic structure 2c*). This is followed by removal of CO_2 (*structure 3c*) and a further compression, *i.e.*, $a = c = 3.3905$ Å, yielding the tetragonal lattice (*structure 4*).

The proposed routes all pass through the common structure, *structure 4**, which is a redefinition of *structure 4*. Redefining the unit cell from *structure 4** to *structure 4* as shown in *Fig 8.2*, represents a cross-over point, transforming the reactant's body-centred unit cell with $Z=2$ ($CaCO_3$) to the face centred unit cell for the product with $Z=4$ (CaO). The lattice dimensions for *structure 4** were compressed to the indicated values (*i.e.*, tetragonal with $a = c = 3.3905$ Å, $b = 4.795$ Å) so that the redefined unit cell (*structure 4*) would have the same dimensions as that of CaO (*structure 5*).

Fig 8.1 Three postulated symmetry-controlled routes, PATH I, PATH II and PATH III for the decomposition of $CaCO_3$. *Fig 8.2* completes the transformations from *structure 4** for PATH III.

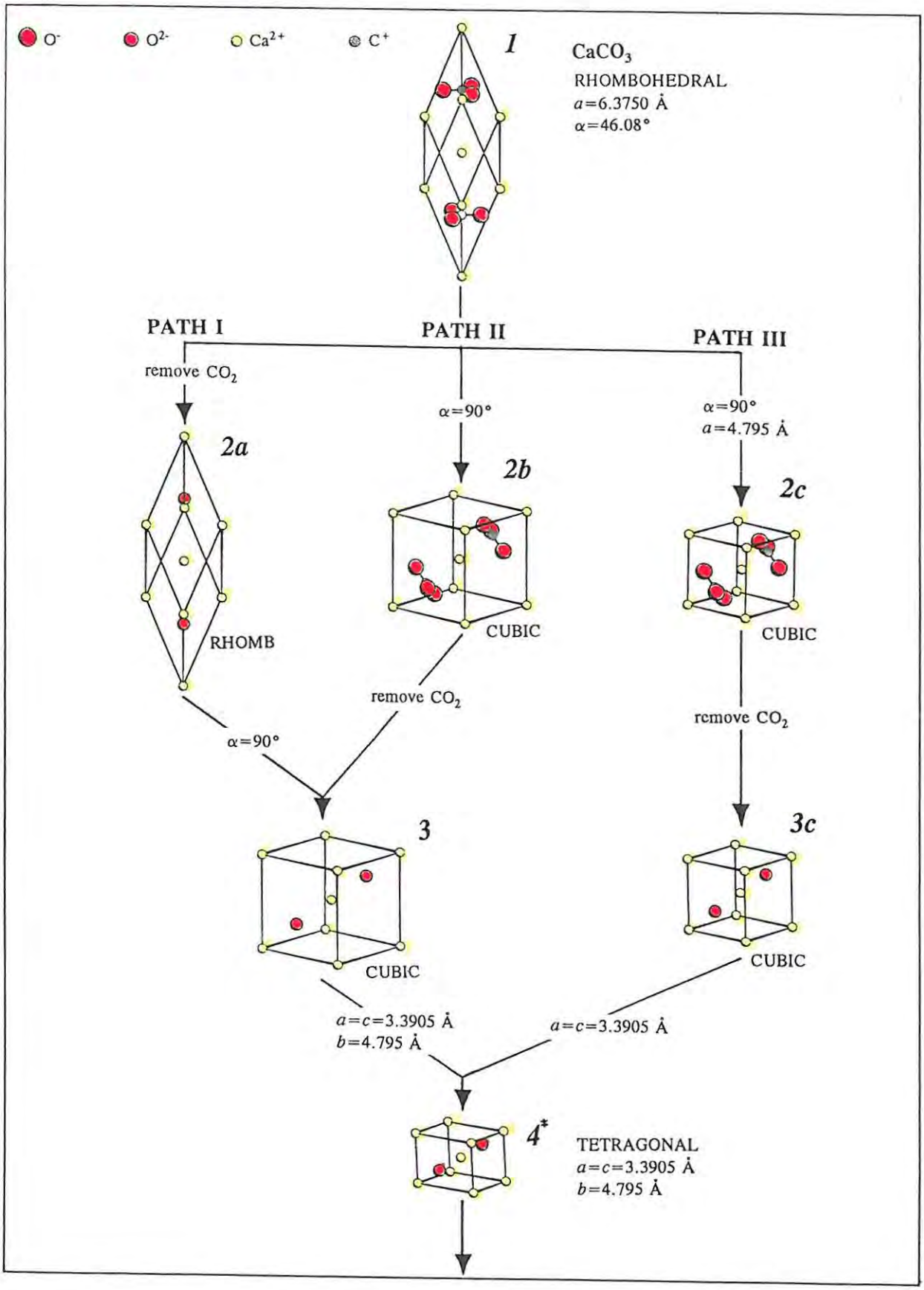

Fig 8.2 Complete symmetry-controlled transformation for the postulated route, PATH III, for the decomposition of $CaCO_3$ to CaO.

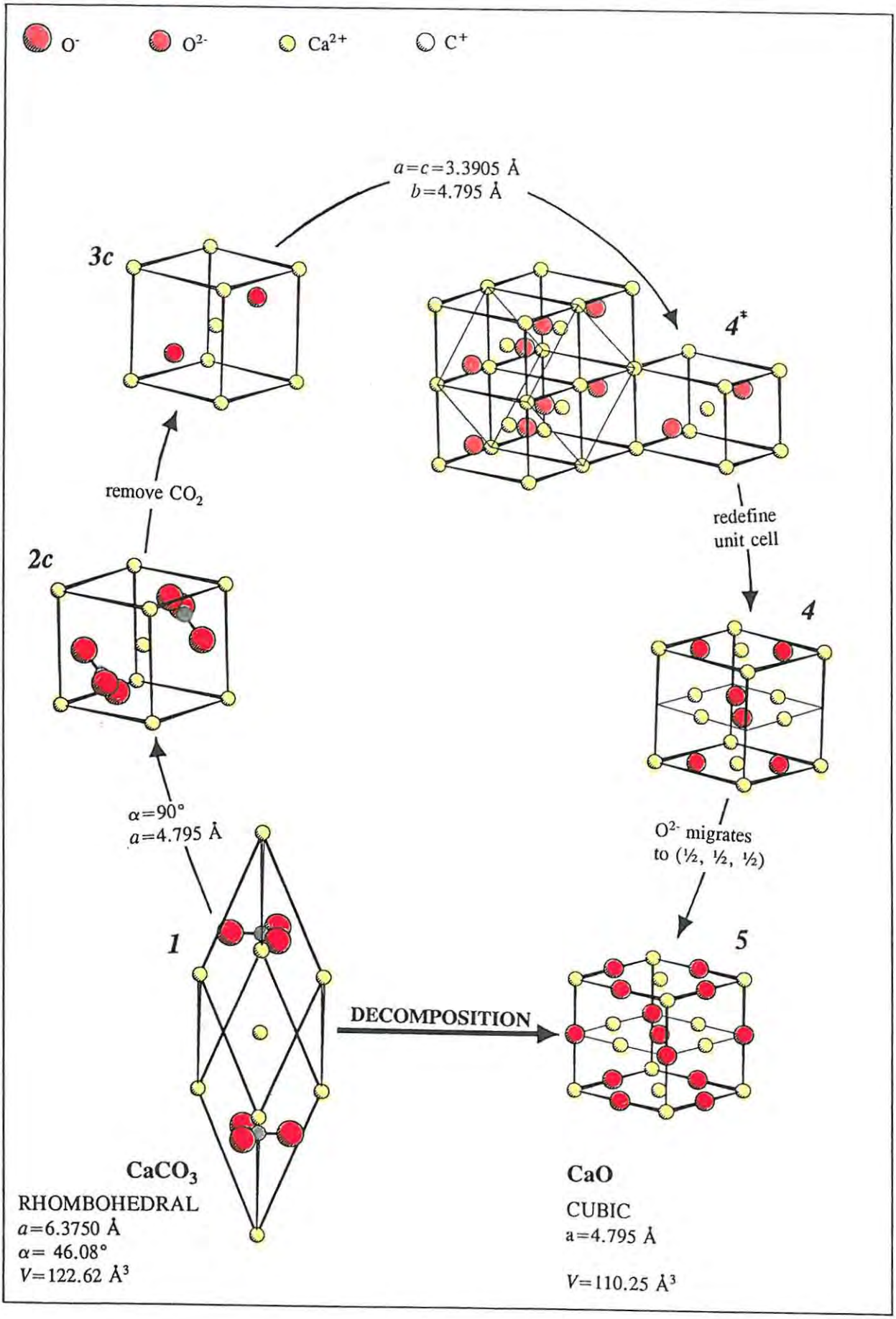

The calcium and oxygen atomic positions in *structures 4* and *5* are closely related, both being generated by the same symmetry operations (see *Section 5.2*), *i.e.*, if the translational vectors (½, ½, 0), (½, 0, ½) and (0, ½, ½) are added to any one of the O^{2-} fractional coordinates, the remaining positions are generated (see *Table 8.11*). Thus, the migration of O^{2-} from, for example, (¼, ¾, ½) in *structure 4* to (½, ½, ½) in *structure 5*, produces the full symmetry set of $Fm\bar{3}m$ displayed by the cubic product CaO.

Table 8.11 Fractional coordinates for atoms in *structures 4* and *5*.

Structure 4				
Ca^{2+}	(0, 0, 0)	(½, ½, 0)	(½, 0, ½)	(0, ½, ½)
O^{2-}	(¼, ¼, 0)	(¾, ¾, 0)	(¾, ¼, ½)	(¼, ¾, ½)
Structure 5				
Ca^{2+}	(0, 0, 0)	(½, ½, 0)	(½, 0, ½)	(0, ½, ½)
O^{2-}	(½, 0, 0)	(0, ½, 0)	(½, ½, ½)	(0, 0, ½)

The positions of the atoms are required to be in fractional coordinates for WMIN. Thus, for any alteration to the unit cell while it still includes the CO_3^{2-} ion (*e.g.*, *structures 2b* and *2c*), the atomic coordinates of the complex ion had to be redetermined to preserve the space group symmetry and the geometry of the carbonate ion (*i.e.*, bond angles = 120° and bond lengths = 1.281 Å). These calculations were performed by means of a program, DELRHOMB.MCD, written by Prof L Glasser [103], for transforming rhombohedral coordinates and is run by the package MATHCAD [104]. (The file can be seen in *Appendix G*).

8.3.3 The kinetics of the aragonite-calcite transformation

The kinetics of the aragonite-calcite transformation has been extensively studied [105-115]. The transition (orthorhombic ⟶ rhombohedral) has a small, positive enthalpy of transition (ΔH_{tr}), but has a high activation energy (E_a). Experimental values of the transition temperature (T_{tr}), the enthalpy of transition and the activation energy are given in *Table 8.12*. The thermodynamic and kinetic parameters for the transition are sensitive to particle-size, impurities content and sample treatment, *e.g.*, grinding, thus a wide range of values, depending on the experimental conditions, has been reported.

The aragonite-calcite transformation is described as a *first-coordination reconstructive transformation* [102], where first coordination bonds are broken and reformed, *i.e.*, the coordination number of Ca^{2+} changes from 9 (in aragonite) to 6 (in calcite). Such transformations involve high activation energies and give rise to large discontinuities, for example, in the cell dimensions, symmetry, internal energy, *etc.*

It has recently been proposed that the aragonite ⟶ calcite phase transition could be achieved by a dislocation glide mechanism [106] instead of the classical diffusion one [116]. According to this model, the transition takes place by motion of partial dislocation causing a shear of the Ca^{2+} sublattice. The Ca^{2+} sublattice is hexagonal close-packed in aragonite and cubic close-packed in calcite. The transition between these two stackings can be achieved by successive layers being shifted laterally over each other, dragging stacking faults which have structures identical with, or closely related to, those of the other polymorph (explained in detail in *ref.* 103).

Table 8.12 Reported values of the transtion temperature (T_{tr}), the enthalpy of transition (ΔH_{tr}) and the activation energy (E_a) for the arogonite-calcite transition.

Reference		T_{tr} /°C	ΔH_{tr} /kJ mol^{-1}	E_a /kJ mol^{-1}	Experimental condition
1973: Rao	[107]	476	0.36	410	DTA
1975: Rao	[108]	387-478	0.21	420	DTA
1978: Rao and Mehrotra	[109]	480-513	3.50	360	DTA
			0.98-4.88	160-703	effect of impurities
1980: Topot, *et al.*	[110]	330-420		205	thermodilatometry
1982: Morales, *et al.*	[111]	485	0.43	566±40	isothermal
				250	DTA
				575±30	DSC
1983: Morales, *et al.*	[112]			561	isothermal
				251-749	DTA
1992: Perić, *et al.*	[113]	410-499		251-276	DTA
1992: Lui and Yund	[114]			247	polycrstaline
				163	single-crystal
1993: Dubrawski and England	[115]	420-505	0.30-0.56		

8.3.4 Aragonite, strontianite and witherite

The symmetry-controlled transformations postulated for the decomposition of the aragonite structures were based on those of calcite on the assumption that the aragonite ⟶ calcite phase transitions [108] precede decomposition. Modelling of the transition, although an interesting problem, was not attempted. PATH III (*Fig 8.3*) was used to compare the behaviour of $CaCO_3$, $SrCO_3$ and $BaCO_3$. *Fig 8.3* omits *structure 4**, since *structure 4** and *4* are derived from the same lattice and have the same lattice energy. The dimensions of *structure 4* are however, dependent on those of *structure 4** (as shown in *Fig 8.2*) and are listed for $CaCO_3$, $SrCO_3$ and $BaCO_3$ in *Table 8.13*.

Table 8.13 Lattice dimensions for *structures 3c*, *4** and *4* in the decompositions of $CaCO_3$, $SrCO_3$ and $BaCO_3$. See *Fig 8.2* for explanation of *structure 4**.

Dimentions /Å	$CaCO_3$	$SrCO_3$	$BaCO_3$
structure 3c: (CUBIC)			
a	4.795	5.1396	5.496
*structure 4**: (TETRAGONAL)			
a=c	3.3905	3.6342	3.886
b	4.795	5.1369	5.496
structure 4: (CUBIC)			
a	4.795	5.1396	5.496

The lattice dimensions of all the calculated structures (from *structure 2* onwards) are based more on the dimensions of the product oxide than on the reactant carbonate. The assumption is that, since the decomposition is endothermic, the structure of the activated complex would be more similar to that of the product oxide than to the reactant carbonate [117]. The proposed route for aragonite is identical to that of calcite (PATH III), and modifications made for $SrCO_3$ and $BaCO_3$ (involving the lattice dimension, *a*, *b*, and *c*) were based on the dimensions of the resultant oxides.

8.3.5 Refined symmetry-controlled route

On the assumption that the energy barrier would result from the removal of CO_2, the transition from *structure 2c* to *3c*, *i.e.*, the point of removal of CO_2, was investigated. The lattice energies of the two structures (*i.e.*, before and after release of CO_2) are related to each other, since both structures have the same lattice dimensions. To find the dimensions which would yield the lowest lattice energies in both *2c* and *3c*, the structures were compressed in stages starting from the dimensions of the product oxide, *i.e.*, 4.795 Å, 5.496 Å, 5.496 Å for $CaCO_3$, $SrCO_3$ and $BaCO_3$, respectively.

Fig 8.3 Postulated symmetry-controlled route, PATH III, for the decomposition of $SrCO_3$ and $BaCO_3$. *Structure* 4^* has been omitted (*cf. Fig 8.2*), since *structures* 4^* and *4* are derived from the same lattice and have the same lattice energy.

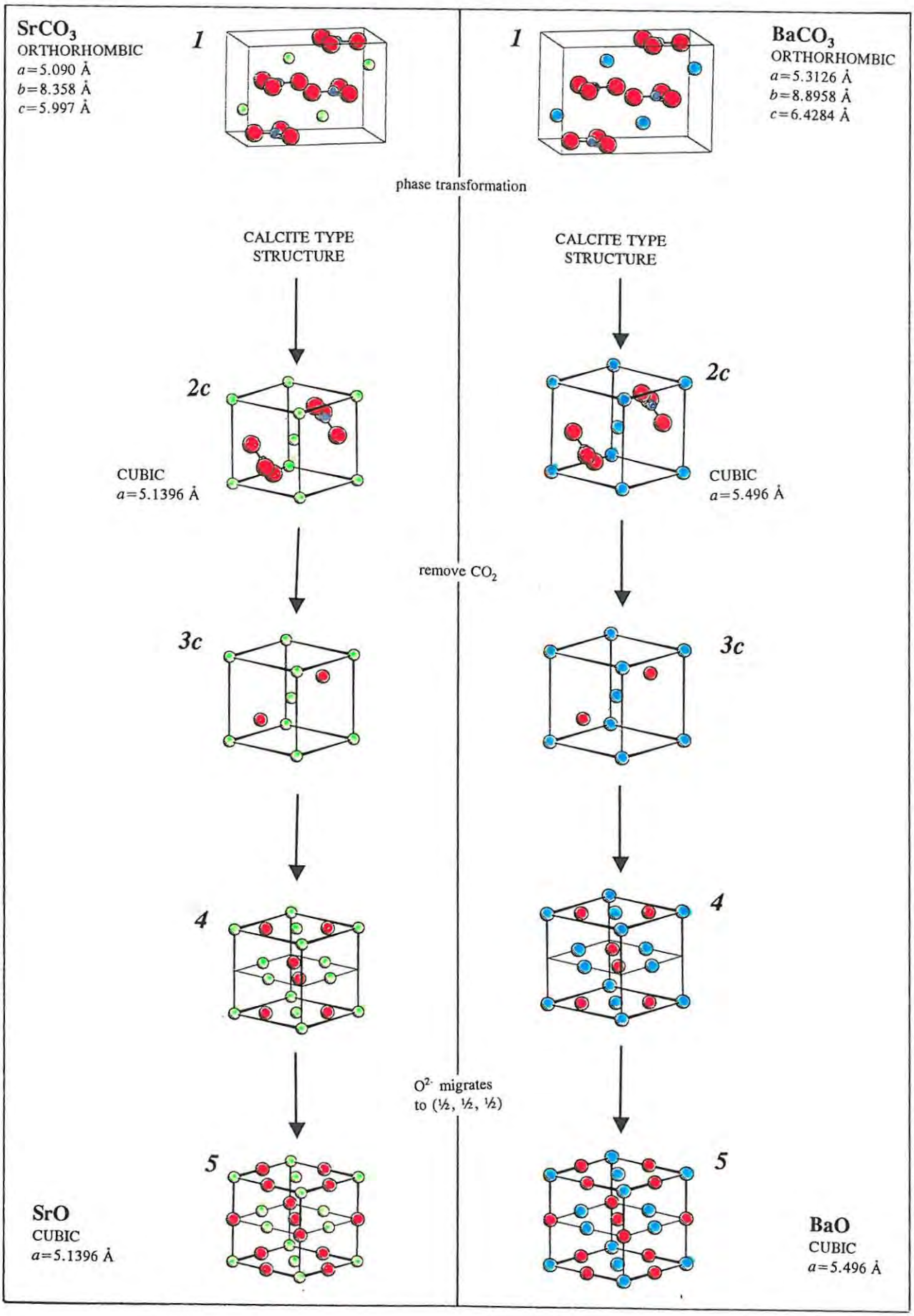

9. RESULTS AND DISCUSSION

9.1 CALCULATED LATTICE ENERGIES

Lattice energies (W) calculated using WMIN for the structures in the proposed decomposition routes, *i.e.*, PATH I, PATH II and PATH III (*Fig 8.1* and *8.2*) for calcite and PATH III (*Fig 8.3*) for aragonite, strontianite and witherite, are listed in *Table 9.1* and *9.2*. The lattice energies corrected for the removal of CO_2 ($W_{corrected}$) (see *Section 9.2*) and the change in the corrected lattice energy with reference to *structure 1* (ΔW_1), are also shown.

Table 9.1 Calculated lattice energies (W) for the decomposition of calcite. $W_{corrected}$ = W corrected for the removal of CO_2 and ΔW_1 = change in the corrected energies with reference to *structure 1* ($CaCO_3$).

Structure	W /kJ mol^{-1}	$W_{corrected}$ /kJ mol^{-1}	ΔW_1 /kJ mol^{-1}
PATH I			
1	-2907	-2709	0
2a	-2926	-2169	738
3	-2758	-2001	906
4	-3403	-2646	261
5	-3486	-2729	178
PATH II			
1	-2907	-2907	0
2b	-2357	-2357	550
3	-2758	-2001	906
4	-3403	-2646	261
5	-3486	-2729	178
PATH 111			
1	-2907	-2907	0
2c	-2921	-2590	317
3c	-3402	-2447	460
4	-3403	-2646	261
5	-3486	-2729	178

Table 9.2 Calculated lattice energies (W) for the decomposition of aragonite, strontianite and witherite. $W_{corrected}$ = W Corrected for the removal of CO_2 and ΔW_1 = change in the corrected energies with reference to *structure 1*.

Structure	W /kJ mol^{-1}	$W_{corrected}$ /kJ mol^{-1}	ΔW_1 /kJ mol^{-1}
$CaCO_3$ (*aragonite*)			
1	-2921	-2921	0
2c	-2590	-259	331
3c	-3204	-2461	460
4	-3403	-2660	199
5	-3486	-2743	178
$SrCO_3$ (*strontianite*)			
1	-2782	-2782	0
2c	-2502	-2502	280
3c	-2951	-2258	524
4	-3176	-2483	299
5	-3240	-2547	235
$BaCO_3$ (*witherite*)			
1	-2431	-2431	0
2c	-2207	-2207	224
3c	-2707	-1851	580
4	-2969	-2113	318
5	-3020	-2164	267

The energies derived for the known structures, *i.e.*, the reactant carbonates (*structure 1*) and solid product oxides (*structure 5*), were compared with thermochemical values [74] and values calculated with the Kapustinskii equation [85] (see *Table 9.3*). The difference in lattice energy between the reactant and product, $\Delta W = W(MCO_3) - W(MO)$, should decrease as the cation size increases from Ca to Ba; this trend is observed for the thermochemical values. For the Kapustinskii equation, ΔW for Ba is slightly greater than for Sr but the obvious deviation of this trend is for Ba (WMIN), where ΔW for Ba is much greater than for Sr. Both the Kapustinskii equation and the potential model used in this investigation to calculate the lattice energies are based on a purely ionic model which does not account for any covalency. The modelling has failed to represent the $BaCO_3$ structure adequately, *i.e.*, using OPT9^{c+a}, the cell constants *a*, *b* and *c*, of $BaCO_3$ deviate by 0.05%, 2.1% and -3.2%, repectively (see *Table 8.6*). To compensate for the simple ionic model used *i.e.*, omitting an explicit description of covalency, the repulsion plus van der Waal energy terms have increased from an average of 7.1% in calcite, aragonite and strontianite to 14.2% in $BaCO_3$ (see *Table 8.7*). Explicit modelling parameters would have to be introduced to account for covalent interaction in $BaCO_3$, making the model more flexible and improving the description of the lattice energy. Otherwise there is good agreement between the three sets of values (*cf.* ΔW in peroxides, *Table 7.2*).

Table 9.3 Comparison of lattice energies (kJ mol^{-1}) for the reactant carbonates and solid product oxide, calculated using WMIN with reported values. The difference between the lattice energies, $\Delta W = W(MCO_3) - W(MO)$, are also shown.

W/kJ mol^{-1}		^{c}Ca	^{a}Ca	Sr	Ba
WMIN:	$W(MCO_3)$	-2907	-2921	-2782	-2431
	W(MO)	-3486	-3486	-3240	-3021
	ΔW	**579**	**565**	**458**	**590**
Kapust. eqn:	$W(MCO_3)$	-2873	*	-2730	-2647
[85]	W(MO)	-3465	-3465	-3261	-3088
	ΔW	**592**		**531**	**534**
Therm. cycle:	$W(MCO_3)$	-2810	*	-2688	-2554
[74]	W(MO)	-3401	-3401	-3223	-3054
	ΔW	**591**		**535**	**500**

*No lattice energy is available for aragonite using the thermochemical cycle [74] or Kapustinskii equation [85]. ^{c}Ca - refers to calcite in MCO_3, ^{a}Ca - refers to aragonite in MCO_3

9.2 CORRECTION FOR THE REMOVAL OF CO_2

To relate the changes in lattice energy to the changes in energy associated with the decomposition of the carbonate, corrections have to be made for the removal of CO_2 from the lattice. The procedure is the same as in the peroxides, *Section 7.2, i.e.*, the processes under consideration are:

$$MCO_3(s) \longrightarrow M^{2+}(g) + CO_3^{2-}(g) \quad .....\Delta H_1 \qquad (1)$$

$$MO(s) \longrightarrow M^{2+}(g) + O^{2-}(g) \quad .....\Delta H_2 \qquad (2)$$

$$MCO_3(s) \longrightarrow MO(s) + CO_3^{2-}(g) - O^{2-}(g) \quad .....\Delta H_3 \qquad (3)$$

$$MCO_3(s) \longrightarrow MO(s) + CO_2(g) \quad .....\Delta H_4 \qquad (4)$$

$$CO_3^{2-}(g) \longrightarrow CO_2(g) + O^{2-}(g) \quad .....\Delta H_5 \qquad (5)$$

Reaction (5) represents the reaction that takes place on removal of CO_2 from the lattice and therefore ΔH_5 must be added to those energies calculated from the lattice devoid of CO_2. The standard enthalpy changes for the carbonate decompositions, $\Delta H_4 = \Delta H_f^{\ominus}(MO) - \Delta H_f^{\ominus}(MCO_3)$, were calculated from tables of thermodynamic data [88]. The ΔH values for reactions (1) to (5) are listed in *Table 9.4*. The energies corrected for the removal of CO_2 are shown in *Table 9.1* (for calcite) and *Table 9.2* (for aragonite, strontianite and witherite). From the decomposition profile *i.e.*, lattice energies corrected for the removal of CO_2 ($W_{corrected}$) plotted against course of reaction, an apparent activation energy (E_a) can be calculated. From the proposed decomposition routes for calcite, *i.e.*, PATH I, PATH II and PATH III, E_a was calculated to be 906, 906 and 460 kJ mol^{-1} repectively. For aragonite, strontianite and witherite (PATH III), E_a was calculated to be 460, 524 and 580 kJ mol^{-1}, respectively.

Table 9.4 Enthalpies of reaction (in kJ mol^{-1}) of the reactions defined in the text.

	calcite	*aragonite structures*		
	$^cCaCO_3$	$^aCaCO_3$	$SrCO_3$	$BaCO_3$
$\Delta H_1 \approx$ -W $(MCO_3)^*$	2907	2921	2782	2431
$\Delta H_2 \approx$ -W $(MO)^*$	3486	3486	3240	3020
$\Delta H_3 = \Delta H_1 - \Delta H_2$	579	565	458	589
ΔH_4	178	178	235	267
$\Delta H_5 = \Delta H_4 - \Delta H_3$	757	743	693	856

*Lattice energies calculated for the carbonates with $OPT9^{c+a}$ and for the oxides with OPT2
$^cCaCO_3$ = calcite; $^aCaCO_3$ = aragonite

9.3 ACTIVATION ENERGIES FOR THE REFINED SYMMETRY-CONTROLLED ROUTE

The proposed reaction routes, PATH III (*Fig 8.2*) for calcite and the aragonite structured carbonates (*Fig 8.3*) were refined, as described is *Section 8.3.5*, by compressing the dimensions of *structures 2c* and *3c* in stages. The lattice energy for *structure 2c* increases while that for *structure 3*c decreases, as the initial unit cell dimensions are compressed. This trend is shown for calcite in *Table 9.5* . After the lattice energies are corrected for the removal of CO_2 (in *structure 3c*) and calculated with reference to the lattice energy of the reactant (ΔW_1), the energy barrier for each structure can be seen. For calcite, a contraction of 5% in the initial unit cell dimension yields the lowest combined E_a, *i.e.*, 408 and 422 kJ mol^{-1} for *structure 2c* and *3c* repectively. This refinement reduces the overall E_a for PATH III from 460 kJ mol^{-1} (a=4.795 Å) to 422 kJ mol^{-1} (a=4.555 Å). Further contraction of a results in a overall higher E_a (see Table 9.5). The same procedure decreased the activation energies (of PATH III) from 460, 524 and 580 kJ mol^{-1} to 422, 465 and 499 for $CaCO_3$ (aragonite), $SrCO_3$ and $BaCO_3$ respectively.

Table 9.5 The lattice energies calculated with WMIN (W) are shown for *structure 2c* and *3c* in the decomposition of $CaCO_3$ (calcite), see *Fig 8.2*. $W_{corrected}$ = W corrected for the removal of CO_2 and ΔW_1 = change in the corrected lattice energy with reference to *structure 1* ($CaCO_3$)

% contraction	a/Å	*structure 2c* W	ΔW_1	*structure 3c* W	$W_{corrected}$	ΔW_1
0	4.795	-2590	317	-3204	-2447	460
4	4.603	-2525	328	-3238	-2481	426
5	4.555	-2499	**408**	-3242	-2485	**422**
6	4.507	-2468	439	-3244	-2487	420

Fig 9.1 Lattice energies corrected for the removal of CO_2 ($W_{corrected}$) plotted against course of reaction (for calcite, PATH III refined as discussed in *Section 9.3*).

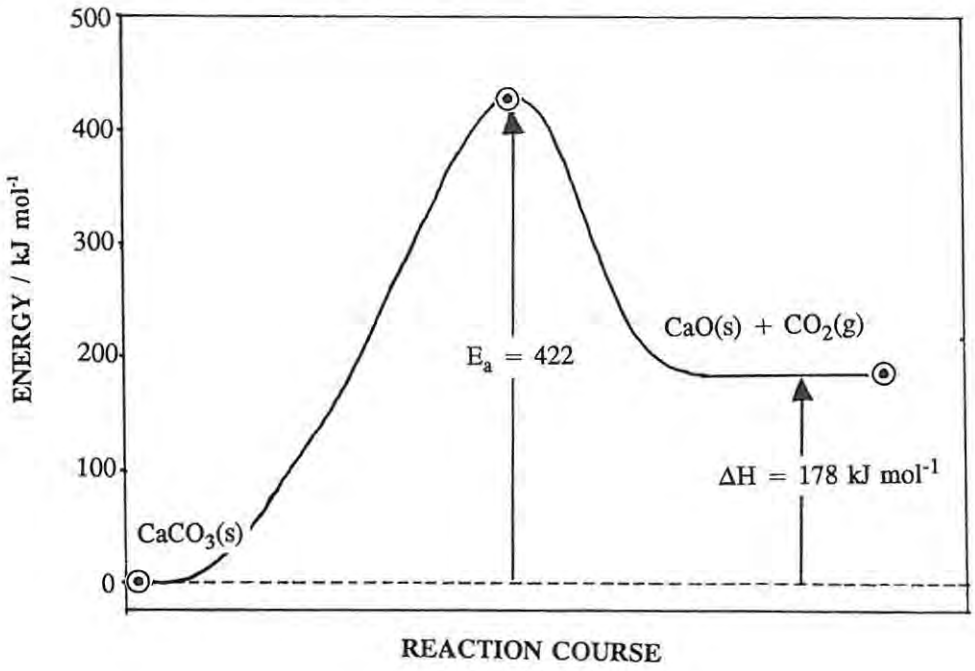

9.4 EXPERIMENTAL VALUES FOR THE ACTIVATION ENERGY OF DECOMPOSITION OF ALKALINE-EARTH CARBONATES

9.4.1 Calcite

The kinetics of the thermal decomposition of $CaCO_3$ are well known to be dependent upon many factors, for example, the nature of the solid reactant (single crystal, powder) its pretreatment (grinding, *etc.*, which influence the defect content), the sample mass and experimental conditions, *i.e.*, the presence or absence of CO_2, the temperature, pressure, *etc.* Due to the influence of these varying conditions, experimental E_a values ranging from ~ 110 to ~ 1600 kJ mol^{-1} have been reported. Perhaps the most clearly-defined experiments are those of Powell and Searcy [118]. They used single crystals of calcite, and the decomposition was studied in vacuum in an attempt to remove any influence of heat transfer or product gas diffusion. The product was shown to be crystalline CaO. They reported an E_a value of 205 $\pm$ 13 kJ mol^{-1} for the decomposition of $CaCO_3$ under negligible back-pressure of CO_2.

Both the presence of CO_2 and a decrease in sample mass produce an increase in the experimental values of E_a [119]. The presence of CO_2 is not taken into account in the present calculation based on lattice energies, where the total removal of CO_2 is in effect, assumed. The reported influence of decreasing sample mass suggests that the E_a value obtained (422 kJ mol^{-1}) in the symmetry-controlled route could fit into the extrapolation pattern given by Gallagher and Johnson [119] of 303 kJ mol^{-1} for a 1μm particle; 378 kJ mol^{-1} for a 10 nm particle, continuing quite feasibly to about 420 kJ mol^{-1} for a single unit cell (~ 0.6 nm).

The standard enthalpy of decomposition of $CaCO_3$ is 178 kJ mol^{-1} at 298 K. In vacuum, decomposition occurs at a measurable rate at about 1100 K. The value of the enthalpy of reaction at 1100 K is calculated from

$$\Delta H_{1100K} = \Delta H_{298K} + \int_{298}^{1100} \Delta C_P \, dT$$

and $\Delta H_{1100\,K} = 170$ kJ mol^{-1}.

Some of the activation energies reported lie below the value of 178 kJ mol^{-1} for the standard enthalpy of reaction at 298 K (or 170 kJ mol^{-1} at 1100 K). One of the fundamental problems in comparing values of E_a and ΔH is that the "mole" referred to may not be the same species. ΔH refers to a mole of *reactant*, while E_a refers to a mole of *activated complex*. In the decomposition of solids it is usually

assumed, perhaps without justification, that the "activated complex" (whatever its interpretation is) is derived from the unit of reactant, *e.g.*,

$$CaCO_3(s) \longrightarrow [CaCO_3]^{\#} \longrightarrow \text{products}$$

Shannon [117] has applied *activated complex theory* (ACT) to the thermal decomposition of solids and discussed the possible nature of the activated complex in the calcite decomposition. The study was prompted by the success of ACT in predicting rates of evaporation of solids, and expanded on earlier work by Polanyi and Wigner [120]. The estimation of the partition function for the activated complex involved in the decomposition for calcite was described, *i.e.*, $CaCO_3$ was considered as a single unit and the degrees of freedom arise from:

(1) External vibrations (analogous to translation degrees of freedom in a gas)

(2) Torsional oscillations (equivalent to rotational freedom in the gaseous stage)

(3) Free rotations of the CO_3^{2-} ion.

(4) Internal vibrations of the CO_3^{2-} ion.

Fig 9.2 The activated complex as it may occur in the decomposition of a carbonate (proposed by Shannon) [117].

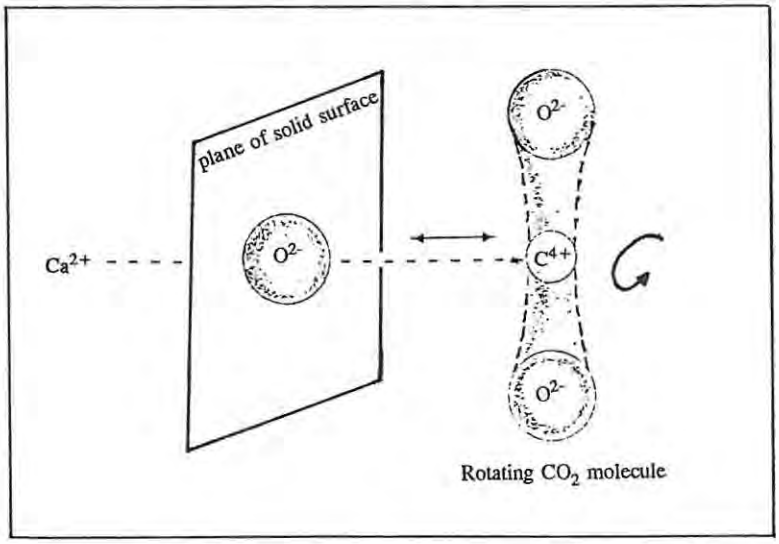

The assumption was made that the Ca^{2+} ions undergo only minor changes in position during formation of the activated complex, and no changes in energy. The only atoms actively involved in the reaction are those in the CO_3^{2-} ion. From experimental evidence for the torsional motion of the CO_3^{2-} ion during phase transitions, Shannon proposed complete rotation of the CO_3^{2-} ions at decomposition temperatures,

and hence, estimated partition functions for the reactant (Q_R), as well as for the products, CaO(s) and CO_2(g), (Q_P). Although the partition function of the products does not appear in the Eyring equation for estimation of the rate constant, the value of the partition function for the activated complex (Q^*) must lie somewhere between that of the reactant and that of the products. The assumption was made that for exothermic reactions, Q^* is close to Q_R, and for endothermic decompositions (such as that of calcite) Q^* is close to Q_P.

Shannon used experimental values of vibrational and rotational frequencies to estimate partition functions for various possible forms of the activated complex. He obtained reasonable agreement between experimental and predicted pre-exponential factors when free rotation of the CO_3^{2-} ion was allowed, but reports no estimates of the activation energy.

9.4.2 Aragonite, strontianite and witherite

The aragonite-structured carbonates first undergo a phase transition to the calcite structure [102] (discussed in *Section 8.3.3*) and therefore, in several respects, the decomposition behaviour of the aragonite-structured carbonates is similar to that for calcium carbonate. Criado, *et al.* [121], made a comparative study of the alkaline-earth metal carbonates and postulated that the decomposition of each MCO_3 gives rise to the same activated complex. Judd and Pope [122] found that the mechanism of decomposition of $SrCO_3$ and $BaCO_3$ is similar to that described by Hills [123] for calcite.

The thermal stability of the alkaline-earth metal carbonates increases as the cation size increases [124], hence the activation energy increases across the series $CaCO_3 \longrightarrow BaCO_3$. There is a wide range of reported E_a values (as for $CaCO_3$), with most lower than or equal to the standard enthalpy of decomposition. Judd and Pope [122] reported E_a = 222 kJ mol^{-1} for $SrCO_3$ and 283 kJ mol^{-1} for $BaCO_3$. Criado, *et al.*, [121] reported similar values, *i.e.*, 251 and 259 kJ mol^{-1} respectively. The respective enthalpies of decomposition are 235 and 267 kJ mol^{-1}. Calvo, *et al.* [125], found that the activation energy of aragonite decomposition is smaller (by 24 kJ mol^{-1}) than that for calcite and reported values of 111 and 87 kJ mol^{-1} for calcite and aragonite repectively. Compared to the more reliable value reported by Powell and Searcy [118] for calcite, *i.e.*, 205 kJ mol^{-1}, a more reasonable activation energy for aragonite would be ~180 kJ mol^{-1}.

9.5 DISCUSSION

The activation energies predicted in this study for the decompositions of the carbonates are in the correct order but higher than experimental values, *i.e.*, 422, 422, 465 and 499 kJ mol^{-1} compared to the experimental values of 205, 87(?), 222 and 283 kJ mol^{-1} for $CaCO_3$ (calcite), $CaCO_3$ (aragonite), $SrCO_3$ and $BaCO_3$. The elevated values could suggest that the lowest energy route has not been found. There are many ways in which the crystal structure of a reactant could be converted into the crystalline product, while losing some gaseous fragments. Three proposed decomposition route were investigated for calcite (*i.e.*, PATH I, PATH II and PATH III) giving energy barriers of 906, 906 and 460 kJ mol^{-1} respectively, and after further refinements to PATH III, an E_a value of 422 kJ mol^{-1} was obtained. Other pathways may lead to even lower energy barrier reaction pathways.

Defects (deviations from perfect periodicity in a crystal), although present in small concentrations, are known to play a role in lowering the activation energy. The sites in the crystal at which decomposition is initiated are undoubtedly regions of crystallographic disorder [126]. The full range from point defects, through line defects, to extended defects such as crystallographic shear (CS) planes has been invoked in decomposition mechanisms. Some reasons proposed [126] for enhanced reactivity at defect sites are:
(1) the strain energy of the defect (*e.e.*, dislocation) lowers the activation energy for nucleation;
(2) there may be favourable stereochemical factors in operation around defects;
(3) defects may act as a source of, or sink for, impurities, which may alter the electron distribution; and
(4) defects may provide "relaxation space" and/or preferential diffusion pathways.
The introduction of defect energy calculations may decrease the E_a for the symmetry-controlled routes proposed in this investigation, thus bringing the calculated activation energies closer to the experimental values.

The reliability of the interatomic potentials was assessed by calculating crystal structural properties and lattice energies (which were not included in the fitting) The overall agreement (except for $BaCO_3$) between experimental and calculated values provides support for the general adequacy and success of the potential model used. It is significant that the small difference (*i.e.*, 14 kJ mol^{-1}) in the lattice energies of calcite and aragonite was observed. However, the potential model (which is based on the Born model of ionic solids) could be improved and made more flexible to include the bonding features of the carbonates, *i.e.*, strong covalent interactions inside the CO_3 unit, and ionic polarization which is most prevalent in $BaCO_3$. The inadequacy of the simple (rigid-ion) ionic model for $BaCO_3$ can be seen by the increase of the repulsion plus van der Waals energy terms, *i.e.*, $W_{r,v}/W_c$ increased from the average

of 7.1% in calcite, aragonite and strontianite to 14% in $BaCO_3$. This trend does not occur for the oxides, where the short-range energy terms remain relatively constant for the series MgO, CaO, SrO and BaO (*i.e.*, $W_{r,v}/W_c$ is 15.6, 14.0, 14.4, 14.6 respectively). Pavese, *et al.*, [46] proposed extra parameters which model the inter- and intra-molecular interactions in $CaCO_3$ more effectively.

The crystal data of the carbonates used as reference are very accurate (*i.e.*, R-values range between 0.02 and 0.033 and calculated densities all fall within the 5% error range) and this seems to make a large difference to the reliability of the interatomic parameters (*cf.* the peroxides).

10. CONCLUDING REMARKS

Possible pathways for the decompositions of ionic solids: A(s) ⟶ B(s) + gases, have been modelled by calculating the lattice energies of the solid structures possibly involved in the reaction. The substances chosen for modelling were the alkaline-earth metal peroxides and carbonates. The changes of lattice energy of an ionic compound, during its transformation from crystalline reactant to crystalline product with accompanying release of a gaseous molecule have been examined to see whether they can be related to experimentally determined activation energies for the thermal decomposition ionic solids. Any model only becomes useful when it is proved to be physically realistic. We have demonstrated the feasibility of the model by calculating reasonable activation energies for the decomposition of the alkaline-earth metal carbonates. The values calculated for the peroxides are less satisfactory, but could be a reflection of the poor structural data used for the peroxides.

Lattice energy is a bulk property, but decomposition of a solid will, at highest resolution, involve the breakdown of individual ions, e.g., the conversion of a single peroxide ion into an oxide ion and an oxygen atom (*i.e.*, $O_2^{2-} \longrightarrow O^{2-} + O$), or decomposition of the carbonate ion with release of CO_2 (*i.e.*, $CO_3^{2-} \longrightarrow O^{2-} + CO_2$). This process takes place in a matrix of the appropriate cations. Several different environments will be experienced by the anion depending upon the symmetry of the surrounding matrix. This symmetry decreases as one compares anions in the bulk of the crystal with anions on a planar surface; on a surface step or crystal edge; or on a crystal corner or sharp protuberance; or at a grain boundary, dislocation or within fine cracks. In this study, only anions in the bulk of the crystals have been considered and the possible influences of lattice energy on such decompositions have been investigated. Decomposition of anions in the other environments is physically more realistic and might be expected to occur with lower energy barriers.

Experimental studies of decompositions of solids are, with few exceptions, low resolution bulk measurements of changes in mass of a sample, or accumulated pressure of gas evolved from the sample [1]. Such measurements thus average out the individual behaviour at the molecular level. This averaging effect of the experimental technique would thus justify comparison of experimentally measured activation energies with a lattice energy profile. No allowance was made in the calculation of lattice energies for the presence of defects of any kind, so the profiles obtained should correspond to the limit of experimental work on perfect crystalline material.

A key factor in determining lattice energies is the determination of accurate and transferable potentials. In this study a simple ionic model (with non-polarizable atoms) was chosen in order to establish what might be the simplest possible viable model. The reliability of the interatomic potentials was assessed by calculating crystal structures and lattice energies (which were not included in the fitting). The lattice enegies for the peroxides could not be accurately evaluated since the reference lattice energies showed inconsistensies. The overall agreement between experimental and calculated values for the carbonates (except for $BaCO_3$) provides support for the adequacy of the potential model used. The transferability of the potentials (from the perfect lattice to the hypothetical intermediate structures in the proposed decomposition routes) is not known, but there is evidence which indicates that potentials of the present form are transferable.

There are inherent problems in the determination of interatomic potentials by *empirical fitting*, for example, having sufficient independent observables. It is also preferable to use a wide range of crystal properties (*i.e.*, structural, elastic, vibrational and dielectric properties) in the fitting procedure, but this is not always possible since only the lattice constants are available for many compounds. The procedure, used in this investigation, of reducing the structures of the known compounds to triclinic systems, seems successful in increasing the number of independent observables in the fitting.

Basic improvements to the calculation which could be made include making the potential model more consistent with the actual bonding of the system involved (by including interatomic parameters which account for the explicit description of covalency and ionic polarization) and including defect energy calculations. There is considerable experimental evidence [1], that decomposition is favoured in regions of a crystal of decreased symmetry relative to the bulk material In computational methods, an essential component of any quantitative study of defect energies, is *lattice relaxation*, since there are always extensive displacements of the surrounding atoms following the formation of a defect. The original computer program HADES by Norgett [127] for calculating defect energies in cubic ionic crystals and the revised codes [128] to treat defects in crystals of any symmetry, were landmarks in the development of defect chemistry and physics. Other more sophisticated programs are now available for investigating the role of defects.

There are many ways in which the crystal structure of a reactant could be converted into a crystalline product, while losing some gaseous constituents. In this study, it has been assumed that this conversion will occur *via* a relatively high degree of symmetry, with the unit cell dimensions and angles adjusting in a regular fashion. This may not appear to be a useful assumption if one is looking at the detailed

process within a *single* unit cell. Removal of a gaseous constituent will then occur through one face (say) of the unit cell, with corresponding distortions of the other parts of the cell. This situation is most similar to the application of activated complex theory suggested by Shannon [117]. The closest experimental approach to such a situation is probably the work of Searcy *et al.*[118] on gas evolution from selected crystal faces.

Many systems can be suggested for extending the exploratory study of this thesis. The removal of H_2O and SO_2, respectively, in the decomposition of $Ca(OH)_2$ and $CaSO_3$ would both yield CaO as the solid product, *i.e.*,

$$Ca(OH)_2(s) \longrightarrow CaO(s) + H_2O(g)$$

$$CaSO_3(s) \longrightarrow CaO(s) + SO_2(g)$$

and the decompositions of the alkaline-earth metal oxalates, *via* MCO_3, which are well-documented experimentally, would be an interesting extension.

$$M(C_2O_4)(s) \longrightarrow MCO_3(s) + CO(g)$$

Other more general systems which could be considered include the removal of (a) H_2O from hydrates, (b) N_2 from azides and (c) ligands from coordination compounds.

A more complex model of the $CaCO_3$ system might include:

(a) a perfect crystal surface

(b) a defective crystal surface (point defects)

(c) internal defects (dislocations, *etc.*)

APPENDIX A

KAPUSTINSKII EQUATION

Kapustinskii [85] advocated the use of *eqn* (A.1), known as the Kapustinskii equation, to calculate the lattice energy of ionic solids of unknown lattice structure. The Kapustinskii equation includes only the Coulombic and repulsion energy terms and replaces the interatomic distance, r_0, with the sum of ionic radii, $\langle r \rangle$, and thus the lattice energies are not as exact as those produced by extended calculations.

$$W/kJ\ mol^{-1} = \frac{1213.9}{\langle r \rangle}\left(1 - \frac{0.345}{\langle r \rangle}\right) \nu\, z_1 z_2 \qquad (A.1)$$

where $\langle r \rangle = r_C + r_A$, *i.e.*, the sum of the ionic radii. r_C is the cation radius and r_A is the anion radius, ν is the number of ions in the formula unit and z_1, z_2 are the valencies of the ions.

The accuracy of the calculated lattice energy dependens on the ionic radii used in the equation. No ion (or atom) has a precisely defined radius and therefore assumptions are required to get an empirically useful set of radii. Early efforts to do this were made by Goldschmidt [129] and Pauling [130] and later (with the availability of relatively accurate experimental electron density maps) by Shannon [131]. The lattice energies (listed in *Table A.2*) of all the alkaline-earth metal oxides, peroxides and carbontes have been calculated using the ionic radii (and thermochemical radii for the complex anion) [132] shown in *Table A.1*.

Table A.1 Ionic Radii [132]

Ion	Radius/Å	Ion	Radius/Å
Cation:		**Anion:**	
Mg^{2+}	0.78	O^{2-}	1.32
Ca^{2+}	1.06	O_2^{2-}	1.73
Sr^{2+}	1.27	CO_3^{2-}	1.78
Ba^{2+}	1.43		

Table A.2 Lattice energies (kJ mol^{-1}) calculated using the Kapustinskii equation and ionic radii from *Table A.1*

	Oxides	Peroxides	Carbonates
Mg	-3865	-3337	-3282
Ca	-3489	-3050	-3004
Sr	-3250	-2865	-2824
Ba	-3088	-2738	-2700

APPENDIX B

ATOMIC FRACTIONAL COORDINATES

The fractional coordinates of all atoms in one unit cell for $CaCO_3$ (aragonite), $SrCO_3$ (strontianite) and $BaCO_3$ (witherite).

	$CaCO_3$	$SrCO_3$	$BaCO_3$
Cation: M^{2+}			
M1	0.2500 0.4150 0.7597	0.2500 0.4160 0.7569	0.2500 0.4163 0.7549
M2	0.7500 0.5850 0.2403	0.7500 0.5840 0.2431	0.7500 0.5837 0.2451
M3	0.7500 0.9150 0.7403	0.7500 0.9160 0.7431	0.7500 0.9163 0.7451
M4	0.2500 0.0850 0.2597	0.2500 0.0840 0.2569	0.2500 0.0837 0.2549
Anion: CO_3^{2-}			
C1	0.2500 0.7622 0.9138	0.2500 0.7601 0.9136	0.2500 0.7570 0.9190
$O1_a$	0.2500 0.9225 0.9038	0.2500 0.9119 0.9054	0.2500 0.9011 0.9122
$O1_b$	0.4736 0.6810 0.9138	0.4694 0.6821 0.9161	0.4595 0.6839 0.9210
$O1_c$	0.0264 0.6810 0.9138	0.0306 0.6821 0.9161	0.0405 0.6839 0.9210
C2	0.7500 0.2378 0.0862	0.7500 0.2399 0.0864	0.7500 0.2430 0.0810
$O2_a$	0.7500 0.0775 0.0962	0.7500 0.0881 0.0946	0.7500 0.0989 0.0878
$O2_b$	0.5264 0.3190 0.0862	0.5306 0.3179 0.0839	0.5264 0.3161 0.0790
$O2_c$	0.9736 0.3190 0.0862	0.9694 0.3179 0.0839	0.9736 0.3161 0.0790
C3	0.7500 0.2622 0.5862	0.7500 0.2601 0.5864	0.7500 0.2570 0.5810
$O3_a$	0.7500 0.4225 0.5962	0.7500 0.4119 0.5946	0.7500 0.4011 0.5878
$O3_b$	0.9736 0.1810 0.5862	0.9694 0.1821 0.5839	0.9736 0.1839 0.5790
$O3_c$	0.5264 0.1810 0.5862	0.5306 0.1821 0.5839	0.5264 0.1839 0.5790
C4	0.2500 0.7378 0.4138	0.2500 0.7399 0.4136	0.2500 0.7430 0.4190
$O4_a$	0.2500 0.5775 0.4038	0.2500 0.5881 0.4054	0.2500 0.5989 0.4122
$O4_b$	0.0264 0.8190 0.4138	0.0306 0.8179 0.4161	0.0405 0.8161 0.4210
$O4_c$	0.4736 0.8190 0.4138	0.4694 0.8179 0.4161	0.4595 0.8161 0.4210

APPENDIX C

WMIN INPUT DATA FILE

C.1 Format

The input data file is in a highly structured format. Data must be entered in the specified lines and within the specified column range. The file can be divided into three sections:

(a) dimensions used to set up array storage; input (1)

(b) title card, control card and common parameter cards; inputs (2) to (10)

(c) substance data cards; inputs (11) to (35)

(Note: all input numbers will be abbreviated as "INP X", where X is the number.

C.2 Array storage

WMIN uses many arrays with dimensions which depend on the particular problem under study. Since there is such a broad range of problems, dynamic dimensioning of arrays is used, rather than fixed dimension statements, to conserve storage. The storage for these arrays is set up by the first 16 integers (INP 1). If the storage space is insufficient when WMIN is run, the user is prompted as to the dimension needed and correction must be made before continuing. The overall size of the storage is established by a subroutine MASTER. This size may be enlarged by re-compiling only that small routine. The dynamic dimensioning procedure is a feature of WMIN which is likely to cause difficulties when different computers, or different operating systems, are used [45].

C.3 Overall title, control card and common parameter cards

The *overall title card* (INP 2) allows a title (using up to 72 characters) to be given to the problem under study.

There are 14 entries for the *overall control card* (INP 3). The MODE is the first and has been discussed in *Section 4.2*. The number of cycles of refinement (NC) is important for the optimisation functions. If only the lattice energy calculation is needed, this indicator can be set to zero. Printed output is controlled by the output print indicator IPRT, which may be set by the user to a value from 0 to 5. A value of 0 causes all output (all the intermediate quantities and matrices used in the calculation) to be printed; a value of 3 may be suitable for normal problems and an IPRT of 5 severely limits the output.

The *common parameter* cards, INP 4 to 10, deal with the energy parameters of the model. The energy parameters are named (NAMPC) and assigned values (PC), and the indicator KPC allows one to set which energy parameter(s) are to be adjusted in MODE 0.

C.4 Substance data cards

These data entries are specific to a particular substance and they begin with the *substance identification card*, where a title (preferably a comprehensive title) is given, for example, "$CaCO_3$ (calcite) SG: R3-C #167 RHOMBOHEDRAL". This provides immediate recognition of the substance, space group and number in the International Tables for X-ray Crystallography [58] and lattice type.

The *control card*, INP 12, (which is different from the overall control card, INP 3) contains 22 entries. The items NA, NS, NRB (number of atoms in asymmetric unit, number of symmetry cards and number of rigid bodies, respectively), are not unique values, they are related through the choice of the asymmetric unit. For example, the atom coordinates can be entered with appropriate matrices to generate repeats of the asymmetric unit. Alternatively, atoms can be entered explicitly with only the identity symmetry operation, resulting in the unit cell becoming the asymmetric unit. These different methods of modelling the same structure lead to different values of NA, NS and NRB. If IZAM, the indicator which controls the size of the formula unit for which the energy is calculated, is set to zero, then the program selects the smallest unit (the asymmetric unit) which contains an integral number of each atom. The number of formula units can be cross-checked in the output, by examining the values ZMC.

The indicators which govern the selection of energy terms to be included in the calculation are also in the *control card*. There are options for Coulombic, van der Waals and repulsive energies, with indicators ICMB, IVDW and IREP, respectively. ICMB and IVDW can be set to either 1 or 0, indicating that the energy will, or will not, be calculated. The repulsion, on the other hand, can be calculated in the standard way by the user's routine REPL, and/or by the user's routine GPOT; the indicator IREP can be set to a value from 0 to 7 depending on which terms are to be included

The energy unit, which can be either kcal mol^{-1} or kJ mol^{-1}, is determined by the indicator IKJ. If IKJ = 0, the units are kcal mol^{-1}, otherwise for IKJ = 1 the units are kJ mol^{-1}. The factor applied to the Coulomb terms is adjusted accordingly, but the user must supply input energy parameters AR, BR, PL, WOBS, *etc.*, in the selected units. Energy parameters for each chemically different kind of atom (K) are entered in INP 19: Q(K) is the charge in units of protons; PL(K) the coefficient in the van der Waals energy; AR(K) the radius of the atom for the repulsion energy; BR(K) the softness coefficient in the repulsion energy; and AMASS(K) the mass in atomic mass units (only required for vibrational analysis).

The crystallographic data are entered as follows:

- Lattice parameters, INP 16: cell constants a, b, c and cosines of α, β, γ
- Symmetry operations, INP 18: only one card for each symmetry generation is needed to generate all the atoms in the cell. Redundant symmetry cards (cards which repeat symmetry already present) can be included since the program omits replicated atoms.
- Fractional atomic coordinates, INP 20: one card for each atom in the asymmetric unit.

INP 21 to 23 deal with rigid bodies; IRB(K) is an integer which specifies the rigid body (defined as an atom or group of atoms which translates or rotates independently) to which atom K belongs. INP 22 assigns rigid-body reference axes, either to the crystal axes or to specified atoms. If a group of atoms acts as a rigid body, then the connection table, INP 23, allows the "backbone" and the associated atoms to be linked. For example, for the rigid body CO_3, the three oxygen atoms are recorded as bonded to the C backbone atom.

APPENDIX D

GPOT: An Algorithm to calclulate short-range energy terms

The algorithm used to calculate the van der Waals and repulsion energy in the form of the Buckingham potential, *i.e.*,

$$\phi(r) = Ae^{-\frac{r}{\rho}} - \frac{C}{r^6}$$

```
C  FOR ISB=1:  Ca=1  C=2  O=3
C  FOR ISB=2:  Ca=1  C=2  O=3
C  FOR ISB=3:  Sr=1  C=2  O=3
C  FOR ISB=4:  Ba=1  C=2  O=3

      IF (ISB.EQ.1. OR .ISB.EQ.2. OR .ISB.EQ.3. OR. ISB.EQ.4) THEN
C   O-O INTERACTION
        IF ( (IK.EQ.3.AND.JK.EQ.3) ) THEN
          GPOT = A(1) * DEXP( -R/B(1) ) - ( C(1)/(R**6.0) )
C   C-O INTERACTION
C       ELSEIF ( (IK.EQ.2.AND.JK.EQ.3).OR.(IK.EQ.3.AND.JK.EQ.2)) THEN
C         GPOT = A(2) * DEXP( -R/B(2) )
        ENDIF
      ENDIF
C
C
      IF (ISB.EQ.1. OR. ISB.EQ.2) THEN
C   Ca-O INTERACTION
        IF ( (IK.EQ.1.AND.JK.EQ.3).OR.(IK.EQ.3.AND.JK.EQ.1) ) THEN
          GPOT = A(3) * DEXP( -R/B(3) )
        ENDIF
      ENDIF

      IF (ISB.EQ.3) THEN
C   Sr-O INTERACTION
        IF ( (IK.EQ.1.AND.JK.EQ.3).OR.(IK.EQ.3.AND.JK.EQ.1) ) THEN
          GPOT = A(4) * DEXP( -R/B(4) )
        ENDIF
      ENDIF
C
      IF (ISB.EQ.4) THEN
C   Ba-O INTERACTION
        IF ( (IK.EQ.1.AND.JK.EQ.3).OR.(IK.EQ.3.AND.JK.EQ.1) ) THEN
          GPOT = A(5) * DEXP( -R/B(5) )
        ENDIF
      ENDIF
```

APPENDIX E

WMIN DATA FILES

E.1 Oxides: calculates lattice energies using OPT2

```
      15        2        2        4        2        0        1        1:INP  1
       0      200    10000       15      200       10       30       15:     1
CALCULATE LATTICE ENERGY for CaO SrO BaO                                :INP  2
  3  3 12  0  0  0  3  5  0   0.0001 0.000001    0.001    0.01     10.0:INP  3
        D      Aoo      Boo      Coo     Amgo     Bmgo     Acao     Bcao:INP  4
     Asro     Bsro     Abao     Bbao                                    :     4
        0 80.38090   0.1733 20.49640 12.13607   0.3004 11.17443   0.3391:INP  5
  8.97697   0.3722  7.56742   0.4049                                    :     5
        1     0.01    0.001     0.01    0.001     0.01    0.001     0.01:INP  6
     0.01    0.001     0.01    0.001                                    :     6
000000000000                                                            :INP  9
000000000000                                                            :INP 10
  2  CaO      SG: Fm3m   #225    CUBIC F                                 :INP 11
  2  2  4  2  0  0  0  2  0 -9  1  0  4  0  0  0  0  1  1  2  0  1      :INP 12
     0.25  2  3                                                         :INP 13
     0.60     0.70                                                      :INP 14
    12.00    13.00    14.00                                            :INP 15
    4.795    4.795    4.795        0        0        0                 :INP 16
             0  1  0  0              0  0  1  0              0  0  0  1:INP 18
             0  1  0  0            0.5  0  1  0            0.5  0  0  1:     18
          0.5  1  0  0              0  0  1  0            0.5  0  0  1:     18
          0.5  1  0  0            0.5  0  1  0              0  0  0  1:     18
Ca           2.0                                                        :INP 19
O           -2.0                                                        :     19
Ca      1                         0        0        0                 :INP 20
O       2                       0.5      0.5      0.5                 :     20
  1  2                                                                  :INP 21
  1  0                                                                  :INP 22
  2  0                                                                  :     22
  0       -0000.0                                                       :INP 29
100000000000                                                            :INP 30
000000000000                                                            :INP 31
  3 SrO    SG: Fm3m  #225    CUBIC F                                    :INP 11
  2  2  4  2  0  0  0  2  0 -9  1  0  4  0  0  0  0  1  1  2  0  1      :INP 12
     0.25  2  3                                                         :INP 13
     0.60     0.70                                                      :INP 14
    12.00    13.00     1540                                           :INP 15
   5.1396   5.1396   5.1396        0        0        0                 :INP 16
             0  1  0  0              0  0  1  0              0  0  0  1:INP 18
             0  1  0  0            0.5  0  1  0            0.5  0  0  1:     18
          0.5  1  0  0              0  0  1  0            0.5  0  0  1:     18
          0.5  1  0  0            0.5  0  1  0              0  0  0  1:     18
Sr           2.0                                                        :INP 19
O           -2.0                                                        :     19
Sr      1                         0        0        0                 :INP 20
O       2                       0.5      0.5      0.5                 :     20
  1  2                                                                  :INP 21
  1  0                                                                  :INP 22
  2  0                                                                  :     22
  0       -0000.0                                                       :INP 29
100000000000                                                            :INP 30
000000000000                                                            :INP 31
  4  BaO      SG: Fm3m   #225    CUBIC F                                 :INP 11
  2  2  4  2  0  0  0  2  0 -9  1  0  4  0  0  0  0  1  1  2  0  1      :INP 12
     0.25  2  3                                                         :INP 13
     0.60     0.70                                                      :INP 14
    12.00    13.00    14.00                                            :INP 15
    5.496    5.496    5.496        0        0        0                 :INP 16
             0  1  0  0              0  0  1  0              0  0  0  1:INP 18
             0  1  0  0            0.5  0  1  0            0.5  0  0  1:     18
          0.5  1  0  0              0  0  1  0            0.5  0  0  1:     18
          0.5  1  0  0            0.5  0  1  0              0  0  0  1:     18
Ba           2.0                                                        :INP 19
O           -2.0                                                        :     19
Ba      1                         0        0        0                 :INP 20
O       2                       0.5      0.5      0.5                 :     20
  1  2                                                                  :INP 21
  1  0                                                                  :INP 22
  2  0                                                                  :     22
  0       -0000.0                                                       :INP 29
100000000000                                                            :INP 30
000000000000                                                             :INP 31
                                                                        :end
```

E.2 Peroxides: calculates lattice energies using OPT4

```
      15        3        2        4        2        0        1        1:INP  1
       0      200    10000       50      200       10       30       15:     1
CALCULATE LATTICE ENERGY for SrO2  BaO2                                 :INP  2
  3  3 10  0  0  0  3  5  0   0.0001 0.000001    0.001    0.01     10.0:INP  3
       D       Aoo       Boo       Coo       Acao      Bcao      Asro     Bsro:INP  4
    Abao      Bbao                                                      :      4
       0 35.86485   0.1546 33.89678  0.00000  0.00000  7.31160   0.3751:INP  5
 1.70120   0.5152                                                      :      5
       1     0.01     0.001     0.01      0.01     0.001     0.01     0.001:INP  6
    0.01    0.001                                                      :      6
000000000000                                                          :INP  9
000000000000                                                          :INP 10
  3 SrO2  SG: I4/mmm  #139    TETRAGONAL I                            :INP 11
  3  2  2  2  0  0  0  2  0 -5  1  0  4  0  1  0  0  1  1  1  0  1    :INP 12
    0.25  2  3                                                        :INP 13
    0.60     0.70                                                     :INP 14
   12.00    13.00    14.00                                           :INP 15
   3.568    3.568    6.616        0        0        0                :INP 16
            0  1  0  0              0  0  1  0              0  0  0  1:INP 18
          0.5  1  0  0            0.5  0  1  0           0.5  0  0  1:     18
Sr            2.0                                                     :INP 19
O            -1.0                                                     :      19
Sr       1                        0        0        0                :INP 20
O1a      2                        0        0   0.3875                :      20
O1b      2                        0        0   0.6125                :      20
  1  2  2                                                            :INP 21
  1  0                                                               :INP 22
  2  0                                                               :      22
  2     3  0  0  0                                                   :INP 23
  0           0                                                       :INP 29
101000000000                                                          :INP 30
000000000000                                                          :INP 31
  4  BaO2    SG: I4/mmm   #139    TETRAGONAL                         :INP 11
  3  2  2  2  0  0  0  2  0 -5  1  0  4  0  1  0  0  1  1  1  0  1    :INP 12
    0.25  2  3                                                        :INP 13
    0.60     0.70                                                     :INP 14
   12.00    13.00    14.00                                           :INP 15
   3.807    3.807    6.841        0        0        0                :INP 16
            0  1  0  0              0  0  1  0              0  0  0  1:INP 18
          0.5  1  0  0            0.5  0  1  0           0.5  0  0  1:     18
Ba            2.0                                                     :INP 19
O            -1.0                                                     :      19
Ba       1                        0        0        0                :INP 20
O1a      2                        0        0   0.3911                :      20
O1b      2                        0        0   0.6089                :      20
  1  2  2                                                            :INP 21
  1  0                                                               :INP 22
  2  0                                                               :      22
  2     3  0  0  0                                                   :INP 23
  0           0                                                       :INP 29
101000000000                                                          :INP 30
000000000000                                                          :INP 31
                                                                      :end
```

E.3 Carbonates: (a) optimizes energy parameters OPT9^{c+a} (symmetry released)

```
      15        20         3         1         8         0         4        40:INP  1
       0      1000     20000        50       200        30       100        15:     1
OPTIMIZE ENERGY PARAMETERS for all carbonates:  (OPT9c+a)                    :INP  2
  0  8 12   0  0  0  3  5  0   0.0001 0.000001    0.001     0.010     10.0:INP  3
        D        Aoo       Boo       Coo       Aco       Bco      Acao      Bcao:INP  4
     Aero       Bsro      Abao      Bbao                                        :     4
        0    4.73143    0.2694   7.82344   0.00000    0.0000   4.50897    0.2625:INP  5
  3.21931     0.2860   0.15098    0.4903                                        :     5
        1       0.01     0.001      0.01      0.01     0.001      0.01     0.001:INP  6
     0.01      0.001      0.01     0.001                                        :     6
000000000000                                                                  :INP  9
011100111111                                                                  :INP 10
  1  CaCO3 (calcite)  SG R3-C  #167  Rhombohedral                             :INP 11
 10  3  1  2  1  1  0  4  0 -5  1  0  4  0  2  0  0  1  1  0  0  1            :INP 12
     0.31  2  2                                                               :INP 13
     0.60     0.70                                                           :INP 14
     12.0     13.0                                                           :INP 15
   6.3750   6.3750   6.3750   0.6937   0.6937   0.6937                       :INP 16
               0  1  0  0              0  0  1  0                 0  0  0  1:INP 18
Ca               2                                                          :INP 19
C             0.985                                                          :     19
O            -0.995                                                          :     19
Ca1      1                            0         0         0                 :INP 20
Ca2      1                       0.5000    0.5000    0.5000                 :     20
C1       2                       0.2500    0.2500    0.2500                 :     20
O1a      3                       0.5068   -0.0068    0.2500                 :     20
O1b      3                      -0.0068    0.2500    0.5068                 :     20
O1c      3                       0.2500    0.5068   -0.0068                 :     20
C2       2                       0.7500    0.7500    0.7500                 :     20
O2a      3                       0.4932    1.0068    0.7500                 :     20
O2b      3                       1.0068    0.7500    0.4932                 :     20
O2c      3                       0.7500    0.4932    1.0068                 :     20
  1  2  3  3  3  3  4  4  4  4                                               :INP 21
  1  0                                                                      :INP 22
  2  0                                                                      :     22
  3  0                                                                      :     22
  4  0                                                                      :     22
  3     4  5  6                                                            :     23
  7     8  9 10                                                            :     23
  0              0        0                                                 :INP 29
111111000000000000                                                            :INP 30
000000000000000000                                                            :INP 31
  2  CaCO3 (Aragonite)  SG Pmcn  #62    ORTHORHOMBIC P                       :INP 11
 20  3  1  2  1  1  0  8  0 -5  1  0  4  0  4  0  0  0  1  0  0  1            :INP 12
  0.28730  2  3                                                              :INP 13
     0.60     0.70                                                           :INP 14
    14.00    15.00    16.00                                                 :INP 15
   4.9614   7.9671   5.7404         0         0         0                   :INP 16
               0  1  0  0              0  0  1  0              0  0  0  1:INP 18
Ca              2.0                                                        :INP 19
C             0.817                                                          :     19
O            -0.939                                                          :     19
Ca1      1                       0.2500    0.4150    0.7597                 :INP 20
Ca2      1                       0.7500    0.5850    0.2403                 :     20
Ca3      1                       0.7500    0.9150    0.7403                 :     20
Ca4      1                       0.2500    0.0850    0.2597                 :     20
C1       2                       0.2500    0.7622    0.9138                 :     20
O1a      3                       0.2500    0.9225    0.9038                 :     20
O1b      3                       0.4736    0.6810    0.9138                 :     20
O1c      3                       0.0264    0.6810    0.9138                 :     20
C2       2                       0.7500    0.2378    0.0862                 :     20
O2a      3                       0.7500    0.0775    0.0962                 :     20
O2b      3                       0.5264    0.3190    0.0862                 :     20
O2c      3                       0.9736    0.3190    0.0862                 :     20
C3       2                       0.7500    0.2622    0.5862                 :     20
O3a      3                       0.7500    0.4225    0.5962                 :     20
O3b      3                       0.9736    0.1810    0.5862                 :     20
O3c      3                       0.5264    0.1810    0.5862                 :     20
C4       2                       0.2500    0.7378    0.4138                 :     20
O4a      3                       0.2500    0.5775    0.4038                 :     20
O4b      3                       0.0264    0.8190    0.4138                 :     20
O4c      3                       0.4736    0.8190    0.4138                 :     20
  1  2  3  4  5  5  5  5  6  6  6  6  7  7  7  7  8  8  8  8                  :INP 21
  1  0                                                                      :INP 22
  2  0                                                                      :     22
  3  0                                                                      :     22
  4  0                                                                      :     22
  5  0                                                                      :     22
  9  0                                                                      :     22
 13  0                                                                      :     22
 17  0                                                                      :     22
  5     6  7  8  0                                                         :     23
```

```
  9    10 11 12  0                                                          :    23
 13    14 15 16  0                                                          :    23
 17    18 19 20  0                                                          :    23
  0       -0000.0                                                          :INP 29
1111110000000000000000000000000                                            :INP 30
0000000000000000000000000000000                                            :INP 31
  3  SrCO3 (Strontianite)  SG Pmcn  #62    ORTHORHOMBIC P                   :INP 11
 20  3  1  2  1  1  0  8  0 -9  1  0  4  0  4  0  0  1  1  0  0  1         :INP 12
  0.28085  2  3                                                            :INP 13
     0.60     0.70                                                         :INP 14
    14.00    15.00    16.00                                                :INP 15
    5.090    8.358    5.997       0        0        0                      :INP 16
             0  1  0  0                0  0  1  0              0  0  0  1:INP 18
Sr             2.0                                                         :INP 19
C             0.817                                                        :    19
O            -0.939                                                        :    19
Sr1     1                        0.2500   0.4160   0.7569                 :INP 20
Sr2     1                        0.7500   0.5840   0.2431                 :    20
Sr3     1                        0.7500   0.9160   0.7431                 :    20
Sr4     1                        0.2500   0.0840   0.2569                 :    20
C1      2                        0.2500   0.7601   0.9136                 :    20
O1a     3                        0.2500   0.9119   0.9054                 :    20
O1b     3                        0.4694   0.6821   0.9161                 :    20
O1c     3                        0.0306   0.6821   0.9161                 :    20
C2      2                        0.7500   0.2399   0.0864                 :    20
O2a     3                        0.7500   0.0881   0.0946                 :    20
O2b     3                        0.5306   0.3179   0.0839                 :    20
O2c     3                        0.9694   0.3179   0.0839                 :    20
C3      2                        0.7500   0.2601   0.5864                 :    20
O3a     3                        0.7500   0.4119   0.5946                 :    20
O3b     3                        0.9694   0.1821   0.5839                 :    20
O3c     3                        0.5306   0.1821   0.5839                 :    20
C4      2                        0.2500   0.7399   0.4136                 :    20
O4a     3                        0.2500   0.5881   0.4054                 :    20
O4b     3                        0.0306   0.8179   0.4161                 :    20
O4c     3                        0.4694   0.8179   0.4161                 :    20
  1  2  3  4  5  5  5  5  6  6  6  6  7  7  7  7  8  8  8  8               :INP 21
  1  0                                                                     :INP 22
  2  0                                                                     :    22
  3  0                                                                     :    22
  4  0                                                                     :    22
  5  0                                                                     :    22
  9  0                                                                     :    22
 13  0                                                                     :    22
 17  0                                                                     :    22
  5     6  7  8  0                                                         :    23
  9    10 11 12  0                                                         :    23
 13    14 15 16  0                                                         :    23
 17    18 19 20  0                                                         :    23
  0       -0000.0                                                          :INP 29
1111110000000000000000000000000                                            :INP 30
0000000000000000000000000000000                                            :INP 31
  4  BaCO3 (Witherite)  SG Pmcn  #62    ORTHORHOMBIC P                     :INP 11
 20  3  1  2  1  1  0  8  0 -9  1  0  4  0  4  0  0  1  1  0  0  1         :INP 12
  0.33623  2  3                                                            :INP 13
     0.80     0.90                                                         :INP 14
    14.00    15.00    16.00                                                :INP 15
   5.3126   8.8958   6.4284       0        0        0                      :INP 16
             0  1  0  0                0  0  1  0              0  0  0  1:INP 18
Ba             2.0                                                         :INP 19
C             0.817                                                        :    19
O            -0.939                                                        :    19
Ba1     1                        0.2500   0.4163   0.7549                 :INP 20
Ba2     1                        0.7500   0.5837   0.2451                 :    20
Ba3     1                        0.7500   0.9163   0.7451                 :    20
Ba4     1                        0.2500   0.0837   0.2549                 :    20
C1      2                        0.2500   0.7570   0.9190                 :    20
O1a     3                        0.2500   0.9011   0.9122                 :    20
O1b     3                        0.4595   0.6839   0.9210                 :    20
O1c     3                        0.0405   0.6839   0.9210                 :    20
C2      2                        0.7500   0.2430   0.0810                 :    20
O2a     3                        0.7500   0.0989   0.0878                 :    20
O2b     3                        0.5405   0.3161   0.0790                 :    20
O2c     3                        0.9595   0.3161   0.0790                 :    20
C3      2                        0.7500   0.2570   0.5810                 :    20
O3a     3                        0.7500   0.4011   0.5878                 :    20
O3b     3                        0.9595   0.1839   0.5790                 :    20
O3c     3                        0.5405   0.1839   0.5790                 :    20
C4      2                        0.2500   0.7430   0.4190                 :    20
O4a     3                        0.2500   0.5989   0.4122                 :    20
O4b     3                        0.0405   0.8161   0.4210                 :    20
O4c     3                        0.4595   0.8161   0.4210                 :    20
  1  2  3  4  5  5  5  5  6  6  6  6  7  7  7  7  8  8  8  8               :INP 21
  1  0                                                                     :INP 22
```

```
  2  0                                                                    :     22
  3  0                                                                    :     22
  4  0                                                                    :     22
  5  0                                                                    :     22
  9  0                                                                    :     22
 13  0                                                                    :     22
 17  0                                                                    :     22
  5     6  7  8  0                                                       :     23
  9    10 11 12  0                                                       :     23
 13    14 15 16  0                                                       :     23
 17    18 19 20  0                                                       :     23
  0        -0000.0                                                      :INP 29
11111100000000000000000000000000                                       :INP 30
00000000000000000000000000000000                                       :INP 31
                                                                       :end
```

E.3 Carbonates: (b) calculates lattice energies using OPT9^{c+a}

```
      15        5        3       12        2        0        1       40:INP  1
       0      500    15000       50      200       30      100       15:     1
CALCULATE LATTICE ENERGY for CaCO3 (a+c) SrCO3 BaCO3                   :INP  2
  3  0 12  0  0  0  3  5  0   0.0001 0.000001    0.001    0.010     10.0:INP  3
       D      Aoo      Boo      Coo      Aco      Bco     Acao     Bcao:INP  4
    Asro     Bsro     Abao     Bbao                                    :     4
       0 4.731430   0.2694  7.82344  0.00000   0.0000  4.50897   0.2625:INP  5
 3.21931   0.2860 0.150976   0.4903                                    :     5
       1     0.01    0.001     0.01     0.01    0.001     0.01    0.001:INP  6
    0.01    0.001     0.01    0.001                                    :     6
000000000000                                                           :INP  9
000000000000                                                           :INP 10
  1  CaCO3 (calcite)  SG R3-C  #167  Rhombohedral                       :INP 11
  5  3 12  2  1  1  0  2  0 -5  1  0  4  0  1  0  0  1  1  0  0  1      :INP 12
    0.30  2  2                                                         :INP 13
    0.60     0.70                                                      :INP 14
    12.0     13.0                                                      :INP 15
  3.3905   3.3905   4.7950   0.0000   0.0000   0.0000                  :INP 16
sA1          0  1  0  0            0  0  1  0            0  0  0  1:INP 18
sB1          0  0  0  1            0  1  0  0            0  0  1  0:     18
sC1          0  0  1  0            0  0  0  1            0  1  0  0:     18
sA2        0.5  0  1  0          0.5  1  0  0          0.5  0  0  1:     18
sB2        0.5  0  0  1          0.5  0  1  0          0.5  1  0  0:     18
sC2        0.5  1  0  0          0.5  0  0  1          0.5  0  1  0:     18
sA3          0 -1  0  0            0  0 -1  0            0  0  0 -1:     18
sB3          0  0  0 -1            0 -1  0  0            0  0 -1  0:     18
sC3          0  0 -1  0            0  0  0 -1            0 -1  0  0:     18
sA4        0.5  0 -1  0          0.5 -1  0  0          0.5  0  0 -1:     18
sB4        0.5  0  0 -1          0.5  0 -1  0          0.5 -1  0  0:     18
sC4        0.5 -1  0  0          0.5  0  0 -1          0.5  0 -1  0:     18
Ca             2                                                       :INP 19
C          0.985                                                       :     19
O         -0.995                                                       :     19
Ca1    1                     0.5000   0.5000  0.5000                  :INP 20
C1     2                     0.2500   0.2500  0.2500                  :     20
O1a    3                     0.5172  -0.0173  0.2500                  :     20
O1b    3                    -0.0173   0.2500  0.5172                  :     20
O1c    3                     0.2500   0.5172 -0.0173                  :     20
  1  2  2  2  2                                                        :INP 21
  1  0                                                                 :INP 22
  2  0                                                                 :     22
  2     3  4  5                                                       :     23
  0              0        0                                           :INP 29
100100000000                                                           :INP 30
000000000000                                                           :INP 31
  2  CaCO3 (Aragonite)  SG Pmcn  #62    ORTHORHOMBIC P                 :INP 11
  5  3  8  2  0  0  0  2  0 -9  1  0  4  0  1  0  0  1  1  0  0  1      :INP 12
  0.29000  3  3                                                        :INP 13
     0.50     0.60     0.70                                           :INP 14
    13.00    14.00    15.0                                            :INP 15
   4.9614   7.9671   5.7404        0        0        0                :INP 16
          0  1  0  0            0  0  1  0            0  0  0  1:INP 18
          0 -1  0  0            0  0 -1  0            0  0  0 -1:     18
        0.5 -1  0  0          0.5  0 -1  0          0.5  0  0  1:     18
        0.5  1  0  0          0.5  0  1  0          0.5  0  0 -1:     18
```

```
            0.5 -1  0  0              0  0  1  0              0  0  0  1:    18
            0.5  1  0  0              0  0 -1  0              0  0  0 -1:    18
              0  1  0  0            0.5  0 -1  0            0.5  0  0  1:    18
              0 -1  0  0            0.5  0  1  0            0.5  0  0 -1:    18
Ca             2.0                                                        :INP 19
C             0.817                                                       :    19
O            -0.939                                                       :    19
Ca1     1                      0.2500    0.4150    0.7597                 :INP 20
C1      2                      0.2500    0.7622    0.9138                 :    20
O1a     3                      0.2500    0.9225    0.9038                 :    20
O1b     3                      0.4736    0.6810    0.9138                 :    20
O1c     3                      0.0264    0.6810    0.9138                 :    20
  1  2  2  2  2                                                           :INP 21
  1  0                                                                    :INP 22
  2  0                                                                    :    22
  2     3  4  5  0                                                       :    23
  0        -0000.0                                                       :INP 29
111000000000                                                            :INP 30
000000000000                                                            :INP 31
  3  SrCO3 (Strontianite)  SG Pmcn  #62    ORTHORHOMBIC P                 :INP 11
  5  3  8  2  0  0  0  2  0-15  1  0  4  0  1  0  0  1  1  0  0  1       :INP 12
  0.29000  3  3                                                         :INP 13
     0.50     0.60     0.70                                             :INP 14
    13.00    14.00    15.00                                             :INP 15
    5.090    8.358    5.997        0         0         0                 :INP 16
              0  1  0  0              0  0  1  0              0  0  0  1:INP 18
              0 -1  0  0              0  0 -1  0              0  0  0 -1:    18
            0.5 -1  0  0            0.5  0 -1  0            0.5  0  0  1:    18
            0.5  1  0  0            0.5  0  1  0            0.5  0  0 -1:    18
            0.5 -1  0  0              0  0  1  0              0  0  0  1:    18
            0.5  1  0  0              0  0 -1  0              0  0  0 -1:    18
              0  1  0  0            0.5  0 -1  0            0.5  0  0  1:    18
              0 -1  0  0            0.5  0  1  0            0.5  0  0 -1:    18
Sr             2.0                                                        :INP 19
C             0.817                                                       :    19
O            -0.939                                                       :    19
Sr1     1                      0.2500    0.4160    0.7569                 :INP 20
C1      2                      0.2500    0.7601    0.9136                 :    20
O1a     3                      0.2500    0.9119    0.9054                 :    20
O1b     3                      0.4694    0.6821    0.9161                 :    20
O1c     3                      0.0306    0.6821    0.9161                 :    20
  1  2  2  2  2                                                           :INP 21
  1  0                                                                    :INP 22
  2  0                                                                    :    22
  2     3  4  5  0                                                       :    23
  0        -0000.0                                                       :INP 29
111000000000                                                            :INP 30
000000000000                                                            :INP 31
  4  BaCO3 (Witherite)  SG Pmcn  #62    ORTHORHOMBIC P                   :INP 11
  5  3  8  2  0  0  0  2  0-15  1  0  4  0  1  0  0  1  1  0  0  1       :INP 12
  0.34000  3  3                                                         :INP 13
     0.60     0.70     0.80                                             :INP 14
    12.00    13.00    14.00                                             :INP 15
   5.3126   8.8958   6.4284        0         0         0                 :INP 16
              0  1  0  0              0  0  1  0              0  0  0  1:INP 18
              0 -1  0  0              0  0 -1  0              0  0  0 -1:    18
            0.5 -1  0  0            0.5  0 -1  0            0.5  0  0  1:    18
            0.5  1  0  0            0.5  0  1  0            0.5  0  0 -1:    18
            0.5 -1  0  0              0  0  1  0              0  0  0  1:    18
            0.5  1  0  0              0  0 -1  0              0  0  0 -1:    18
              0  1  0  0            0.5  0 -1  0            0.5  0  0  1:    18
              0 -1  0  0            0.5  0  1  0            0.5  0  0 -1:    18
Ba             2.0                                                        :INP 19
C             0.817                                                       :    19
O            -0.939                                                       :    19
Ba1     1                      0.2500    0.4163    0.7549                 :INP 20
C1      2                      0.2500    0.7570    0.9190                 :    20
O1a     3                      0.2500    0.9011    0.9122                 :    20
O1b     3                      0.4595    0.6839    0.9210                 :    20
O1c     3                      0.0405    0.6839    0.9210                 :    20
  1  2  2  2  2                                                           :INP 21
  1  0                                                                    :INP 22
  2  0                                                                    :    22
  2     3  4  5  0                                                       :    23
  0        -0000.0                                                       :INP 29
111000000000                                                            :INP 30
000000000000                                                            :INP 31
                                                                        :end
```

APPENDIX F

PLUTO DATA FILES

The PLUTO files for CaO (cubic), CaO_2 (tetragonal), $CaCO_3$ (calcite-rhombohedral) and $CaCO_3$ (aragonite-orthorhombic), are included. To improve the clarity of the unit cell diagrams, the size of the ionic radii was reduced to 30% of the values given in the "Handbook of Chemistry and Physics" [74].

```
DATA CAO  (cubic)
CELL 4.795 4.795 4.795 90 90 90
SYMM X,Y,Z
CA1    0  0  0
CA2    0 -1  0
CA4    0  0  1
CA5    0 -1  1
CA6    1  0  0
CA7    1 -1  0
CA8    1  0  1
CA9    1 -1  1
CA10   0.5 0 0.5
CA11   0.5 -1 0.5
CA12   0.5 -0.5 0
CA13   0.5 -0.5 1
CA14   0 -0.5 0.5
CA15   1 -0.5 0.5
O1     0.75 -0.25 0
O2     0.25 -0.75 0
O3     0.75 -0.25 1
O4     0.25 -0.75 1
O5     0.25 -0.25 0.5
O6     0.75 -0.75 0.5
OPT SOLID DIRICH NOLABEL
JOIN CA1  CA4
JOIN CA1  CA2
JOIN CA1  CA6
JOIN CA4  CA8
JOIN CA4  CA5
JOIN CA2  CA7
JOIN CA2  CA5
JOIN CA5  CA9
JOIN CA6  CA8
JOIN CA6  CA7
JOIN CA7  CA9
JOIN CA8  CA9
RAD ATOMS CA .297  O .396
SHADE 120 -45 .8
VIEW XO YROT -50 XROT -15
SIZE 220 SCALE 9
RAD BONDS TAPER 15
PLOT
```

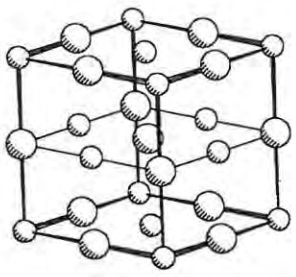

```
DATA CAO2  (tetragonal)
CELL 3.54 3.54 5.92 90 90 90
SYMM X,Y,Z
CA1    0  0  0
CA2    0 -1  0
CA3    0  0  1
CA4    0 -1  1
CA5    1  0  0
CA6    1 -1  0
CA7    1  0  1
CA8    1 -1  1
CA9    0.5 -0.5 0.5
O1     0   0   0.39
O2     0   0   0.61
O3     1  -1   0.39
O4     1  -1   0.61
O5     0  -1   0.39
O6     0  -1   0.61
O7     1   0   0.39
O8     1   0   0.61
O9     0.5 -0.5 0.11
O10    0.5 -0.5 0.89
OPT SOLID DIRICH NOLABEL
JOIN CA1  CA2
JOIN CA1  CA3
JOIN CA1  CA5
JOIN CA2  CA4
JOIN CA2  CA6
JOIN CA3  CA4
JOIN CA3  CA7
JOIN CA4  CA8
JOIN CA5  CA6
JOIN CA5  CA7
JOIN CA6  CA8
JOIN CA7  CA8
RAD ATOMS CA .297  O .528
SHADE 120 -45 .8
VIEW XO YROT -60 XROT -15
SIZE 220 SCALE 9
RAD BONDS TAPER 15
PLOT
```

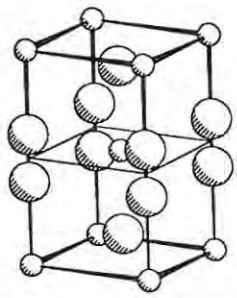

```
DATA CACO3  (calcite-rhombohedral)
CELL 6.3750 6.3750 6.3750 46.08 46.08 46.08
SYMM X,Y,Z
CA1  0.5  0.5  0.5
CA2  0  0  0
CA3  0  0  1
CA4  0  1  1
CA5  0  1  0
CA6  1  0  0
CA7  1  0  1
CA8  1  1  0
CA9  1  1  1
C1  0.25  0.25  0.25
C2  0.75  0.75  0.75
O1  -.0068 .25 .5068
O2  .5068 -.0068 .25
O3  .25 .5068 -.0068
O4  .4932 1.0068 .75
O5  1.0068 .75 .4932
O6  .75 .4932 1.0068
OPT SOLID DIRICH NOLABEL
JOIN C2 O6
JOIN C2 O5
JOIN C2 O4
JOIN C1 O1
JOIN C1 O2
JOIN C1 O3
JOIN CA4 CA5
JOIN CA5 CA2
JOIN CA2 CA3
JOIN CA3 CA4
JOIN CA9 CA8
JOIN CA8 CA6
JOIN CA6 CA7
JOIN CA7 CA9
JOIN CA9 CA4
JOIN CA8 CA5
JOIN CA6 CA2
JOIN CA7 CA3
MOLE 1 0 0 0
SHADE 120 -45 .8
RAD BONDS TAPER 15
VIEW LINE CA1 C1 YROT 75 ZROT 90
RAD ATOMS CA .297  O .528  C .3
SIZE 220 SCALE 9
PLOT
```

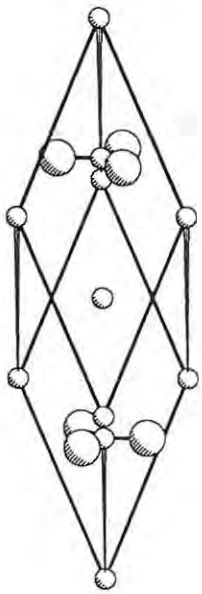

```
DATA CACO3  (aragonite-orthorhombic)
CELL 4.9614 7.9671 5.7404 90 90 90
SYMM X,Y,Z
CA1    0.2500 0.4150 0.7597
CA2    0.7500 0.5850 0.2403
CA3    0.7500 0.9150 0.7403
CA4    0.2500 0.0850 0.2597
C1     0.2500  0.7622 0.9138
O1     0.2500  0.9225 0.9038
O2     0.4736  0.6810 0.9138
O3     0.0264  0.6810 0.9138
C2     0.7500  0.2378 0.0862
O4     0.7500  0.0775 0.0962
O5     0.5264  0.3190 0.0862
O6     0.9736  0.3190 0.0862
C3     0.7500  0.2622 0.5862
O7     0.7500  0.4225 0.5962
O8     0.9736  0.1810 0.5862
O9     0.5264  0.1810 0.5862
C4     0.2500  0.7378 0.4138
O10    0.2500  0.5775 0.4038
O11    0.0264  0.8190 0.4138
O12    0.4736  0.8190 0.4138
OPT SOLID DIRICH NOLABEL ATOM CELL PLOT
JOIN C1 O1
JOIN C1 O2
JOIN C1 O3
JOIN C2 O4
JOIN C2 O5
JOIN C2 O6
JOIN C3 O7
JOIN C3 O8
JOIN C3 O9
JOIN C4 O10
JOIN C4 O11
JOIN C4 O12
RAD ATOMS   CA .297  C 0.3  O .528
SHADE 120 -45 .8
SIZE 220 SCALE 9
VIEW XO YROT -15 XROT -10
RAD BONDS TAPER 15
PLOT
```

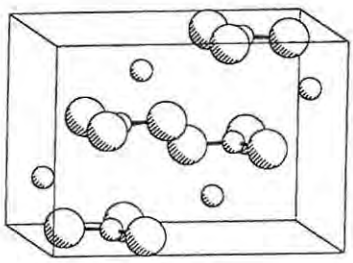

APPENDIX G

DELRHOMB.MCD

Alter rhombohedral cell constants DELRHOMB.MCD LG 26/3/95
(Subscripts: o=original; r=rhombohedral; h=hexagonal)

Original rhombohedral constants: $\alpha_o := 48.18 \cdot deg$ $a_o := 5.6751$

$$\alpha'_o := \operatorname{acos}\left[\sqrt{1 - \frac{4}{3}\cdot\sin\left[\frac{\alpha_o}{2}\right]^2}\right]$$

<- (Internal angle: triad to polar axis)

$\alpha'_o = 0.491$ $\alpha'_o = 28.12 \cdot deg$

$$x := \begin{bmatrix} 0 \\ 0.25 \\ 0.5274 \end{bmatrix} \quad y := \begin{bmatrix} 0 \\ 0.25 \\ -0.0274 \end{bmatrix} \quad z := \begin{bmatrix} 0 \\ 0.25 \\ 0.25 \end{bmatrix}$$

(Set of atom fractional coords)

$x_r := x \cdot a_o$ $y_r := y \cdot a_o$ $z_r := z \cdot a_o$

$$x_r = \begin{bmatrix} 0 \\ 1.419 \\ 2.993 \end{bmatrix} \quad y_r = \begin{bmatrix} 0 \\ 1.419 \\ -0.155 \end{bmatrix} \quad z_r = \begin{bmatrix} 0 \\ 1.419 \\ 1.419 \end{bmatrix}$$

Convert to hexagonal:

$$\overrightarrow{x_h := \left[x_r \cdot \sin\left[\alpha'_o\right] - z_r \cdot \sin\left[\alpha'_o\right]\right]}$$

$$\overrightarrow{y_h := \left[y_r \cdot \sin\left[\alpha'_o\right] - z_r \cdot \sin\left[\alpha'_o\right]\right]}$$

$$\overrightarrow{z_h := \left[\left[x_r + y_r + z_r\right] \cdot \cos\left[\alpha'_o\right]\right]}$$

Global definitions:

$rad \equiv 1$

$deg \equiv \frac{\pi}{180} \cdot rad$

$$x_h = \begin{bmatrix} 0 \\ 0 \\ 0.742 \end{bmatrix} \quad y_h = \begin{bmatrix} 0 \\ 0 \\ -0.742 \end{bmatrix} \quad z_h = \begin{bmatrix} 0 \\ 3.754 \\ 3.754 \end{bmatrix}$$

New rhombohedral constants: $\alpha := 50 \cdot deg$ $a := 5.6751$

$$\alpha' := \operatorname{acos}\left[\sqrt{1 - \frac{4}{3}\cdot\sin\left[\frac{\alpha}{2}\right]^2}\right]$$

$\alpha' = 29.209 \cdot deg$

New fractional coords

$$\overrightarrow{x_r := \left[\frac{z_h}{\cos(\alpha')} + \frac{2 \cdot x_h}{\sin(\alpha')} - \frac{y_h}{\sin(\alpha')}\right]} \qquad \frac{x_r}{3 \cdot a} = \begin{bmatrix} 0 \\ 0.25261 \\ 0.52053 \end{bmatrix}$$

$$\overrightarrow{y_r := \left[\frac{z_h}{\cos(\alpha')} + \frac{2 \cdot y_h}{\sin(\alpha')} - \frac{x_h}{\sin(\alpha')}\right]} \qquad \frac{y_r}{3 \cdot a} = \begin{bmatrix} 0 \\ 0.25261 \\ -0.01531 \end{bmatrix}$$

$$\overrightarrow{z_r := \left[\frac{z_h}{\cos(\alpha')} - \frac{x_h}{\sin(\alpha')} - \frac{y_h}{\sin(\alpha')}\right]} \qquad \frac{z_r}{3 \cdot a} = \begin{bmatrix} 0 \\ 0.25261 \\ 0.25261 \end{bmatrix}$$

REFERENCES

1. M.E. Brown, D. Dollimore and A.K. Galwey, "Reactions in the Solid State", Comprehensive Chemical Kinetics, Vol 22, Elsevier, Amsterdam, 1980.

2. A. Coetzee, "Thermal decomposition of mixed metal oxalates", MSc Thesis, Rhodes University, Grahamstown, South Africa, 1993.

3. E.K. Powell and A.W. Searcy, *Metall. Trans.*, **11B** (1980) 427.

4. M.J. Tribelhorn and M.E. Brown, *Thermochim. Acta.*, **225** (1995) 143.

5. W.C. Mackrodt and R.F. Stewart, *J. Phys. C: Solid State Phys.*, **12** (1979) 5015.

6. C.R.A. Catlow, *Computational Techniques and Simulation of Crystal Structure*, ch 7, in "Solid State Chemistry: Techniques", A.K. Cheetham and P. Day (Eds), Clarendon Press, Oxford, 1987.

7. C.R.A. Catlow and W.C. Mackrodt, *Theory of Simulation Methods for Lattice and Defect Energy Calculations in Crystals*, ch 1 and C.R.A. Catlow, M.Dixon and W.C. Mackrodt, *Interionic Potentials in Ionic Solids*, ch 10, in "Lecture Notes in Physics", Vol 166: Computer Simulation of Solids, C.R.A. Catlow and W.C. Mackrodt (Eds), Springer-Verlag, Berlin, 1982.

8. J.H. Harding, *Rep. Prog. Phys.*, **53** (1990) 1404.

9. C.R.A. Catlow, R.G. Bell and J.D. Gale, *J. Mater. Chem.*, **4** (1994) 781.

10. C.R.A. Catlow and G.D. Price, *Nature*, **347** (1990) 243.

11. C.R.A. Catlow, J.D. Gale and R.W. Grimes, *J. Solid State Chem.*, **106** (1993) 13.

12. C.R.A Catlow, J.M. Thomas, C.M. Freeman, P.A Wright and R.G Bell, *Proc. R. Soc. (London) A*, **442** (1993) 85.

13. C.R.A Catlow and A.N. Cormack, *Chem. Br.*, (1982) 627.

14. J.M. Thomas and C.R.A. Catlow, *Prog. Inorg. Chem.*, **35** (1987) 1.

15. J.D. Gale, C.R.A. Catlow and W.C. Mackrodt, *Modelling Simul. Mater. Sci. Eng.*, **1** (1992) 73.

16. C.R.A Catlow and J.M. Thomas, *Phil. Trans. R. Soc. (London) A*, **341** (1992) 255.

17. W.H. Press, B.P. Flannery, S.A. Teukolsky and W.T. Vetterling, "Numerical Recipes", Cambridge University Press, Cambridge, 1989.

18. P.E. Gill, W. Murray and M.H. Wright, "Practical Optimization", Academic Press. London, 1989.

19. T. Schlick, "Optimization Methods in Computational Chemistry" in *Reviews in Computational Chemistry*, Vol 3, K.B. Lipkowitz and D.B. Boyd (Eds.), VCH Publishers, New York, 1992.

20. A.R. Learch, "A Survey of Methods for Searching the Conformational Space of Small and Medium-Sized Molecules" in *Reviews in Computational Chemistry*, Vol 2, K.B. Lipkowitz and D.B. Boyd (Eds.), VCH Publishers, New York, 1991.

21. J. Blazejowski and J. Lubkowski, *J. Therm. Anal.*, **38** (1992) 2195.

22. E.S. Oran and J.P. Boris, "Numerical Simulation of Reactive Flow", Elsevier, New York, 1987.

23. M.P. Tosi, *Solid State Phys.*, **16** (1964) 1.

24. T.C. Waddington, *Adv. Inorg. Radiochem.*, **1** (1959) 158.

25. E.L. Burrows and S.F.A. Kettle, *J. Chem. Educ.*, **52** (1975) 59.

26. E. Madelung, *Phys Z.*, **19** (1918) 524.

27. G.C. Benson, *Can. J. Phys.* **34** (1956) 888.

28. H.M. Evjen. *Phys. Rev.* **39** (1932) 675.

29. F.C. Frank, *Phil. Mag.* **41** (1950) 1287.

30. P.P. Ewald, *Ann. Phys.*, **64** (1921) 253.

31. F.J. Bertaut, *J. Phys. Radium*, **13** (1952) 499.

32. D.E. Williams, *Acta Crystallogr.*, **A27** (1971) 452; **A28** (1972) 629; *Top. Curr. Phys.*, **26** (1981) 3.

33. R.C. Evans, "An Introduction to Crystal Chemistry", Cambridge University Press, London, 1966.

34. S.M.P. Verma and R.K. Singe, *Phys. Stat. Sol.*, **36** (1969) 335.

35. G. Brink, L. Glasser and R.C. Mboweni, *J. Phys. Chem.*, **93** (1989) 2927.

36. R. Eisberg and R.Resnick, "Quantum Physics of Atoms, Molecules, Solids, Nuclei and Particles", John Wiley & Sons, New York, 1985.

37. M.W. Lister, *Thermochim. Acta*, **8** (1974) 341.

38. S.C. Parker, *Solid State Ionics*, **8** (1983) 179.

39. S.C. Parker, E.T. Kelsey, P.M. Oliver and J.O. Titiloye, *Faraday Discuss.*, **95** (1993) 75.

40. T.S. Bush, J.D. Gale, C.R.A. Catlow and P.D. Battle, *J. Mater. Chem.*, **4** (1994) 831.

41. N. Allan, A.L. Rohl, D.H. Gay, C.R.A. Catlow, R.J. Davey and W.C. Mackrodt, *Faraday Discuss.*, **95** (1993) 275.

42. S.M.P. Lyddane and M. Herzfield, *Phys. Rev.*, **54** (1938) 846.

43. B.G. Dick and A.W. Overhauser, *Phys. Rev.*, **112** (1958) 90.

44. H. Bilz, M Buchanan, K Fischer, K. Haberkorn and U. Schröder, *Solid State Commun.*, **16** (1975) 1023.

45. W.R. Busing, WMIN: A computer program to model molecules and crystals in terms of potential energy functions, ORNL-5747, U.S., Oak Ridge National Laboratory, 1981. Revised version: March 1994.

46. A. Pavese, M. Catti, G.D. Price and R.A. Jackson, *Phys. Chem. Minerals*, **19** (1992) 80.

47. G. Brink and L. Glasser, *J. Mol. Struct.*, **244** (1991) 277.

48. S. Kirkpatrick, C.D. Gelatt and M.P. Vecchi, *Science*, **220** (1983) 671.

49. A.J. Pertsin and A.I. Kitaigorodsky, "The Atom-Atom Potential Method", Vol 43, Springer Series in Chemical Physics, M. Cardona (Ed), Springer-Verlag, Berlin, 1987.

50. C.R.A. Catlow and A.M. Stoneham, *J. Phys. C: Solid State Phys.*, **16** (1983) 4321.

51. G.V. Lewis and C.R.A. Catlow, *J. Phys. C: Solid State Phys.*, **18** (1985) 1149.

52. E. Clementi, G. Corongiu and G. Ranghino, *J. Chem. Phys.*, **74** (1081) 578.

53. G. Brink and L. Glasser, *J. Phys. Chem.*, **94** (1990) 981.

54. T.L. Gilbert, *J. Chem. Phys.*, 49 (1968) 2640. See also: T.L. Gilbert, O.C. Simpson and M.A. Williamson, *J. Chem. Phys.*, **63** (1975) 4061.

55. C. Giacovazzo, *International Union of Crystallography Newsletter*, **2** (1994) 2.

56. L.V. Azároff and M.J. Buerger, "The Powder Method in X-ray Crystallography", McGraw-Hill Book Company, New York, 1958.

57. Inorganic Crystal Structure Database (ICSD), maintained by FIZ Karlsruhe and Gmelin Institute.

58. N.F.M. Henry and K. Lonsdale (Eds), "International Tables for X-ray Crystallography", Vol 1, The Kynoch Press, Birmingham, 1952.

59. S. Motherwell, PLUTO: a computer program for molecular drawings, Cambridge, England.

60. H. Ellis (Chief Ed), "Revised Nuffield Advanced Science Book of Data", Longman Ltd., Essex, 1986.

61. S. Sasaki, K. Fujino and Y. Takeuchi, *Proc. Jpn. Acad.*, **55** (1979) 43.

62. G. Natta and L Passerini, *Gazz. Chim. Ital.*, **59** (1929) 129.

63. W. Primak, H. Kaufman and R. Ward, *J. Am. Chem. Soc.*, **70** (1948) 2043.

64. W. Gerlach, *Z. Phys.*, **9** (1929) 184.

65. P. Luger, "Modern X-Ray Analysis on Single Crystals", Walter de Gruyter, Berlin, 1980.

66. J.D. Bernal, E. Djatlowa, P. Kasarnwsky, S Reichstein and A.G. Ward, *Z. Krist.*, **92** (1935) 344.

67. V. Kotov and S. Reichstein, *Zh. Fiz. Khim.*, **15** (1941) 1057.

68. A. F. Wells, "Structural Inorganic Chemistry", Clarendon Press, Oxford, 1962.

69. T.E. Harr, Thesis, Syracuse University, USA, 1952. (Found on ICSD Nos 30570, 30571, 30572, 30573, 30574, 30575).

70. S.C. Abrahams and J. Kalnajs, *Acta Cryst.*, **7** (1954) 838.

71. N.G. Vannerber, *Ark. Kemi.*, 14 (1959) 99.

72. C. Brosset and N.G. Vannerberg, *Nature (London)*, **177** (1956) 238.

73 J.V. Smith, "Powder Diffraction File", No. 7-234 (1956).

74. R.C. Weast (Chief Ed), "Handbook of Chemistry and Physics", 64th edition, CRC Press, Boca Raton, 1983.

75. S.I. Reichstein and I. Kazarnovskii, *Zh. Fiz. Khim.*, **3** (1932) 83.

76. H.J. Meyer, *Z. Krist.*, **128** (1969) 183.

77. S.R. Kamhi, *Acta Cryst.*, **16** (1963) 770.

78. T.C.W. Mak and G. Zhou, "Crystallography in Modern Chemistry, A Resource Book of Crystal Structures", John Wiley & Sons, New York, 1992.

79. H. Effenberger, K. Mereiter and J. Zemann, *Z. Krist.*, **156** (1981) 233.

80. J.P.R. de Villiers, *Am. Mineral.*, **56** (1971) 768.

81. M.J.L. Sangster and A.M. Stoneham, *Phil. Mag.*, **43** (1981).

82. C.R.A. Catlow, W.C. Mackrodt, M.J. Norgett and A.M. Stoneham, *Phil. Mag.*, **35** (1977) 177.

83. J.E. Post and C.W. Burnham, *Am. Mineral.*, **71** (1986) 142.

84. M.L. Huggins and Y. Sakamoto, *J. Phys. Soc. Japan*, **12** (1957) 241.

85. A.F. Kapustinskii, *Z. Physik. Chem. (Leipzig)*, **B22** (1933) 257; *J. Phys. Chem. (USSR)*, **5** (1943) 59.

86. M.G. Evans and N. Uri, *Trans. Faraday Soc.*, **45** (1949) 224.

87. A.V. Vedeneev, L.I. Kazarnovskaya and I.A. Kazarnovskii, *Zhur. Fiz. Khim.*, **26** (1952) 1808.

88. R.H. Wood and L.A. D'Orazio, *J. Phys Chem.*, **69** (1965) 2558.

89. F.D. Rossini, D.D. Wagman, W.H. Evans, S. Levine and Irving Jaffe (Eds), "Selected Values of Chemical Thermodynamic Properties", Circular of the National Bureau of Standards 500, United States Government Printing Office, Washington, D.C., 1952.

90. A.B. Tsentsiper and Z.I. Kuznetsova, *Izv. Akad. Nauk SSR*, (1965) 1902.

91. M.M. Pavlyuchenko and T.I. Popova, *Geterogennye Khim. Reacktsii Inst. Obshch. i Neorgan Khim. Akad. Nauk Belorussk. SSR*, **80** (1965) 5: *Chem. Abstr.*, **64** (1966) 13440c.

92. V.J. Brunere and A.N. Dokuchaeva, *Izv. Akad. Nauk. Latvijskoj SSR, Ser. Chim.*, **3** (1990) 332: *Chem. Abstr.*, **113** (1990) 104146v.

93. B.J. Erofeev and N.D. Sokolova, Topokinetic Equation Tables, *Akad. Nauk BSSR, Minsk*, (1963) 3.

94. M.A. Fahim and J.D. Ford, *J. Chem. Eng.*, **27** (1983) 21.

95. M.F.C. Ladd, *Trans. Faraday Soc.*, **65** (1969) 2712.

96. M.F.C. Ladd, *Theor. Chim. Acta*, **25** (1972) 400.

97. H.D.B. Jenkins and T.C. Waddington, *Nature (London), Phys. Sci.*, **232** (1971).

98. H.D.B. Jenkins, K.F. Pratt, B.T. Smith and T.C. Waddington, *J. Inorg. Nucl. Chem.*, **38** (1976) 371.

99. P.S. Yuen, M.W. Lister and S.C. Nyburg, *J. Chem. Phys.*, **68** (1978) 1937.

100. M.F.C. Ladd, *Nature (London)*, **238** (1972) 125; H.D.B. Jenkins and T.C. Waddington, *Nature (London)*, **238** (1972) 126.

101. W.R. Busing, *Trans. Am. Cryst. Assoc.*, **6** (1(70) 57.

102. C.N.R. Rao and K.J. Rao, "Progress in Solid State Chemistry", Vol 4, Pergamon, Oxford, 1967.

103. L. Glasser, DELRHOMB.MCD: a computer program for transforming rhombohedral coordinates, University of Witwatersrand, Johannesberg, 1994.

104. Mathcad PLUS 5.0, MathSoft, P.O. Box 58, Livingston, EH54 7AE, UK

105. N.S. Brar and H.H. Schloessin, *Can. J. Earth Sci.*, **16** (1979) 1402.

106. M. Madon and P. Gillet, *Earth Planet. Sci. Lett.*, **67** (1984) 400.

107. M.S. Rao, *Indian J. Chem.*, **11** (1973) 280.

108. C.N.R. Rao, "Crystal Structural Transitions in Inorganic Nitrites, Nitrates and Carbonates", National Bureau of Standards, Washington, D.C., 1975.

109. C.R.M. Rao and P.N. Mehrotra, *Can. J. Chem.*, **56** (1978) 32.

110. N.D. Topor, L.I. Tolokonnikova and B.M. Kadenatsi, *J. Therm. Anal.*, **20** (1981) 169.

111. J. Morales, L Hernán, L.V. Flores and A. Ortega, *J. Therm. Anal.*, **24** (1982) 23.

112. J. Morales, L Hernán, M. Macias and A. Ortega, *J. Mater. Sci.*, **18** (1983) 2117.

113. J. Perić, R. Krstulović, T. Ferić and M. Vučak, *Thermochim. Acta*, **207** (1992) 245.

114. M. Liu and R.A. Yund, *Contrib. Mineral. Petrol.*, **114** (1993) 465.

115. J.V. Dubrawski and B.M. England, *J. Therm. Anal.*, **39** (1993) 987.

116. P. Gillet and M. Madon, *Bull Mineral.*, **105** (1982) 590.

117. R. Shannon, *Trans. Faraday Soc.*, **60** (1964) 1902.

118. E.K. Powell and A.W. Searcy, *Metall. Trans.*, **IIB** (1980) 427.

119. P.K. Gallagher and D.W. Johnson, Jr., *Thermochim. Acta*, **6** (1973) 67.

120. M. Polanyi and E Wigner, *Z. Physik. Chem. A*, **139** (1928) 439.

121. J.M. Criado, F. González and J. Morales, *Thermochim. Acta*, **32** (1979) 99.

122. M.D. Judd and M.I. Pope, *J. Therm. Anal.*, **4** (1972) 31.

123. A.W.D. Hills, *Chem. Eng. Sci.*, **23** (1968) 297.

124. K.F. Purcell and J.C. Kotz, "Inorganic Chemistry", W.B. Saunders Company, London, 1977.

125. E.G. Calvo, B. Aparicio and A.R. Salvador, *Thermochim. Acta*, **143** (1989) 339.

126. M.E. Brown, *Chemsa*, **5**(5) (1979) 74.

127. M.J. Norgett, UKAEA report, AERE-R7650, USA.

128. C.R.A. Catlow, *J. Phys. (Paris)*, **C6** (1980) 53.

129. V.M. Goldschmidt, *Trans. Faraday Soc.*, **25** (1929) 253.

130. L. Pauling, "The Nature of the Chemical Bond", Cornell University Press, New York, 1960.

131. R.D. Shannon, *Acta Crystallogr.*, **A32** (1976) 751.

132. W.E. Dasent, "Inorganic Energetics", 2nd ed., Cambridge University Press, Cambridge, 1982.